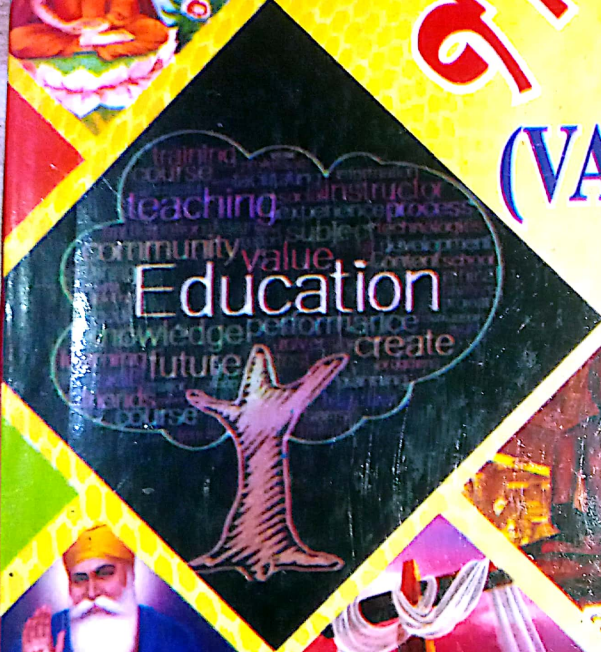


इन्दिरा गांधी विश्वविद्यालय, रेवाड़ी के समस्त स्नातकोत्तर पाठ्यक्रमों के लिए

मूल्य शिक्षा

(VALUE EDUCATION)



डॉ. सुनील यादव
डॉ. आशीष कुमार

महावीर प्रकाशन, दिल्ली

मूल्य शिक्षा

(Value Education)

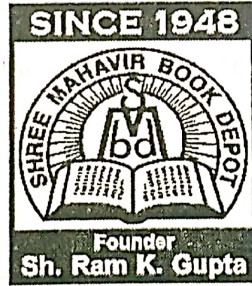
(इंदिरा गांधी विश्वविद्यालय, रेवांडी के समस्त स्नातकोत्तर पाठ्यक्रमों के लिए)

डॉ. सुनील यादव

असिस्टेंट प्रोफेसर, वाणिज्य विभाग
राजकीय महाविद्यालय, नारनौल

डॉ. आशीष कुमार

असिस्टेंट प्रोफेसर, संस्कृत विभाग
राजकीय महाविद्यालय, नारनौल



श्री महावीर बुक डिपो (पब्लिशर्स)

An ISO 9001 : 2015 Certified

नई सड़क, दिल्ली - 110006

दूरभाष : 23262993, 23283331, फैक्स : 011-23270792

वेबसाइट : www.mahavirpublications.com

ई-मेल : info@mahavirpublications.com

प्रकाशक :

श्री महावीर बुक डिपो (पब्लिशर्स)

2603, नई सड़क, दिल्ली-110006

फोन : 23262993, 23270792

टेली फैक्स : 011-23270792

मूल्य : ₹ 150.00

द्वितीय संशोधित संस्करण

Every effort has been made to avoid errors or omissions in this publication. In spite of this, some errors might have crept in. Any mistake, error or discrepancy noted may please be brought to our notice which shall be taken care of in the next edition. It is notified that neither the publishers nor the authors or sellers will be held responsible for any damage or loss to any one, of any kind, in any manner, therefrom. The authors and publishers specifically disclaim any implied warranties as to merchantability or fitness of the publication for any particular purpose.

टाइपसेट :

साहिल कम्प्यूटर्स

कमला नगर, दिल्ली-7 [Mulya Shiksha]

मुद्रक :

फाईन आर्ट एजेन्सी, दिल्ली

डिपार्ट्मन्ट् , गृहकार्य , अलाहाबादराजी डिपार्ट्मन्ट्

संस्कृतभाषा विभाग

पुस्तकालय

क-इण्ड
पूजनीय दादाजी स्व. श्री गणेशीलाल जी
एवं
दादीजी स्व. श्रीमती गिन्दोड़ी देवी
को समर्पित

ख-इण्ड

-डॉ. सुनील यादव

ग-इण्ड

कॉलेज ऑफ़ इण्डियन लैंग्वेज

अलाहाबाद विश्वविद्यालय, अलाहाबाद, उत्तर प्रदेश, भारत

पृष्ठ संख्या

पृष्ठ संख्या

इन्दिरा गांधी विश्वविद्यालय, मीरपुर, रेवाड़ी

अनिवार्य पाठ्यक्रम

मूल्य शिक्षा

निर्देश-पूरे पाठ्यक्रम से कुल आठ प्रश्न पूछे जायेंगे। प्रत्येक खण्ड में दो-दो प्रश्न होंगे, जिनमें परीक्षार्थियों को कुल पाँच प्रश्न करने होंगे। प्रत्येक खण्ड से एक प्रश्न करना अनिवार्य होगा।

खण्ड-क

मूल्य शिक्षा-अर्थ और प्रकृति

1. मूल्य और मूल्य शिक्षा की अवधारणा
2. मूल्य शिक्षा का उद्देश्य
3. मूल्य शिक्षा की आवश्यकता और महत्ता
4. मूल्य शिक्षा के नियामक तत्त्व

खण्ड-ख

मूल्य शिक्षा के विभिन्न रूप

1. परिवार और मूल्य शिक्षा
2. समाज और मूल्य शिक्षा
3. राजनीति और मूल्य शिक्षा
4. मूल्य शिक्षा का धार्मिक और सांस्कृतिक पक्ष
5. मूल्य शिक्षा का आर्थिक और पर्यावरण सम्बन्धी स्वरूप

खण्ड-ग

मूल्य शिक्षा के स्रोत

1. हिन्दू धर्म-वेद, उपनिषद्, गीता, चाणक्य नीति, शुक्रनीति, रामचरित मानस।
2. जैन धर्म
3. बौद्ध धर्म

4. सिक्ख धर्म
5. ईसाई धर्म
6. इस्लाम धर्म



खण्ड-घ

प्रसिद्ध दार्शनिक और विचारक

1. महात्मा गांधी
2. स्वामी विवेकानन्द
3. लोकमान्य गंगाधर तिलक
4. राधाकृष्णन
5. हेमचन्द्र विक्रमादित्य
6. राव तुलाराम
7. बालमुकुन्द गुप्त

विषय सूची

क्र.सं.	अध्याय	पृष्ठ
	खण्ड-1	
1.	मूल्य शिक्षा : अर्थ और प्रकृति (Value Education : Meaning and Nature)	1-31
	खण्ड-2	
2.	मूल्य शिक्षा के सामाजिक एवं पारिवारिक पहलू (Social and Domestic Aspects of Value Education)	32-48
3.	मूल्य शिक्षा के राजनीतिक, आर्थिक एवं धार्मिक पहलू (Political, Economic and Religious Aspects of Value Education)	49-60
	खण्ड-3	
4.	मूल्य शिक्षा के वैदिक स्रोत (Vedic Sources of Value Education)	61-107
5.	मूल्य शिक्षा के धार्मिक स्रोत (Religious Sources of Value Education)	108-123
6.	मूल्य शिक्षा में अन्य धर्मों का योगदान (Contribution of Other Religions in Value Education)	124-138
	खण्ड-4	
7.	प्रसिद्ध दार्शनिक और विचारक (Leading Philosophers and Thinkers)	139-156
8.	मूल्य शिक्षा में तिलक और राधाकृष्णन का योगदान (Contribution of Tilak and Radha Krishnan in Value Education)	157-167
9.	मूल्य शिक्षा में अन्य विचारकों का योगदान (Contribution of Other Thinkers in Value Education)	168-175

1

मूल्य शिक्षा : अर्थ और प्रकृति (Value Education : Meaning and Nature)

अध्याय के मुख्य बिन्दु

- मूल्य और मूल्य शिक्षा की अवधारणा
(Concept of Value and Value Education)
- मूल्य शिक्षा के उद्देश्य
(Objectives of Value Education)
- मूल्य शिक्षा की आवश्यकता और महत्त्व
(Need and Importance of Value Education)
- मूल्य शिक्षा के नियामक तत्त्व
(Regulatory Elements of Value Education)

भूमिका (Introduction)

हमारे देश की सभ्यता व संस्कृति विश्व की अन्य सभ्यताओं व संस्कृतियों की तुलना में प्राचीन व सनातन है। समय व काल में परिवर्तन के थपेड़ों को झेलती हुई गंगा के अखण्ड प्रवाह के समान अपने अस्तित्व को बनाये हुए हैं। भारतीय (आर्य) संस्कृति के समय की अन्य संस्कृतियाँ (बेबीलोन, मेसोपोटामिया, मिस्र और सिन्धु घाटी सभ्यतायें इत्यादि) इतिहास की सामग्री बन चुकी है। हमारे देश में विश्व की अनेक जाति व संस्कृतियों का आगमन हुआ परन्तु उनका भी विलय व संगम इस महान् संस्कृति ने बड़ी सहृदयता से स्वीकार कर लिया और अपनी संस्कृति को अक्षुण्ण बनाये रखा। हमारे भारत देश (आर्य देश) को विश्व का आध्यात्मिक गुरु माना जाता था। इसका एकमात्र कारण इस



Shree Mahavir Book Depot (Publishers)

ISO 9001:2015 Certified

2603, Nai Sarak, Delhi-110006 (India)

Ph. : 23262993, 23270792 Fax: 011-23270792

E-mail : info@mahavirpublications.com

Visit us : www.mahavirpublications.com

Follow us on: [facebook.com/mahavirpublications](https://www.facebook.com/mahavirpublications)

ISBN : 978-93-87909-10-6



9 789387 1909106

ओ३म्

भारतीय संस्कृति का मूलाधार
पुरुषार्थ चतुष्टय

(विदुरनीति, चाणक्यनीति, हितोपदेश, पञ्चतन्त्र के आलोक में)

Publishing-in-support-of,

EDUCREATION PUBLISHING

RZ 94, Sector - 6, Dwarka, New Delhi - 110075
Shubham Vihar, Mangla, Bilaspur, Chhattisgarh - 495001

Website: *www.educreation.in*

© Copyright, Authors

All rights reserved. No part of this book may be reproduced, stored in a retrieval system, or transmitted, in any form by any means, electronic, mechanical, magnetic, optical, chemical, manual, photocopying, recording or otherwise, without the prior written consent of its writer.

ISBN: 978-1-5457-0813-2

Price: ₹ 315.00

The opinions/ contents expressed in this book are solely of the authors and do not represent the opinions/ standings/ thoughts of Educreation or the Editors . The book is released by using the services of self-publishing house.

Printed in India

ओ३म्

भारतीय संस्कृति का मूलाधार
पुरुषार्थ चतुष्टय

(विदुरनीति, चाणक्यनीति, हितोपदेश, पञ्चतन्त्र के आलोक में)

लेखक
आशीष कुमार



EDUCREATION PUBLISHING

(Since 2011)

www.educreation.in

ओ३म्
विषयानुक्रणिका

क्र.		
	पुरोवाक्	vi
	प्रस्तावना	viii
1	प्रथम अध्याय – विषय प्रवेश	1
2	द्वितीय अध्याय- धर्म का स्वरूप	6
3	तृतीय अध्याय- अर्थ का स्वरूप	46
4	चतुर्थ अध्याय– काम का स्वरूप	73
5	पञ्चम अध्याय- मोक्ष का स्वरूप	100
6	षष्ठ अध्याय – उपसंहार	147

पुरोवाक्

भारत का अभिज्ञान इसके महनीय ग्रन्थों एवं लोककल्याणकारी विपुल वाङ्मय में सन्निहित है। यह समग्र वाङ्मय भारतीय संस्कृति को उद्भासित करता है, जिससे यह देश विश्व-गुरु के महनीय आसन पर आसीन हो सका। भारतीय संस्कृति में ब्रह्मज्ञान तथा आत्मविश्वास के आयामों की ओर विशेषरूप से ध्यान दिया जाता है। आत्मा की पवित्रता के लिए तप एवं साधनों को अनिवार्य माना गया है। इस अध्यात्म भावना के अनुसार यह माना गया है कि इस संसार से परे भी एक सत्ता है, वही समस्त प्राणियों में व्याप्त है।

इसी भारतीय संस्कृति में कमल के पुष्प सौन्दर्य, कोमलता, पवित्रता और मांगल्य का प्रतीक माना गया है। आम्रपल्लवों के वन्दनवारों से शुभ अवसरों पर गृहसज्जा और पूजा हेतु कलश की स्थापना आवश्यक मानी जाती है। तुलसी और पीपल के वृक्ष को देवता माना जाता है। नारियल के बिना तो शायद ही कोई धार्मिक अनिष्ठान पूर्ण होता हो। ऐसी कोमल व मनोहर भारतीय संस्कृति ने पुरुषार्थ चतुष्टय को जन्म दिया, तथा पुरुषार्थ चतुष्टय को विशेष महत्त्व प्रदान किया।

विद्वानों ने पुरुषार्थ के सिद्धान्त को भारतीय संस्कृति की आत्मा माना है। पुरुषार्थ चतुष्टय को धार्मिक, भौतिक एवं आध्यात्मिक तत्त्वों का निवेशन बताया है।

मानव जीवन का चरम लक्ष्य मोक्ष की प्राप्ति है। अर्थ और काम इस लक्ष्य तक पहुँचाने के माध्यम हैं। माध्यमों का प्रयोग किस प्रकार किया जायें, इसे स्पष्ट करने काम धर्म का है। इस प्रकार मनुष्य के मोक्ष के लिए धर्म, अर्थ, काम, मोक्ष को पुरुषार्थ चतुष्टय के अन्तर्गत स्वीकार किया गया है।

प्रस्तुत लेखक ने पुरुषार्थ चतुष्टय पर शोधपूर्ण गहन विवेचन किया है। ये आरम्भिक अध्ययन होने के कारण इसकी उपादेयता है। इस विषय के विवेचन के अनेकविध दृष्टिकोण हो सकता है। लेखक का दृष्टिकोण सहानुभूतिपूर्ण है, जो इस अवधारणा की मूलभावना को समझने में सहायक है। अपने इस परिश्रम के लिए वे साधुवाद के पात्र हैं। मैं इनके ग्रन्थ की अनुशंसा करती हूँ।



डा. अर्चना कुमारी

सहायक प्राध्यापिका

राजकीय महाविद्यालय बौन्द कलाँ

हरियाणा

प्रस्तावना

भारत के ऐतिहासिकता विकासक्रम से यह स्पष्ट हो जाता है कि सामाजिक संगठन, रीति-नीति और दर्शन सभी कट्टर सिद्धान्तवादिता की अपेक्षा भारतीय संस्कृति ने सदैव उदार समन्वयवादिता का परिचय दिया है। बदलती हुई परिस्थितियों के अनुकूल अपने स्वरूप में संतुलित परिवर्तन करके अपने अस्तित्व को सुरक्षित रखने का प्राणीशास्त्रीय सिद्धान्त संस्कृतियों पर भी लागू होता है। एक तरह से देखा जाए तो विविध संस्कृतियों की महत्वपूर्ण विशेषताओं को आत्मसात करते-करते उदारता और अनुकूलन के गुण सहज ही भारतीय संस्कृति में विकसित हुए हैं। व्यक्ति के पुरुषार्थ की भावना समन्वय से मानी गयी है। भौतिक और आध्यात्मिक जीवन का सुख समन्वय पर ही आधारित रहा है। मनुष्य का विकास इहलौकिक और पारलौकिक दोनों स्थितियों के समन्वय से ही सम्भव है।

अनुकूल और प्रतिकूल तथा सहयोगी और विरोधी प्रवृत्तियों में समन्वय स्थापित करके चलना भारतीय संस्कृति का मूल आधार तत्व रहा है। सम्पूर्ण जगत् चाहे जड़ हो या चेतन सभी में समन्वय की भावना विद्यमान रहती है। जीव और ब्रह्म, आत्मा और परमात्मा, लौकिक और पारलौकिक, कामना और साधना, भोग और योग, ग्रहण और त्याग आदि समन्वय स्थापना के परिचायक हैं।

सामाजिक संस्थाओं के जो आचार-विचार बनाये गये हैं। उनमें समन्वय की भावना परिलक्षित होती है। आश्रम व्यवस्था पूर्णरूपेण समन्वयवादी भावना पर आधारित है। धर्म, अर्थ, काम, मोक्ष सभी समन्वय पर आधारित है। जो भारतीय संस्कृति का एक नियम है। इसी भारतीय संस्कृति को भारतीय ऋषि-मुनियों ने तो स्वीकार किया ही है, अपितु सम्पूर्ण विश्व ने इस संस्कृति का लौहा माना है। इसी भारतीय संस्कृति की आज विलुप्त को देखते हुए मैंने भी इस भारतीय संस्कृति के मूलाधार पुरुषार्थ चतुष्टय नामक पुस्तक की रचना की है। ताकि भारतीय संस्कृति की अमूल्य निधि समाप्त न हों। तथा समाज में विद्यमान बुराईयों से बचा जा सके। वर्तमान में लोग नास्तिक होते जा रहे हैं। इससे लोग आस्तिक बनें। मैंने अपने प्रयास से भारतीय संस्कृति के मूलाधार नामक पुस्तक के विभिन्न अध्यायों को इस प्रकार से संयोजित किया है।

प्रथम अध्याय- विषय प्रवेश

इसमें संस्कृति की परिभाषा, भारतीय संस्कृति का महत्व, पुरुषार्थ का अर्थ तथा पुरुषार्थ का स्वरूप तथा पुरुषार्थ चतुष्टय की वर्तमान में उपयोगिता को प्रस्तुत किया है।

द्वितीय अध्याय- धर्म

इस अध्याय में धर्म का अर्थ, धर्म का स्वरूप, धर्म का फल तथा धर्म के मुख्य मार्ग तथा गौण मार्गों को प्रस्तुत किया है।

तृतीय अध्याय- अर्थ

इस अध्याय में अर्थ का अर्थ, अर्थ का महत्व, अर्थवान् और निर्धन की दशा, अन्याय से उपार्जित धन का फल, धन का विनियोग, आदि विषयों को प्रस्तुत किया है।

चतुर्थ अध्याय- काम

इस अध्याय में काम का अर्थ, काम शब्द के पर्यायवाची शब्द, काम के प्रकार, काम का महत्व तथा काम मनुष्य के लिए साधक तथा बाधक विषयों को प्रस्तुत किया है।

पञ्चम अध्याय- मोक्ष

इस अध्याय में मोक्ष शब्द का अर्थ, मोक्ष के प्राप्ति के साधन, मोक्ष का स्वरूप विषयों को प्रस्तुत किया है।

षष्ठ अध्याय- उपसंहार

इस अध्याय में सभी अध्यायों को एक सार के रूप में प्रस्तुत किया है। इस पुस्तक के कुछ अध्याय में शोधप्रबन्ध के हैं तथा कुछ अध्यायों पर मैंने शोधप्रबन्ध के अनन्तर काम किया है। मेरे इस पुस्तक का उद्देश्य वर्तमान काल की स्थितियों को सुधारने का है। यदि हम कहीं भी जाते हैं, हमें वही पर बेईमानी, अनाचार, दुराचार दिखाई पड़ता है। इन विषम परिस्थितियों से अपनी इस सर्वश्रेष्ठ संस्कृति को बचाना ही ध्येय है इस पुस्तक की सफलता में मैं अपने पुजनीय गुरुजनों तथा अपने माता-पिता को देता हूँ। जिन्होंने मेरे को इस लायक बनाया है। अब ये पुस्तक मैं विद्वानों के करकमलों में सोपता हूँ। गुरुजनों से मेरी अपेक्षा है कि मेरे इस शोधकार्य में हुई त्रुटियों को क्षमा करने की कृपा करें तथा इसे स्वीकार कर

आशीष को शुभाशीष प्रदान करें। अब प्रस्तुत पुस्तक विद्वानों के कर-कमलों में
सोंपता हूँ।

गच्छतः स्खलनं क्वापि भवत्येव प्रमादतः।

उत्थाप्य सानुकम्पं हि समादधति सज्जनाः॥

प्रथम अध्याय विषय प्रवेश

मानव जीवन के तीन पक्ष ज्ञान, भाव एवं कर्म है। जिसे वैचारिक दृष्टि से बुद्धि, हृदय एवं व्यवहार कहा जा सकता है। जीवन में जब इन तीनों तत्त्वों का सामंजस्य होता है तब उसे संस्कृति कहते हैं। संस्कृति शब्द की व्युत्पत्ति सम् उपसर्ग पूर्वक कृ धातु में भाव अर्थ में क्तिन् प्रत्यय लगाने पर हुई है। संस्कृति शब्द का सम्बन्ध **संस्कार** शब्द से है। संस्कृति शब्द का अर्थ है संस्करण, परिमार्जन, शोधन, परिष्करण इत्यादि। ऐसी क्रिया जो व्यक्ति में निर्मलता का संचार करें। किसी वस्तु को यहाँ तक संस्कारित और परिष्कृत करना कि इसका अन्तिम उत्पाद हमारी प्रशंसा और सम्मान प्राप्त कर सके। यह ठिक उसी तरह है जैसे संस्कृत भाषा का शब्द संस्कृति। संस्कृति उन भूषणरूपी सम्यक् चेष्टाओं का नाम है जिनके द्वारा मानव समूह अपने आन्तरिक और बाह्य जीवन को अपनी शारीरिक मानसिक शक्तियों को संस्कारवान विकसित और दृढ़ बनाता है। वस्तुतः संस्कृति इतनी व्यापक और बृहद् चेष्टाओं का भण्डार है जो सनातन काल से क्रमिक रूप में निखरती आई है और जिन्होंने मानव के सर्वांगण विकास में पूरा-पूरा योगदान भी दिया है। संस्कृति मानव समूह के उन आचार-विचारों की प्रणाली का प्रतिनिधित्व करती है जो मनुष्य को सुसंस्कृत बनाकर उसे सभी प्रकार योग्य समर्थ बनाती है।

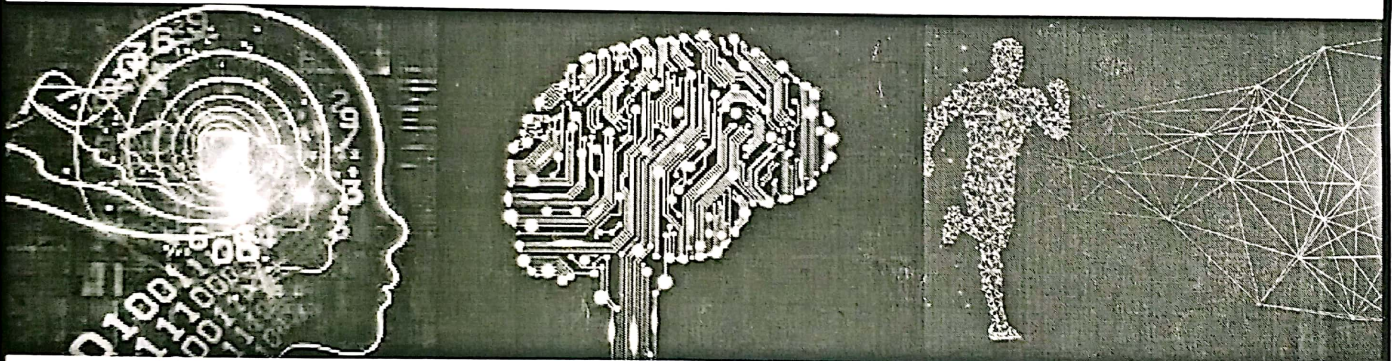
शिक्षाविदों के अनुसार संस्कार मनुष्य एवं जाति दोनों के होते हैं। जातीय संस्कारों को ही संस्कृति की संज्ञा दी जाती है।¹ संस्कृति के द्वारा किसी देश के धर्म, साहित्य, मानवीय मूल्यों, रीति-रिवाजों लक्ष्यों एवं आदर्शों को जाना जा सकता है।

भारतीय चिन्तकों ने विज्ञान, दर्शन, धर्म और संस्कृति की व्याख्या करते हुए कहा गया है कि बाहर की ओर देखना विज्ञान तथा अन्दर की ओर देखना

¹. भारतीय संस्कृति के मूल तत्व पृ.1



**PROCEEDINGS
OF
NATIONAL CONFERENCE
ON
COMPUTATIONAL INTELLIGENCE AND DATA SCIENCE
NCCIDS-23
ISBN:978-93-80544-50-2**



**ORGANIZED BY
DEPARTMENT OF COMPUTER SCIENCE & APPLICATIONS
IN COLLABORATION WITH
CHAUDHRY RANBIR SINGH INSTITUTE OF SOCIAL &
ECONOMIC CHANGE
&
TECHNICAL COLLABORATION WITH
COMPUTER SOCIETY OF INDIA**

**MAHARSHI DAYANAND UNIVERSITY, ROHTAK - 124001 (HARYANA)
NAAC ACCREDITED 'A+' GRADE STATE UNIVERSITY**

www.mdurohtak.ac.in

IIOT SECURITY CHALLENGES AND PROSPECTIVE MEASURES

Dr. Palak^{1*}, Dr. Preeti Gulia², Dr. Satish Kumar³, Ms. Venu⁴

^{1,3}Dept. of Computer Science, Govt. College, Narnaul, Haryana

³Dept. of Computer Science and Applications, MDU, Rohtak, Haryana

⁴Dept. of Computer Science, Govt. College, Sector 9, Gurugram, Haryana

Abstract

The large network of interconnected physical items (i.e., things) that share data with other devices and systems online is known as the Internet of Things (IoT). This paper presents the investigation and analysis of the current situation and problems with Internet of Things (IoT) security. The goal of the Internet of Things (IoT) framework is to globally connect everyone and everything. IoT security is a broad word that refers to the plans, instruments, systems, procedures, and techniques employed to safeguard every facet of the internet of things. In order to guarantee the availability, integrity, and confidentiality of IoT ecosystems, physical components, applications, data, and network connections must all be protected. Perceptual, network, and application layers often make up an IoT architecture. A variety of security principles must be implemented at each tier in order to realize a secure IoT. It can only be ensured that the IoT framework's future security issues are addressed and resolved. For the security problems specific to IoT layers and devices, many researchers have worked to develop suitable countermeasures. This article gives a general overview of security ideas, technological issues, and security risks. It also offers potential fixes and a look at the future of IoT security.

Keywords—Internet of things; IoT; Security, Attacks, connectivity.

I. INTRODUCTION

The Internet of Things (IoT) idea entails expanding Internet connectivity to a variety of gadgets and common objects in addition to traditional devices like desktop and laptop computers, smartphones, and tablets. Offering enhanced device, system, and service connectivity that extends beyond machine-to-machine communications and encompasses a range of protocols, domains, and applications is the ultimate goal of the Internet of Things. IoT has quickly expanded to play a significant role in how

people live, interact, and conduct business. Web-enabled devices are transforming our universal rights into a larger switched-on space to live in all over the world. Transportation, agriculture, healthcare, and the production and distribution of energy are just a few of the IoT's many application fields. IoT devices employ an identity management tactic to set themselves apart from a collection of connected but disparate devices. With the Internet of Things, an IP address can also define a region, although each entity within a region has a distinct address.

By enabling the intelligent gadgets all around us to perform routine tasks, IoT aims to fundamentally alter the way we live today. The words that are used in relation to IoT include "smart" homes, "smart cities," "smart infrastructure," etc. IoT applications can be found in a wide variety of environments, from private homes to commercial buildings [1]. The consequences of IoT security breaches can be highly damaging. This is because the Internet of Things affects both virtual and physical systems. IoT users can engage with their surroundings thanks to applications in the personal and social domain, and human users can uphold and develop social connections. IoT is being used in the transportation sector to provide safe and convenient transportation options through a variety of smart vehicles, smart infrastructure, and smart traffic signals. The technologies of Radio Frequency Identification (RFID) and Wireless Sensor Networks have allowed IoT applications to advance quickly in recent years (WSN).

The remainder of this article is structured as follows. The three-layer IoT architecture is described in Section II. The security concerns related to various security tenets and the characteristics of IoT devices are described in Section III. The section also discusses the security concerns related to each IoT tier. The research that has recently been done to try and find solutions to the IoT security problems is covered in Section IV. The overview of all the IoT work that has been studied is provided in Section V.



DE GRUYTER

Palak
Book Chapter

Requires Authentication Published by De Gruyter 2022

Decision tree-based improved software fault prediction: a computational intelligence approach

From the book Computational Intelligence in Software Modeling

Palak and Preeti Gulia

<https://doi.org/10.1515/9783110709247-011>

Abstract

Software plays a significant role in our daily lives. The use of smart real-time devices has increased dramatically in the recent decade, necessitating the creation of fault-tolerant, high-reliability software. The basic goal of dependable and robust software is to reduce the quantity of failures that occur when a program is executed. Software fault prediction is a key activity for increasing quality assurance efficiency, economy, and precision. Fault prediction is critical for identifying software components that are prone to flaws. The majority of previous software fault prediction research has concentrated on categorizing software modules whether they are faulty or not. The most important criterion for developing an effective fault prediction model is to identify a dependable fault prediction technique. Due to some inherent constraints, manual techniques of forecasting and finding defects in complex systems may not guarantee a fault-free system, and they are generally time intensive. Computational intelligence (CI) techniques provide promising approaches for solving such problems. In this chapter, we investigate the applications of CI in optimizing various phases of software development. Further, the application of decision tree regression (DTR) for improving fault percentage prediction in different scenarios is the main contribution of this chapter. Two datasets of different sizes from PROMISE repository are extracted and used for performance analysis of the proposed model. The results reveal that DTR generated significant prediction accuracy in intra-release projects.

© 2022 Walter de Gruyter GmbH, Berlin/Boston

Printed by: palak.aug6@gmail.com. Printing is for personal, private use only. No part of this book may be reproduced or transmitted without publisher's prior permission. Violators will be prosecuted.

Communication and Computing Systems - Prasad et al. (eds)
© 2019 Taylor & Francis Group, London, ISBN 978-0-367-00147-6

ACO and GA based test suite reduction for component based software: A hybrid approach

Palak & Preeti Gulia

Department of Computer Science and Applications, MDU, Rohtak, India

ABSTRACT: The quality of a software application depends on the effectiveness of the testing carried out during development and maintenance phase. Testing is a crucial but time consuming activity that influences the overall cost of software development. Thus a minimal but efficient test suite selection is the need of the hour. This paper presents a hybrid technique based on ACO (Ant Colony Optimization) and GA (Genetic Algorithm) for selection of promising test cases to reduce the overall development cost and time of the application. We took component based software into consideration as they offer some inherent advantages over traditional software development paradigms.

KEYWORDS: Ant Colony Optimization, Genetic Algorithm, Test Case selection, Components

1 INTRODUCTION

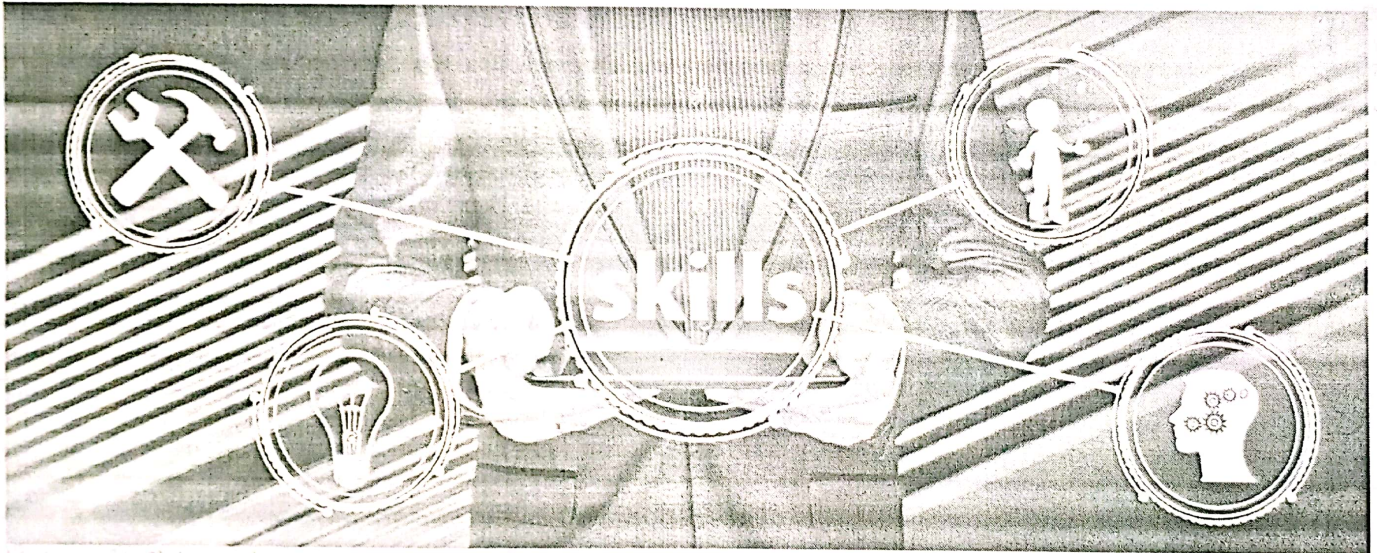
The hardware and software industries are growing together at very fast pace to meet the growing need of smart devices. The smart gadgets have invaded our lives so badly that we can't predict our future without them. The software embedded with these devices play a crucial role to provide best known user experiences to provide the intended functionality. This scenario raises many challenges in front of the software developers to fulfill the quality needs of the end user. Software testing is a crucial and unavoidable step to achieve the same. The role of test cases in the process of testing is very important to verify the functionality and detect faults. A software failure can claim many lives in case of critical systems. Moreover the development paradigms have evolved a long way from traditional procedural approach to a modular component based approach. Component based software engineering (CBSE) (Szyperski, 2002) evolved back in late 1980's and growing since then. It works on the principle of reusability and the software is developed in small chunks called components. Each component has some set of functionality and interacts with other components through interfaces. They provide a black box view of the functionality. Commercial off the shelf (COTS) is gaining popularity with time. Considering the impracticality of the exhaustive testing, it becomes the need of the hour to select a promising suite of test data that is capable of providing higher fault coverage.

Ant Colony Optimization (M. Dorigo et al., 1999) and Genetic Algorithm (Mitchell et al., 1996) are search based techniques that are inspired from nature and natural phenomenon. They are meta-heuristic techniques that are problem independent and can work with incomplete knowledge. In contrast to heuristics, meta-heuristics provide randomness during searching and prevent us to get stuck in local optima. We exploited the advantages of both to develop a hybrid approach that is capable of selecting promising test cases to reduce the size of test suite without compromising with the efficiency and test coverage.

Palak

Book Chapter

New Paradigm in Business & Education



EDITORS

Dr. Deepak Gupta

Ms. Payal Jain



NEW PARADIGM IN BUSINESS AND EDUCATION

EDITORS

Dr. Deepak Gupta

Assistant Professor, Dept. of Commerce
Indra Gandhi University, Meerpur, Rewari, Haryana, India

Payal Jain

Assistant Professor, Dept. of English
Pt. Neki Ram Sharma Govt. College, Rohtak, Haryana, India

ISBN No: 978-81-944303-8-4



Published By:
National Press Associates, New Delhi
www.npapublishing.in

ROLE OF BLOCKCHAIN IN EDUCATION SECTOR

Preeti Gulia, Ayushi Chahal, Palak

Dept. of Computer Science & Applications, Maharshi Dayanand University, Rohtak

Abstract

Blockchain is an emerging technology, which is upgrading day by day. It is a digital platform which is disrupting every market. Blockchain is a digital platform which provides a crypto-currency named Bitcoin. Bitcoin is a most famous application of blockchain, which is the most well-known virtual currency world-wide. But now, Blockchain does not only support the financial sector, it also has deepened its roots in other industries also like healthcare, smart-cities, education etc. Blockchain in the education sector is still very new and unexplored in different areas. Blockchain has considerable amount of potential to completely change conventional education system by providing every facility online. This study discusses different features of Blockchain like trust, data sharing, security, decentralized etc. Blockchain provides decentralized domain, which helps in removing third party involvement in any sort of communication or transaction. This paper presents potential uses for Blockchain technology in the education sector. Blockchain and education system unification could set a very promising trend. Because of its major feature "security", it helps in improving the online education system, by securing the personal data/information of academicians, students, developers, content producers and other employees of education system. In COVID-19 pandemic, only that sector can show their presence to the world which can work online by maintaining social distance. And hence, online education system is widely adopted by students as well as different educational institutes. Online education has become the backbone of education sector which helps it running in this difficult time also. Different application of Blockchain in education system like certification, securing sensitive data, helping in verifying fraudulent degrees etc. are presented in this paper. Blockchain helps in building innovative learning ecosystem for learners which fills the gap in credentialing, copyright protection, and efficient communication.

Keywords: Blockchain, Education technology, healthcare, finance, protection, security.

INTRODUCTION

Blockchain is just a "chain" of "blocks". Here Block is referred as digital information and chain represents public database. So, blockchain is digital information which is stored in a public database.. Blockchain is used to create and store these cryptocurrency electronically using encryption technique.[1]

In blockchain Blocks are made up of three type of information[12]:

Block stores the information like date, time and cost of the transaction.

Block stores information of "who" have participated in the transaction.

Block stores information about their own identities. They store unique hash function which helps in distinguishing between them.

Experiments for blockchain were started on early 1990's but it was introduced in 2008. Blockchain has gained the fame through bitcoin technology. Bitcoin is a cryptocurrency which have existence due to blockchain technology. One can divide Blockchain history in three generation: [6]

First generation: Digital currencies

First existence of Blockchain was as bitcoin. A white paper was released by the name Satoshi Nakamoto from which blockchain gained its popularity. And first well known blockchain is Bitcoin. [2]

Second generation: Smart Contracts

Effect of crystal structure of chemically grown zinc oxide thin film on optical properties

Cite as: AIP Conference Proceedings 2142, 080016 (2019); <https://doi.org/10.1063/1.5122444>
Published Online: 29 August 2019

Pooja Rana, Jyoti Gaur, Arindam Ghosh, Sanjay, and V. Singh



View Online



Export Citation

AIP | Conference Proceedings

Get **30% off** all
print proceedings!

Enter Promotion Code **PDF30** at checkout



Effect of crystal structure of chemically grown Zinc Oxide thin film on optical properties

Pooja Rana^a, Jyoti Gaur^a, Arindam Ghosh^{a*}, Sanjay^a, V. Singh^b

^aDepartment of Physics, GDC Memorial College Bahal, Bhiwani, Haryana

^bDepartment of Physics, RPS Degree College, Mahendergarh-123029, Haryana, India

*Corresponding author: arindamghosh211983@gmail.com.

Abstract: Amongst various metal oxides, Zinc Oxide (ZnO) draws the attention of the scientific community for its various types of properties. For this study purpose, ZnO thin films were prepared by Modified Chemical Bath Deposition (MCBD) technique. To remove out the formation of excessive hydroxide, the bath temperature was maintained at 80°C. There was no change in crystallinity in case of pristine sample. As the annealing temperature increased, the crystallinity goes on improving and then after decreased as it was depicted in the structural morphologies and the variation in the optical properties were also in good correlation with the structural morphologies.

INTRODUCTION

Zinc oxide (ZnO) is a remarkable multifunctional II-VI semiconductor with a unique set of properties. It is a suitable for application a wide range of emerging domains such as solid state lighting, nanotechnology, transparent electronics and Spintronics[1]. Nan crystalline zinc oxide has a wide range of devices such as high power transparent thin film transistors, optical wave guide, conductive gas sensor and transparent electrode for photo electrochemical application. It is a large band gap ($E_g = 3.3\text{eV}$), n-type semiconductor that possesses optical properties which render it importance industrially as a phosphor in a field of emissive displays, cathodoluminescent devices, etc[2]. The properties of ZnO strongly depend on their dimensions and morphologies. Due to the multipurpose use of ZnO a number of research groups have deposited the ZnO thin films by various methods, such as molecular beam epitaxy, chemical vapour deposition, radio frequency magnetron sputtering, chemical bath deposition, spray pyrolysis, successive ionic layer adsorption and reaction (SILAR), etc[3].

Looking forward for the wide application of ZnO, we tried to deposit ZnO thin films using simple and economical Modified chemical bath deposition (MCBD) technique at room temperature. The effect of various annealing temperatures on the physical properties have been studied and discussed.

EXPERIMENTAL DETAILS

Substrate cleaning: Amorphous glass Micro slides, supplied by blue star were cleaned by labolene detergent, than washed by tap water, followed by chromic acid for about 15 minutes. After that the slides were washed by double distilled water and dried well in dust free area.

Preparation of thin films: ZnO thin films were synthesized by Successive Ionic Layer Adsorption and Reaction (SILAR) technique. Zinc sulphate and hydrogen peroxide (LR grade) were used in the deposition of ZnO thin films. The cationic precursor for ZnO was 0.1 M ZnSO_4 with pH nearly 11, the source of O^{2-} ions was H_2O_2 . Trietanolamine (TEA) of GR grade was used as the complexing agent in the cationic precursor solution. For the

deposition of ZnO thin films, the cleaned substrates were immersed in cationic precursor (ZnSO₄) solution for about 10 sec where the Zinc ions were absorbed on the substrates. Then the substrates were rinsed in deionized water for about 20 sec. Thereafter, the substrates were immersed in the anionic precursor solution (H₂O₂) for 10 sec, the oxygen ions reacted with the adsorbed Zn²⁺ ions on the substrates. Lastly, the substrates were immersed in deionized water for 20 sec to remove the loosely bounded ions. This completes, one SILAR cycle for deposition of ZnO thin films. After 25 SILAR cycles, we obtained ZnO thin films of about 0.38 μm terminal thickness. This experimental process was carried out at room temperature with unstirred solution. By several trials, we optimized the following preparative parameters tabulated in (Table 1) for ZnO thin films. The as grown films of ZnO were annealed in air at 350° C for 2h to study the annealing effect on structural, optical and electrical properties.

Deposition Condition	Precursor Solution	
	Cationic	Anionic
Concentration	0.1	---
Complexing agent	TEA	---
pH	11	10
Immersion time (sec)	10	10
Rinsing time (sec)	20	20
Number of immersion cycles	25	25
Deposition temperature (°C)	27	27

Characterization techniques: The thickness of the film was measured by a crude-weight difference method using a sensitive micro-balance provided by K-roy instruments. The identifications of the crystal structure was studied by x-ray diffraction (XRD) data, which was carried out by CuKα (1.5405 Å) radiation using Burker(model: D8 Discover) in the scanning range of 200 to 600. The optical characterization of the films was done in the range 350–800 nm with the help of UV–Vis spectrophotometer lambda 25. The electrical resistivity was calculated from the current voltage measurement system named lab equip. the TEP measurement was done by our home made unit. For all these purpose the silver paste was used as the ohmic contact.

RESULT AND DISCUSSION

Structural Studies

Figure.1 shows the Scanning Electron Microscopy (SEM) image which is obtained from the surface of ZnO thin-film grown by Modified Chemical Bath Deposition Technique (MCBD) technique. The first SEM image shows the pristine(as deposited) film and the second image shows the annealed sample at 400°C. This surface morphological study shows the uniform deposition throughout the surface. From first figure, it is clear that, the phase formation started by not fully crystalline. But as the annealing temperature increases, the sample became more crystalline in comparison of the pristine sample. This surface morphological study shows the improvement in crystallinity as the annealing temperature goes on increasing in this case. This type of result was in good agreement with the previously

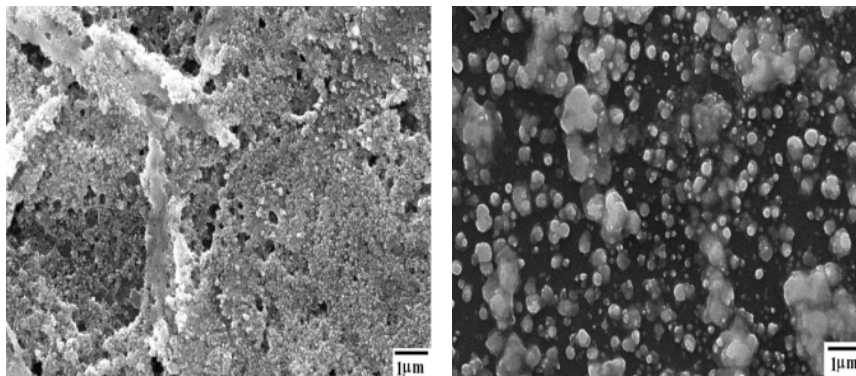


Figure. 1. Scanning Electron Microscopy image of ZnO thin film as-grown and annealed samples

OPTICAL STUDIES

reported data elsewhere [4]. The theory of optical absorption gives the relationship between the adsorption coefficient (α) and the photon energy ($h\nu$) for direct allowed transition as

$$\alpha h\nu = A(h\nu - E_g)^{\frac{1}{2}}$$

Where ' $h\nu$ ' is the photon energy, ' E_g ' is the band gap and ' A ' is constant having separate values for different transition. By extrapolating the linear part of the curve $(\alpha h\nu)^2$ as a function of ' $h\nu$ ', to the energy axis will give the energy band gap [5].

From Fig 2 it is seen that the band gap energy decreases from 3.78eV to 3.67eV with increase in annealing temperature. For as-grown samples, the band gap is higher (3.78eV). It may be due to the presence of zinc hydroxide which might be in amorphous form. But as the annealing temperature increases, the band gap has decreased upto 3.67eV. It may be due to the removal of $Zn(OH)_2$ [6] from the films and/or removal of defect levels from the films [7]. In addition, one can relate the decrease in the bandgap with increase in grain size; which is direct evidence in our

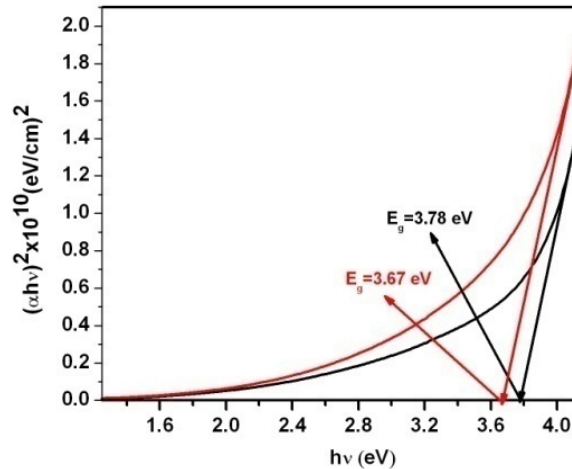


Figure 2. Optical property of the ZnO thin film as-grown and annealed at different temperatures.

CONCLUSION

case. The Zinc Oxide (ZnO) thin films were deposited easily on the amorphous glass substrates using the low cost MCBT technique. For getting good quality thin films, the films were annealed at different temperatures. The improvement in crystallinity was observed in the SEM images which is in well agreement with the structural analysis. Optical absorption study revealed direct band gap nature with band gap energy in the range 3.78 eV to 3.67 eV depending on the annealing temperature. Finally it is concluded that post deposition treatment like annealing helps in improving the physical properties. In addition, it is important to note down that a specific annealing temperature (in our case 4500C) is sufficient to get the improved properties of ZnO thin films for device grade applications.

ACKNOWLEDGMENTS

The author is truly grateful to the Principal, faculty members of science dept. G.D.C. Memorial College, Bahal-127028. I am very thankful to Dr. Arindam Ghosh and Dr. Sanjay Gaur for their persistent support and guidance throughout this work. I am very thankful to UGC-CSR and Dr. B.A.M. University for providing the structural and optical facilities.

REFERENCES

1. Newton M C and Warburton P A *Materials Today* **10** 50(2007).
2. M. Cooke, *Semicond, Today* **2**,37 (2007).
3. A. Ennaoui, M. Weber, R. Scheer, H.J. Lewerenz, *Sol. Energy Mater. Sol. Cells* **54**, 277-286 (1992).
4. A. Ghosh, N.G. Deshpande, Y.G. Gudage, R.A. Joshi, A.A. Sagade, D.M. Phase, Ramphal Sharma, *Journal of Alloys and Compounds* **469**, 56–60(2009)
5. Arindam Ghosh , Ramphal Sharma, Anil Ghule , Vidya S. Taur , Rajesh A. Joshi, Dipalee J. Desale, Yuvraj G. Gudage , K.M. Jadhav, Sung-Hwan Han *Sensors and Actuators B* **146**, 69-74(2010).
6. M.L. de la Olvera, A. Maldonado, R. Asomoza, M. Melendez-Lira, *Sol. Energy Mater. Sol. Cells* **71**, 61 (2002).
7. G. Hodes, A.A. Yaro, F. Decker, P. Motisuke, *Phys. Rev. B* **36**, 4215 (1987).

Effect of annealing on the structural and opto-electrical properties of as-grown ZnO thin films by successive ionic layer adsorption and reaction (SILAR) technique

Cite as: AIP Conference Proceedings 2142, 030009 (2019); <https://doi.org/10.1063/1.5122337>
Published Online: 29 August 2019

Kiran, Poonam, Arindam Ghosh, Sanjay, and Vijender Singh



View Online



Export Citation

AIP | Conference Proceedings

Get **30% off** all
print proceedings!

Enter Promotion Code **PDF30** at checkout



Effect of Annealing on the Structural and Opto-electrical Properties of As-grown ZnO Thin Films by Successive Ionic Layer Adsorption and Reaction (SILAR) Technique

Kiran¹, Poonam¹, Arindam Ghosh^{1, a)}, Sanjay¹, Vijender Singh²

¹*Department of Physics, GDC Memorial College Bahal, Bhiwani (Haryana) India*

²*Department of Physics, RPS Degree College, Mahendergarh (Haryana) India*

^aCorresponding author: arindamghosh211983@gmail.com

Abstract: The Zinc oxide thin films were grown on the amorphous glass substrate using Successive Ionic Layer Adsorption and Reaction (SILAR) technique at room temperature. The various preparative parameters were optimized to obtain good quality films. The as-grown films were annealed at 350° C for 2 h in air. The comparative study of the annealed and the as-grown thin films of ZnO were done for structural, optical and electrical studies. Polycrystalline nature was depicted from the x-ray diffraction (XRD) patterns. The peak intensity of as-grown ZnO thin films enhances after annealing. The average grain size calculated from XRD patterns was 17.66 nm for as-grown, while it increased to 24.66 nm after annealing. The band gap of as-grown ZnO thin films was relatively higher and was found to be 3.80 eV. After air annealing, the band gap decrease to 3.58 eV. The current-voltage characteristics show nearly ohmic behavior with decrease in the film resistance, after annealing in air. N-type conductivity was confirmed from the TEP measurements.

INTRODUCTION

In today's modern physics, the one dimensional (1D) semiconductor structures i.e. nano wires, nano rods, nano tubes etc have attracted their attention due to their unique properties like electronic, magnetic, mechanical, electrical and chemical Properties [1]. Due to the vigorous development of interest in Zinc oxide thin films and the extensive utilization, it became a versatile technologically important material. Such as transparency in the visible range, high electrochemical stability etc. This n-type semiconducting material with a wide band gap (3.37eV) is applicable in various fields, such as solar cells, gas sensors [2], liquid crystal display, heat mirrors. Likewise it can be used in various potential applications such as low voltage and short wavelength optoelectronic devices such as LED and laser diodes. Besides these, this material is of great importance in industrial field as a phosphor in field of emissive displays [3, 4], as cathodoluminescent devices [5], or as the grain medium in UV semiconductor lasers [6]. Due to these great number of applications a number of researchers are working on this transparent semiconducting material (ZnO). They have deposited this film by molecular beam epitaxy (MBE) [7], rf sputtering [8], magnetron sputtering [9], pulsed laser deposition (PLD) [10,11], spray pyrolysis [12], arc plasma evaporation [13], chemical bath deposition [14,16] etc. Due to the significant role of ZnO in optical devices such as short wavelength laser, it is of fundamental interest to understand how air annealing effect the structural, optical and electrical properties of this material.

In the present investigation, we have used simple and economical Successive Ionic Layer Adsorption and Reaction (SILAR) technique to grow thin films of ZnO. This method was employed because of the advantage that wastage due to bulk precipitations in solution can be avoided. This phenomenon is commonly observed in chemical bath deposition technique. In this SILAR technique, thin films can be obtained by immersion of substrates into separately placed cationic and anionic precursor solutions and rinsing between every immersion with ion exchange water.

EXPERIMENTAL DETAILS

Substrate cleaning: Amorphous glass Micro slides, supplied by blue star were cleaned by labolene detergent, than washed by tap water, followed by chromic acid for about 15 minutes. After that the slides were washed by double distilled water and dried well in dust free area.

Preparation of thin films: ZnO thin films were synthesized by Successive Ionic Layer Adsorption and Reaction (SILAR) technique. Zinc sulphate and hydrogen peroxide (LR grade) were used in the deposition of ZnO thin films. The cationic precursor for ZnO was 0.1 M ZnSO_4 with pH nearly 11, the source of O^{2-} ions was H_2O_2 . Trietanolamine (TEA) of GR grade was used as the complexing agent in the cationic precursor solution. For the deposition of ZnO thin films, the cleaned substrates were immersed in cationic precursor (ZnSO_4) solution for about 10 sec where the Zinc ions were adsorbed on the substrates. Then the substrates were rinsed in deionized water for about 20 sec. Thereafter, the substrates were immersed in the anionic precursor solution (H_2O_2) for 10 sec, the oxygen ions reacted with the adsorbed Zn^{2+} ions on the substrates. Lastly, the substrates were immersed in deionized water for 20 sec to remove the loosely bounded ions. This completes, one SILAR cycle for deposition of ZnO thin films. After 25 SILAR cycles, we obtained ZnO thin films of about 0.38 μm terminal thickness. This experimental process was carried out at room temperature with unstirred solution. By several trials, we optimized the following preparative parameters tabulated in (Table 1) for ZnO thin films. The as grown films of ZnO were annealed in air at 350° C for 2h to study the annealing effect on structural, optical and electrical properties.

Table 1: Optimized Parameters for preparation of ZnO thin films

Deposition Condition	Precursor Solution	
	Cationic	Anionic
Concentration (M)	0.1	----
Complexing agent	TEA	----
pH	11	----
Immersion time (sec)	10	10
Rinsing Time (Sec.)	20	20
Number of immersion Cycles	25	25
Deposition temperature (°C)	27	27

Characterization techniques: The thickness of the film was measured by a crude-weight difference method using a sensitive micro-balance provided by K-roy instruments. The identifications of the crystal structure was studied by x-ray diffraction (XRD) data, which was carried out by $\text{CuK}\alpha$ (1.5405 Å) radiation using Burker(model: D8 Discover) in the scanning range of 200 to 600. The optical characterization of the films was done in the range 350–800 nm with the help of UV–Vis spectrophotometer lambda 25. The electrical resistivity was calculated from the current voltage measurement system named lab equip. the TEP measurement was done by our home made unit. For all these purpose the silver paste was used as the ohmic contact.

RESULT AND DISCUSSION

XRD studies: Figure.1 represents the comparative study of the XRD pattern of the as grown and annealed ZnO thin films grown by the SILAR method. The crystal structure of the ZnO thin film was found to be hexagonal (JCPDS card no- 80-0075). From the spectrum it was clear that the thin films of ZnO are highly oriented along (100) at $2\theta=31.7540$ for as grown and 31.7810 for annealed thin films. Other peaks were observed along (002), (101), (110) etc for the as grown and annealed thin films.

While the formation of ZnO thin films, $\text{Zn}(\text{OH})_2$ might have been also formed, since the source solutions were dissolved in distilled water. However, $\text{Zn}(\text{OH})_2$ was not detected in the XRD patterns. This might be due to the fact that the $\text{Zn}(\text{OH})_2$ was present in small extent gets accumulated along the grain boundaries of the crystallites constituting the film or $\text{Zn}(\text{OH})_2$ might be present in amorphous form. However, the peak intensity of the ZnO thin films (mainly along the 100 orientation) increased after air annealing in 350°C for about 2h. This increase in peak intensity implies that the film quality is improved after air annealing. The temperature dependence of the films in

terms of quality could be explained by the mobility of the particle with low temperature. At low temperatures, the particles with low mobility will be located at different position within the substrates. The low mobility of the particles will prevent the formation of well crystallized thin films [17], (Table 3 strengthen this statement.) It was also observed that the peak position gets shift to some extent, which also signifies the decrease in the lattice constant due to the annealing effect. The grain size was calculated using the Scherrer's formula, and is given in (Table 2).

$$D = \frac{K\lambda}{\beta \cos\theta} \quad (1)$$

where, 'D' is crystallite size, ' λ ' is the X-ray wavelength used, ' β ' is the angular line width of half maximum intensity, ' θ ' is Bragg's diffraction angle and 'K' is some constant, which is 0.9. From this calculation it is observed that the grain size has increased after annealing. The increase in grain size could be equally confirmed from the enhancement of the peak intensity.

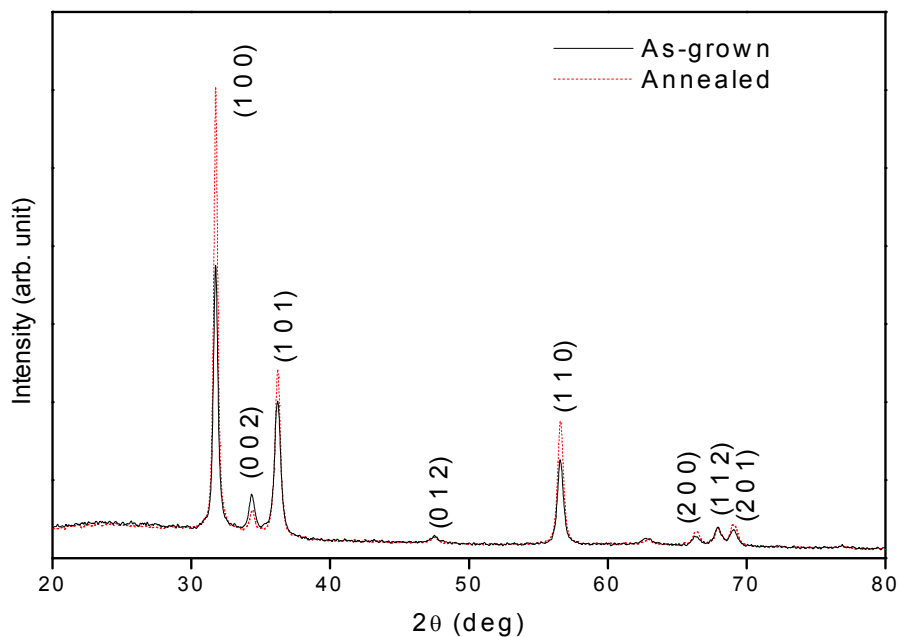


Figure 1: XRD of the as grown and annealed ZnO thin films

Table 2: Comparative study of XRD of as grown and annealed ZnO thin films

Type	d_{st} (Å)	d_{ob} (Å)	hkl	a Å	c Å	Grain size (nm)	Avg Grain size (nm)
As deposited	2.8179	2.8155	100	3.2508	5.222	18	17.66
	2.4785	2.4771	101			17	
	1.6269	1.6248	110			18	
Annealed	2.8179	2.8132	100	3.2490	5.2144	28	24.66
	2.4785	2.4842	101			24	
	1.6269	1.6234	110			22	

Optical Studies

Figure 2 (a) shows the plot of absorbance (αt) versus the wavelength (nm) for as grown and the annealed ZnO thin films. From the spectrum, it is clear that ZnO thin films have low absorbance in the visible region which is one of the characteristics of ZnO. The sharp absorption edges were observed in both the films. Hence one can conclude that the ZnO thin films deposited on glass substrates, prepared by SILAR technique are of high optical quality. The oscillations that are seen in the absorption spectra are originated from the interferences of the lights that refracted from the source of the thin film and the interface.

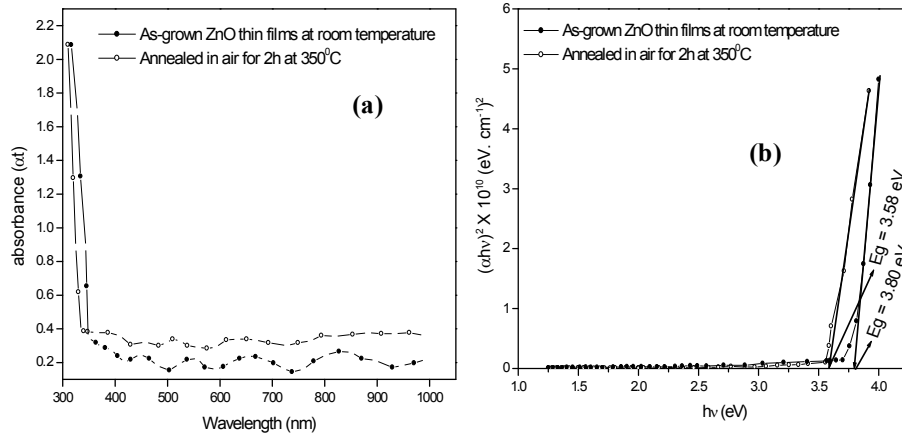


Figure 2: (a) Plot of absorbance versus wavelength and (b) plots of $(\alpha h\nu)^2 \times 10^{10} \text{ (eV.cm}^{-1}\text{)}^2$ versus

The data were analyzed from the following classical relation between absorption coefficient (α) and the photon energy ($h\nu$) can be expressed as,

$$\alpha = (h\nu - E_g)^{1/2} / h\nu \quad (2)$$

In this case the ' $h\nu$ ' is the energy of photon and ' E_g ' is the energy band gap. Figure 2 (b) shows the plot of $(\alpha h\nu)^2$ against ($h\nu$). The energy band gap was obtained by extrapolating the linear part of the curves $(\alpha h\nu)^2$ as a function of $h\nu$ of the incident radiation to intercept the energy axis. From this figure, it is clear that the ' E_g ' for as grown and annealed films was 3.8 eV and 3.58 eV, respectively. This type of high band gap in case of as grown films may be due to the presence of zinc hydroxide. The decrease in band gap energy is due to the increase in the grain size (which was obtained from the XRD) due to annealing. The removal of Zn(OH)_2 [18] or removal of defects may be the other reasons. The ' E_g ' was decreased after annealing was also reported earlier by Jimenez-Gonzalez and Nair [19]. According to the XRD study, the crystallinity of the as grown ZnO thin films is lower than that of the annealed films. Due to the low crystallinity and presence of amorphous Zn(OH)_2 the localization increased in between the conduction and valance band. As a result the as deposited films have comparatively higher band gap as compared to the annealed films. In our XRD study the lattice constants have decreased after annealing. The smaller the lattice constants, the smaller the band gap. The same types of reports have been reported earlier by another research group [20].

Electrical

Current Voltage Characteristics: Figure 3 (a), shows the plot of current (I) versus voltage (V) of the as grown and annealed ZnO thin films. In this case there is a linear dependence of the current on the voltage confirming the ohmic behavior of the contacts. The resistance was calculated by taking the inverse of the slope of the as grown and annealed samples. The resistance was decreased after the annealing effect. It was reported earlier that the resistance may increase due to the decrease in grain size [21]. But in our case the grain size increases (XRD study) after annealing. So the resistance is decreasing.

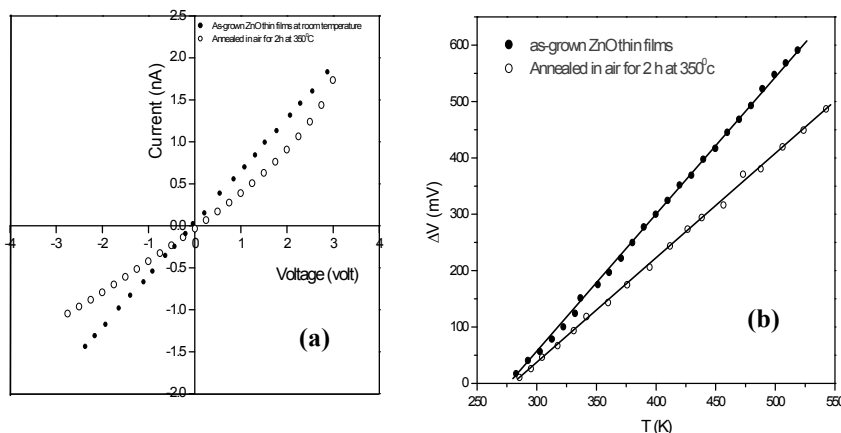


Figure 3: Plot of current versus voltage characteristics of the as grown and annealed ZnO thin films, Plot of ΔV versus ΔT of the as grown and annealed ZnO thin films deposited by SILAR technique.

Table 3: Comparative study of resistivity and TEP measurements of as grown and annealed ZnO thin films

Types of Sample	Resistance (10^9) Ω	Resistivity (10^5) Ω	Conductivity (10^{-5}) Ω cm ⁻¹	Electron density (10^{19}) cm ⁻³	Mobility (10^{-5}) (cm ⁻² V ⁻¹ s ⁻¹)
As grown	2.2	0.919	1.08	2.64	0.25
Annealed	1.6	0.66	1.515	2.66	0.35

Figure 3 (b), shows the plot of ΔV vs ΔT for the as grown and annealed ZnO thin films. From this study we can determine carrier concentration (n), mobility (μ). From the figure, it is clear that ΔV increases with the temperature. In this TEP measurement, it is observed that polarity of thermally generated voltage at the hot end is positive which indicates these films are of n-type.

The electron density can be calculated with the help of the following relation [22],

$$\log n = 3/2 \log T - 0.005TEP + 15.719 \quad (3)$$

The mobility (μ) can also be determined with the help of the following relation,

$$\mu = \sigma / ne \quad (4)$$

The results are tabulated in Table 3. It was seen that the conductivity increases with annealing, as a result mobility also increases. Another explanation might be due to increase in crystallinity, grain size of the annealed ZnO thin films (which is quite well supported by I-V measurements and XRD studies).

CONCLUSION

Almost transparent ZnO thin films were successfully deposited using Successive Ionic Layer Adsorption and Reaction (SILAR) technique at room temperature. From XRD studies it is clear that ZnO is of polycrystalline in nature and it exhibit excellent crystallinity structure with (100) orientation. After heat treatment the peaks were increased. The grain size lies between 17 nm (as grown) to 24 nm (annealed). From optical studies, it is clear that it has low absorbance in the visible region. The energy band gap was found to be 3.8 eV for as grown and 3.58 for annealed samples. From the I-V study its ohmic behavior was seen and its n-type conductivity was confirmed from the TEP measurements.

ACKNOWLEDGEMENT

For this research work, the authors are very much thankful to The Head, of the Department of Physics, G.D.C.Memorial College Bahal for providing us the laboratory facility. At the same time we are also very much thankful to the Director, UGC- DAE Consortium for Scientific Research (CSR), Indore for providing us the characterization of the samples and also for their valuable suggestion during course of our research work.

REFERENCES

1. Y.Cui.,Q.Q.Weï , H.K.Park. and C.M.Liber. *science***293**, 1289 (2001).
2. G.Feng, D.Li,L.Yao, *Vacuum* **68**, 363 (2003).
3. K. Vanheusden ,C.H.Seager,W.L.Warren,D.R.Tallent, J.A.Vight,*J.AppliedPhys***68**, 403(1996).
4. K. Vanheusden, W.L.Warren, C.H.Seager, D.R.Tallent, J.A.Voight, *J.AppliedPhys***79**,7983 (1996).
5. S.Bachir,C.Sandouly,J.Kossanyi,J.C.Ronfard-Harte,*JPhys.Chem.Solids***57**, 1869-79(1996).
6. .L.N.Kurbatov,G.S.Kozina,V.A.Kuznetsov,I.P.Kuzmina,A.A.Shternberg,*KvantovayaElektronika,Moskra***7**, 378-82 (1980).
7. T.Ohgaki,N.Ohashi,H.Kakemoto,S.Wada,Y.Adachi,H.Haneda and .Tsurumi,*J.Appl.Phys***93**, 1961 (2003).
8. .M.Kumar,R.M.Mehra,A.Wakahara,M.Ishida and A.Yoshida, *J.Appl. Phys***93**,3837 (2003).
9. M.Chen,Z.L.Pei,C.Sun and S.Wen,*J.Vac.Sci.Technol.A***19**, 963(2001).
10. V.Cracium,S.Amirhaghi,D.Cracium,J.Elders,J.G.E.Gardeniers and I.W.BFoyd.*Appl.Surf.Sci.***86**, 99 (1995).
11. S.Choopun,R.D.VCispute,W.Noeh,A.Balsamo,R.P.Sharma,T.Venkatesan,A.Iliadis and D.C.Look *Appl.Phys.:Leyy***75**, 3947(1999).
12. A.E.Manouni, F.J.Manjon,M.Mollar,B.Mari,R.Gomez,M.C.Lopez and J.R.Ramos- Barrado,*Superlattice Microstruct.***39**185 (2006).
13. T.Miyata,Y.Minamino,S.Ida and T.Minami,*J.Vac.Sci.Technol. A* **22**,1711 (2004).
14. A.Ennaoui,M.Weber,R.Scher,H.J.Lewerenz,*Sol.EnergyMatter.Sol cells* **54**, 277(1998).
15. M.Ortega-Lopez,A.Avila-Gaccia,M.L.Albor-Aguitera,V.M.Sanchez Resendiz,*Matter.Res.Bull.***38**, 1241(2003).
16. V.R.Shinde,C.D.Lokhande,R.S.Mane,Sung-Hwan Han,*Applied Surface Science* **245**, 407-413(2005).
17. .K.Shan,G.X.Liu,W.J.Lee,B.C.Shin,*J.Appl. Phys.* **101**, 053106(2007).
18. M.L.de la olvera , A.Maldonado,R.Asomoza,A.Melendez-Lira*Sol.Cells.***71**, 61(2002).
19. A.E.Jimenez-Gonzalez,P.K.Nair,*Semcond.Sci.Technol* 10 (1995)1277
20. S.T.L.Tain,B.J.Chen,X.W.Sun,W.J.Fan,H.S.Kwok,X.H.Zang,S.J.Chua, *J.Appl.Phys* 98 (2005) 013505
21. .P.M.Ratheesh,C.SudhaKartha, K.P.Vijaykumar, F.Singh, D.K.Avasthi, T.Abe, Y.Kashiwaba, G.S.Okram,M.Kumar, Sarvesh Kumar *J.Appl.Phys.* 97 (2005) 013509
22. J.S.Curran, R.Phillippe,Proceedings of 14th Internatiopnal Conference on Solar Energy,Stresa.Italy,10-14 May (1982)

Structural and optical properties chemically grown zinc oxide thin film

Cite as: AIP Conference Proceedings 2142, 140034 (2019); <https://doi.org/10.1063/1.5122547>
Published Online: 29 August 2019

Pooja, Krishma, Jyoti Gupta, Arindam Ghosh, Sanjay, and V. Singh



View Online



Export Citation

AIP | Conference Proceedings

Get **30% off** all
print proceedings!

Enter Promotion Code **PDF30** at checkout



AIP
Publishing

Structural and optical properties chemically grown Zinc Oxide thin film

Pooja¹, Krishma¹, Jyoti Gupta¹, Arindam Ghosh^{1a}, Sanjay¹, V. Singh²

¹*Department of Physics, GDC Memorial College Bahal, Bhiwani, Haryana*

²*Department of Physics, RPS Degree College, Mahendergarh-123029, Haryana, India*

^aCorresponding author: arindamghosh211983@gmail.com

Abstract. Amongst various metal oxides, Zinc Oxide (ZnO) is widely used semiconducting material amongst various II-VI group materials due to its various properties like wide energy band gap (3.3 eV), strong binding energy of 60 meV, higher transparency, low electron affinity sensitivity and selectivity for device grade applications. For this study purpose, for this study purpose (ZnO) thin films have been deposited by Successive Ionic Layer Adsorption and Reaction (SILAR) technique on amorphous glass substrate at room temperature. These films were then annealed for about 2 hours in air atmosphere. The structural studies reveal the increase in grain size upto 400°C. The change in crystallite size were observed in the Atomic Force Microscopy (AFM) images. The optical studies were also in well agreement with the structural analysis.

INTRODUCTION

Zinc Oxide (ZnO) is an inorganic compound with the formula ZnO. ZnO is its different forms with unique properties, such as, direct band gap (3.3eV) high exciton binding energy (60meV)[1] and good resistivity is one amongst the widely explored functional metal oxide semiconductor[2]. The properties of ZnO strongly depend on their dimensions and morphologies. ZnO is a white powder that is insoluble in water, and it is widely used as an additive in numerous materials and products including rubbers, plastics, glass, cement, ointments, batteries, first-aid tapes etc. Although it occurs naturally as the mineral zincite, most zinc oxide is produced synthetically[3]. ZnO is a wide-band gap semiconductor of the II-VI semiconductor group. The native doping of the semiconductor due to oxygen vacancies or zinc interstitials in n-type[4]. This semiconductor has several favorable properties, including good transparency, high electron mobility, wide band gap and strong room temperature luminescence. The properties of ZnO strongly depend on their dimensions and morphologies. Due to the multipurpose use of ZnO a number of research groups have deposited the ZnO thin films by various methods, such as molecules beam epitaxy, chemical vapour deposition, radio frequency magnetron sputtering, chemical bath deposition, spray pyrolysis, successive ionic layer adsorption and reaction (SILAR) etc[5]. ZnO is a semiconducting material having piezoelectric properties, has important application in sensors, optoelectronics, transducers and biomedical applications. ZnO has a number of morphological configuration due to its unique crystal structure. Generally, these physical techniques are labor intensive and costly, requiring sophisticated instrumentation and vacuum system. On the other hand, wet chemical technique are simple and cost effective and thus have become the methods of choice. Amongst these technique, SILAR is gaining popularity for its simplicity and environmental friendly procedure for obtaining stoichiometric ZnO thin-film. But according to the literature survey, there are very few reports on the synthesis of ZnO nanoparticle thin film at ambient conditions and their application in LPG sensors[6]. Looking forward for the wide application of ZnO, we tried to deposit ZnO thin film using SILAR technique at room temperature. The effect of various annealing temperatures on the physical properties have been studied and discussed.

EXPERIMENTAL DETAILS

The ZnO thin-films were deposited onto the glass substrates using a cost effective technique, i.e. SILAR. In this process, aqueous solution of 0.1M ZnSO₄ was used in as the cationic precursor solution, to which, ammonia solution

was slowly added to adjust the pH to approx. 10. Two to three drops of tri-ethanolamine (TEA) was added to the cationic precursor solution which helps in achieving uniformity of the thin film over the entire substrate. H₂O was used as the anionic precursor solution. The pre-cleaned glass substrates were dipping into the cationic precursor for about 20s. Then the samples were rinsed in de-ionised water for about 40 sec for getting the uniform layer of cations get adsorbed onto the glass substrate. These films were dipped into the anionic precursor for about 20 sec and again rinsed with de-ionised water for about 40 sec. The thickness of the developed films was found to be approx. 380nm. The film was annealed at 400°C to remove any possible organic contaminates and to minimize the hydroxides to achieve desired purity of ZnO thin films.

Film thickness was measured by gravimetric weight different method using in sensitive microbalance (k-Roy instruments). The morphological image of films were obtained by using Atomic Force Microscopy (AFM). The optical absorption study was performed in the range 300-800nm.

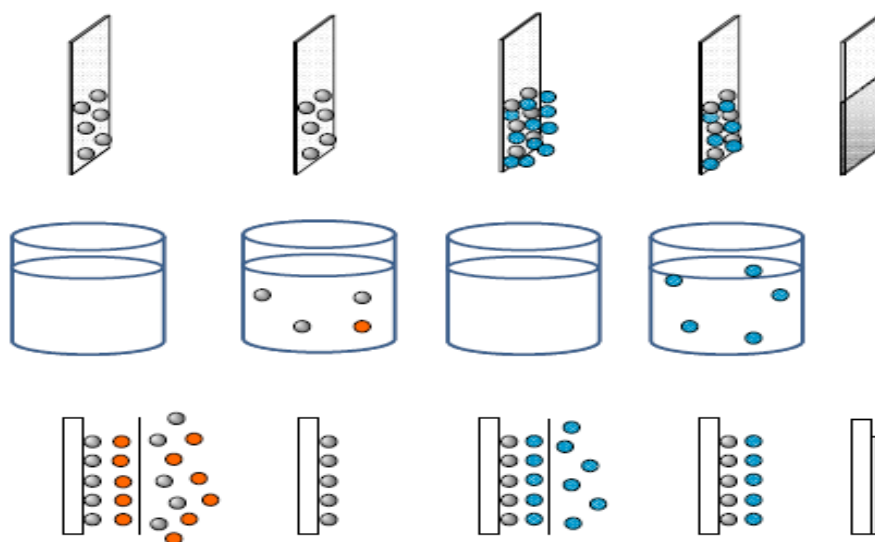


Figure 1: Schematic diagram of Successive Ionic Layer Adsorption and Reaction (SILAR) technique.

RESULT AND DISCUSSION

Structural Studies

Figure.2 shows the Atomic Force Microscope (AFM) image of the Pristine and annealed ZnO thin-film grown by Successive Ionic Layer Adsorption and Reaction(SILAR) technique. The first AFM image shows the pristine(as deposited) film and the second and third image shows the annealed sample at 300°C and 400°C respectively. This study shows the uniform deposition throughout the surface. From these figures, it is also clear that, as the annealing temperature increases, crystallinity of the sample increases.

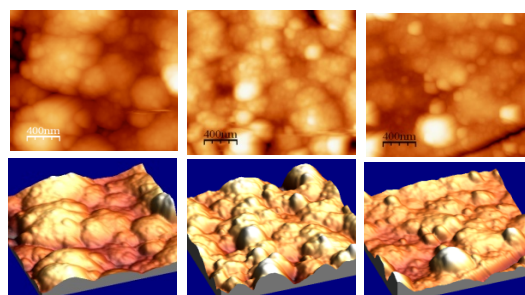


Figure. 2. Atomic Force Microscopy image of ZnO thin film as-grown and annealed samples

OPTICAL STUDIES

The theory of optical absorption gives the relationship between the adsorption coefficient (α) and the photon energy ($h\nu$) for direct allowed transition as

$$\alpha h\nu = A(h\nu - E_g)^{\frac{1}{2}}$$

Where ' $h\nu$ ' is the photon energy, ' E_g ' is the band gap and ' A ' is constant having separate values for different transition. By extrapolating the linear part of the curve $(\alpha h\nu)^2$ as a function of ' $h\nu$ ', to the energy axis will give the energy band gap [7].

From Fig 3 it is seen that the band gap energy decreases from 3.77eV to 3.62eV with increase in annealing temperature. For as-grown samples, the band gap is higher (3.77eV). It may be due to the presence of zinc hydroxide which might be in amorphous form. But as the annealing temperature increases, the band gap has decreased upto 3.62eV. It may be due to the removal of $Zn(OH)_2$ [6] from the films and/or removal of defect levels from the films [7]. In addition, one can relate the decrease in the bandgap with increase in grain size; which is direct evidence in our case.

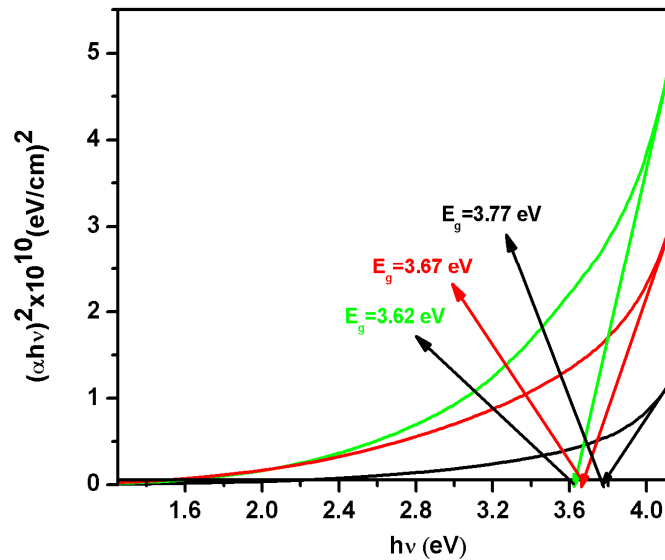


Figure 3. Optical property of the ZnO thin film as-grown and annealed at different temperatures.

CONCLUSION

By using Successive Ionic Layer Adsorption and Reaction (SILAR) technique, the ZnO thin film were deposited on to the glass substrate. The film were annealed at 400°C temp. gives the good quality thin film. The structure is confirmed by the AFM studies. The grain size was also increased from 7.00nm to 18.00nm for as-grown sample (at room temperature) to 400°C. The optical study reveals that the energy band gap of the sample is 3.62ev. Finally it is concluded that annealing treatment helps in improving the physical properties.

ACKNOWLEDGEMENT

The author is truly grateful to the principal, faculty members of science deptt., G. D. C. Memorial College, Bahal. I am very thankful to UGC-CSR and Dr. B.A.M. University for providing the structural and optical facilities.

REFERENCES

1. S.H. Eom, Y.-M. Yu, Y.D. Choi, C.-S. Kim, Optical characterization of ZnO whiskers grown without catalyst by hot wall epitaxy method, *J. Cryst. Growth* **284**, 166–171(2005).
2. U. Ozgur, Y.I. Alivov, C. Liu, A. Teke, M.A. Reshchikov, S. Dogan, V. Avrutin, S.J. Cho, H. Morkoc, A comprehensive review of ZnO materials and devices, *J. Appl. Phys.* **98**, 041301 (2005).
3. De Liedekerke, Marcel (2006) “2.3.Zinc Oxide(Zinc white):Pigments Inorganic,”in Ullmann’s Encyclopedia of Industrial Chem. Wiley-VCH, Weinheim.
4. Ozgur U. ;Alivov, Ya.I.Liu, c.; Teke,A.; Reshchikov, M.A.; Dogan, S.; Avrutin, V.;Cho, S-J.; Morkoc, H.. “A Comprehensive review of ZnO materials and devices”.*Journal of applied physics*. 98(4); 041301-103(2005).
5. A. Ennaoui, M. Weber, R. Scheer, H.J. Lewerenz, *Sol. Energy Mater. Sol. Cells* **54**, 277-286(1992).
6. B.C. Yadav, R. Srivastava, A. Yadav, V. Srivastava, LPG sensing of nanostructured zinc oxide and zinc niobate, *Sensor Lett.* **6**, 714–718 (2008).
7. G. Hodes, A.A. Yaro, F. Decker, P. Motisuke, *Phys. Rev. B* **36**, 4215-4221(1987).

A brief review on effect of grain size on solar energy conversion efficiency of chemically grown Bi_2S_3 thin films

Cite as: AIP Conference Proceedings 2142, 150031 (2019); <https://doi.org/10.1063/1.5122580>

Published Online: 29 August 2019

Poonam, Kiran, Arindam Ghosh, Sanjay, and V. Singh



View Online



Export Citation

AIP | Conference Proceedings

Get **30% off** all
print proceedings!

Enter Promotion Code **PDF30** at checkout



A brief review on effect of grain size on solar energy conversion efficiency of chemically grown Bi₂S₃ thin films

Poonam¹, Kiran¹, Arindam Ghosh^{1a}, Sanjay¹, V. Singh²

¹Department of Physics, GDC Memorial College Bahal, Bhiwani, Haryana

²Department of Physics, RPS Degree College, Mahendergarh-123029, Haryana, India

^aCorresponding author: arindamghosh211983@gmail.com

Abstract. Amongst various semiconductors, Bi₂S₃ is one of the most widely used compounds, used for various types of applications like thermoelectric and optoelectronic applications as well as biological and chemical sensors due to its various types of properties. Bi₂S₃ is a challenging material because of its midway band gap ($E_g=1.74\text{eV}$) and absorption coefficient of the order of 10^4 cm^{-1} . There are a lot of techniques have developed for synthesizing the Bi₂S₃ thin films. Amongst them, Zhehao Zhu et al have revealed that as annealing temperature increases in sulfur vapour atmosphere, the light absorption and charge separation efficiencies enhances by achieving carrier diffusion length that is comparable to the light absorption depth, leading to high solar energy conversion efficiencies in Bi₂S₃. R.S.Mane et al also have reported that, the Photoelectrochemical (PEC) performance of chemically grown Bi₂S₃ is improved with increase in film thickness and grain size.

INTRODUCTION

Solar power a cleanest, new able and amazing source of energy to satisfy the increasing energy demand for the world which taking the attention of researcher toward the Photo electrochemical solar cell for the low cost and acceptable performance. Semiconductor thin films are always important due to their electrical and optical properties which is useful in various optoelectronic devices, among which a non-toxic, n type semiconductor, Bi₂S₃, having its important role having band gap energy nearly 1.7eV in visible solar energy spectrum. There are various methods for the deposition of Bi₂S₃ thin film like CBD (Chemical Bath Deposition), SILAR, spray pyrolysis and electrodeposition etc. Among which SILAR method, also called modified CBD, is a promising, because of newly and less investigated technique because of its simplicity and economics. Some reports says that efficiency of solar cell can be enhance by making the sulfur vapor annealing. Thus promising efficiency leads to makes the interest toward the effective synthesis or processing techniques and to makes study about various material properties. Thus to keep in mind the increase energy demand [1] for the world, some researcher make their study for PEC at low cost and acceptable performance.

Name(Commonly)	Bismuth sulphate (Bi ₂ S ₃)
Colour	Grey to Brown
Appearance	Crystalline Solid
Melting Point	850 °C
Density	6.780 gm / cm ³
Band gap	1.73Ev
Oxidation	Bi(+3) and S(-2)

STUDY ABOUT SYNTHESIS OF Bi_2S_3 THIN FILMS

Recently the synthesis of Bi_2S_3 n-type semiconductor much attention because of their physical and chemical properties and great application in the pigment, solar cell, IR detector, thermo electronic and optoelectronic devices and also because of its band gap lies close to the range of theoretical maximum attainable energy conversion efficiency. There are the various methods for the deposition of thin films such as Electrochemical deposition, Chemical bath deposition [2], vapour deposition, Spray Pyrolysis [3], electrodeposition technique [4] hydrothermal synthesis successive ionic layer adsorption and reaction (SILAR). Because of the facile processing and a lots of application SILAR method is used for the synthesis of Bi_2S_3 into Nano crystalline films. As the poor electric contacts at the semiconductor interface due to the solution deposited film leads to the high resistance, which causes the high concentration of grain boundaries leads to the various defects that could reduce the optoelectronic performance of the material. Some studies reported that the annealing with the sulfur vapour at different temperature to get highly crystalline Bi_2S_3 .

The M-CBD technique is mainly based on adsorption and reaction of the ions from the solutions and rinsing between every immersion with deionized water to avoid homogeneous precipitation in the solution [5] and the preparative parameters are given below were used to prepare Bi_2S_3 thin films were deposited on to FTO coated glass substrate [5].

Parameters	Precursors	
	Cationic (Bismuth nitrate)	Anionic (Thioacetamide)
concentration	0.003M	0.1M
pH	9	9
Immersion time	20sec	20sec
deposition temp	27°C	27°C

During the every process of solution deposition the immersion of Na_2S solution is done for 2 min after 5, 10 or 15 layers of Bi_2S_3 were coated the annealing with sulfur vapour is performed with argon. Temperature used for deposition are 40°C, 445°C and 470°C respectively. For pure argon annealing temperature is 445°C, Annealing pressure – 1 atm, Annealing time - 60 min.

POST DEPOSITION TECHNIQUES

There are various post deposition techniques are available to improve the crystallinity of the required materials. Amongst them, annealing and irradiations with low energy as well as high energy play a significant role in order to improve various types of properties. In accordance to the application point of view, annealing in different atmosphere plays an important role. As to improve the crystallinity and phase purity of solution deposited Bi_2S_3 it is necessary to find the alternate method of annealing among which sulphur vapour annealing is effective one according to Zhehao Zhu et al study. Sulfur vapour annealing, by increasing the crystalline size from 10nm to 50 nm, to improve the crystallinity of the solution deposited Bi_2S_3 Nano crystals. During high temperature annealing, introducing the sulfur vapours, prevents the formation of Bi_2O_3 bulk crystal impurities and leads to phase pure Bi_2S_3 . Sulfur vapour annealing converts the surface oxides of the annealed film to the sulphides which fill in the sulfur vacancies of Unannealed Bi_2S_3 to increase the photo excited carriers lifetimes to get Bi_2S_3 as a promising material for the photovoltaic and the Photoelectrochemical energy conversion applications, sulfur annealed Bi_2S_3 exhibits enhanced light absorption and charge separation efficiency.

PHOTOELECTRICAL ACTIVITY OF Bi_2S_3

The synthesis of well alignment Bi_2S_3 nanowires on the various metal oxides substrates such as TiO_2 , BiVO_4 and ZnO , then it is shown by Mira Park et al that the resulting composite Bi_2S_3 is showed enhanced Photoelectrochemical properties as compared to the sole Bi_2S_3 electrode. This enhancement attributed toward

the charge separation on the Bi_2S_3 layer because of the electron transfer from the Bi_2S_3 conduction band to the that of the metal oxides Some study explained the effect of Na_2S by studying their band tuning properties of $\text{Bi}_2\text{S}_3/\text{TiO}_2$, which says that the in the absence of Na_2S the conduction band of the Bi_2S_3 with large diameter have more positive conduction than the conduction band of TiO_2 which restrict electron injection from Bi_2S_3 to the TiO_2 however in the presence of the Na_2S the this shift is of more negative potential which leads to more negative photocurrent and also the injection of electron increases from Bi_2S_3 to TiO_2 And this alignment of the Na_2S between the $\text{Bi}_2\text{S}_3/\text{TiO}_2$ when the interface of it is exposed to the Na_2S electrolyte which make a direct contact between the interface or the electrolyte. These studies results more negative photocurrent but not their magnitude when bulk $\text{Bi}_2\text{S}_3/\text{TiO}_2$ photo anode is measured in Na_2S electrolyte compared to other electrolyte however there is no report about the influence of Na_2S on Bi_2S_3 , which needs more study on this purpose.

ROLE OF CRYSTAL SIZE

Nanocrystalline Bi_2S_3 thin films of different thickness having their grain size lies in between 7 to 34nm been prepared by CBD which causes the significant change in the Photoelectrochemical cell performance. they change their thickness by making deposition at different time period which shows that the thickness and the grain size is increases with longer time deposition. This change in the size occurs due to the trapping of charge carriers at the surface and the intergrain boundaries which do not depend on the thickness this causes the decrease of the electrical resistivity with the increases of the grain size and thickness. Which attribute to the improved grain size and the reduction of the defects level. Study of RS Mane and et al revealed that the thickness and the grain size of Bi_2S_3 thin films nanowires can increased by deposition at longer time period at bath temperature of 6°C The comparative study of RS Mane et al and Zhehao Zhu et al are tabulize below and tried to compare the effect of thickness and grain size on various properties on the optical and electrical properties of Bi_2S_3 thin films.

Deposition time	Film thickness	Grain size	Band gap energy	Rs (Ω)	Fill factor	efficiency
5	103	7	2.06	53	33.64	0.012
10	230	14	1.90	49	35.16	0.027
15	323	20	1.86	28	39.14	0.039
20	375	27	1.70	25	42.53	0.056
25	437	34	1.60	20	46.77	0.086

COMPARATIVE STUDY

The comparison of the various properties of s-annealed and pristine Bi_2S_3

Bi_2S_3	Pristine	S annealed
Grain Size	10 nm(TEM)	50 nm
Life Time	0.7ps	3 ps-23ps
Band gap	1.37eV	1.24eV
Light Absorption Efficiency	39.6%	60.8%

From the above table it can be understood that the thickness and the grain size of Bi_2S_3 thin films increase with the increase in the time period of deposition which helps in the improvement of performance of Bi_2S_3 electrode.

CONCLUSION

It was found that PEC performance of Bi_2S_3 can be improved with increasing the grain size or thickness and also seen that the light absorption efficiency of S- annealed Bi_2S_3 is more in comparison of annealed which is necessary for solar cell. We will explore the influence of H_2 impurities on the optoelectronic properties and performance of material in future work.

ACKNOWLEDGMENT

The author is truly grateful to the principal, faculty members of science deptt. G.D.C. Memorial College, Bahal-127028.

REFERENCE

1. Lewis, N. S. *Science* 2007, 315, (5813), 798-801
2. Desai J D & Lokhande CD, *Indian J Pure & Applied Phys* 31 (1993) 152
3. Gadakh JD & Bhosale CH, *Meter Res Bull* 35 (2000) 1097
4. Yesugsade NS, Lokhande CD and Bhosale CH *Thin Solid Films* 263 (1995) 145
5. Zhehao Zhu, Project report of B.Sc.
6. R.S. Mane, B.R. Sankapal, C.D. Lokhande, *Materials Chemistry and Physics* 60 (1999) 196-203

Advances in Basic Science (ICABS 2019)

Bahal, India • 7–9 February 2019

Editors • Sanjay Gaur, Arindam Ghosh and Vijender Singh



Investigation on sintered preform with different geometrical shape factor

Cite as: AIP Conference Proceedings 2142, 170023 (2019); <https://doi.org/10.1063/1.5122620>
Published Online: 29 August 2019

Parveen Kumar, R. K. Ranjan, Davender Singh, and Vijender Singh



View Online



Export Citation

AIP | Conference Proceedings

Get **30% off** all
print proceedings!

Enter Promotion Code **PDF30** at checkout



Investigation on Sintered Preform with Different Geometrical Shape Factor

Parveen Kumar^{1a}, R. K. Ranjan², Davender Singh³, Vijender Singh³

1Department of Mathematics, RPS Degree College, Balana (Mahendergarh), India

2Director, NIET Noida, India

3 Department of Physics, RPS Degree College, Balana (Mahendergarh), India

^aCorresponding author: parveengaur1980@gmail.com

Abstract. The proposed research work has been taken up to understand deformation characteristics of compacted and sintered cylindrical preform considering the effect of strain rates by introducing different lubricating conditions at the ends of the preform. The radius of curvature of the bulged preform was measured during the experiments and found to be confirmed with the calculated one. It is assumed that the curvature of the bulge followed the form of a circular arc and accordingly calculated. The experiments were conducted for three aspect ratios. The frictional forces developed between platens/forming tools are important considerations in sintered-preform working process and in addition to this, the variation of strain rates have also been studied. Between various bulge parameters like strain, geometrical shape and stress ratios, the mathematical relationships have been developed and found in good correlation with experimental data. It would be helpful for those who are working in the field of mathematical modeling of sintered metal powder products. The results so obtained are discussed critically and will be presented graphically.

Key word: -Geometrical shape factor, Sintered preform, Strain rate, Friction

INTRODUCTION

Many investigators have carried a series of investigations on the forging of sintered cylindrical preform due to its relevance in powder metallurgy. Earlier investigations on forging of solid cylinders have been done. Jonson and Mellor have published a comprehensive review of literature [1]. During axisymmetric compression testing the mechanical properties of metals i.e. estimation of their forming limit up to plastic instability and fracture are another significant aspect of the study [2]. The existence of frictional constraint between die and work piece directly affect the plastic deformation of the specimen. During axially compression of solid cylinder between top and bottom platens the specimen material which is in contact with the surfaces undergoes heterogeneous deformation that results in barreling of the cylinder. At the faces of the contact, the friction retards plastic flow of metal on the surface and in its vicinity. A conical wedge of a relatively undeformed metal is formed immediately below it, while rest of the cylinder surfaces high strains and bulges out in a form of barrel. A well known principle in plastic deformation is demonstrated showing that the metal goes most easily towards the nearest free surface which is the point of least resistance. However the use of the lubricants reduces bulging and under ideal lubrication condition, even up to zero. Kulkarni and Kalpakjian examined the arc of barrel, assumed it to be a circular or parabolic, whereas Schey et al. presented a comprehensive report on the geometrical factors that affect the shape of the barrel [3,4].

Sowerby R, O'Reilly I, Chandrasekaran N, Dung NL tested the material for cold forging [5]. Banerjee showed theoretically that the barrel radius could be expressed as a function of axial strain and conformed the same through experimental verification [6]. It is presumed a similar behavior should be observed while conducting the experimental investigations with sintered-preforms. Since during the initial phase of upsetting of sintered-preform the densification process occurs and at later stage of upsetting it should resemble with solid cylindrical specimen. This is an attempt to confirm the presumption. Shyam M Keralaverma, A. Amine have investigated and proposed an approximate yield criterion for anisotropic porous media [7].

YU Shihao and others have conducted experiments on preform upsetting closed die forging and studied deformation and densification laws of powder cold forging [8]. S. Malayappan, and others conducted the experiments to generate data of the cold upset forging of solid cylinders of annealed Aluminium [9]. K Manisekar and others through their experiments generated data on cold upset forging of square & rectangular billets of annealed Aluminium under different frictional conditions and aspect ratios [10].

These above two experiments suggest having similar studies of powder preforms. Wikipedia, the free encyclopedia failure theory (material) and Hill yield criterion provides available theories for application in the cases of metal to metal composites [11]. The densification and compression of sintered preform takes place simultaneously therefore volumetric constancy is not possible, as preform's density changes due to closing of inter particle pores. Thus, suitable yield criterion is required, which is dependent on relative density of perform. The high interfacial pressure, which is applied for deformation, breaks the die-work piece interfacial lubricant film therefore have to consider composite friction including both sliding and sticking friction [12]. Earlier investigators have made no experimental attempt to study the sintered-preform considering various strain rates by introducing lubricants at the ends of the preforms. In this investigation the geometrical shape factors namely GSF(1) and GSF(2) and new hoop strain were arrived at based on contact diameters, barrel diameters, truncated portion diameters initial height, deformed height, barreled height and truncated portion height.

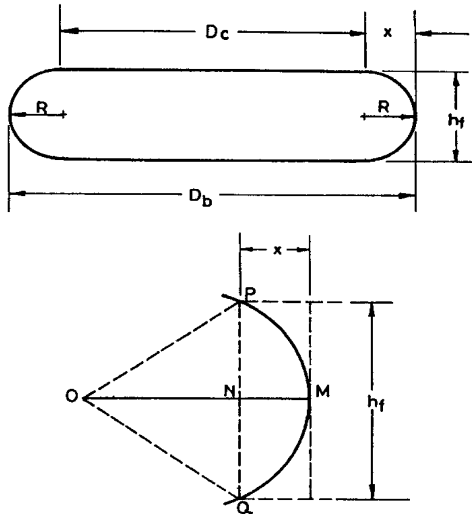


Fig. 1 Barrelling as circular arc of contact

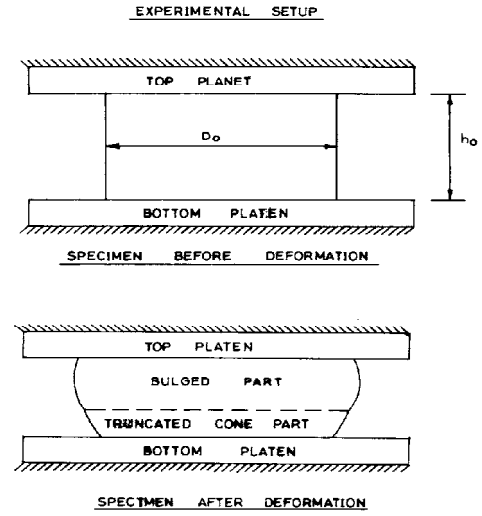


Fig. 2 Preform before and after deformation

MATHEMATICAL CALCULUS

The Experimental set up of the preform is as shown in the figure 1 & 2. The figure 1 shows the barreling as circular arc

of contact, while figure 2 demonstrates the specimen before and after the deformation.

From Fig.1 the expression for bulge radius R can be derived as $X = (D_b - D_c)/2$ (1)

Here D_b is bulged diameter and D_c is contact diameter and the h_b is the height of bulge. As in the Fig.1

$$OP = OQ = OM = R. \text{ and } PN = QN = h_b/2 \quad (2)$$

$$ON = OM - MN = R - x \quad (3)$$

$$\text{Since the triangle PNO is a right angle triangle, hence } (OP)^2 = (ON)^2 + (PN)^2. \quad (4)$$

$$R^2 = (R - x)^2 + (h_b/2)^2. \quad (5)$$

$$\text{The above equation after expansion reduces to: } R = (x/2) + (h_b^2/8x). \quad (6)$$

$$\text{Also } x = OM - ON = R - (OP^2 - PN^2)^{0.5}, \text{ therefore } X = R - (R^2 - (h_b/2)^2)^{0.5} \quad (7)$$

Once the diameters namely (D_c) and bulged (D_b) and height after deformation (h_f) are known, the radius of curvature of the bulge surface (of the bulged-upset sample) can be determined. The mass constancy principle is considered for sintered-powder-preform and the new GSF⁽²⁾ is derived as follows

$$(\pi/4)(h_0 d_0^2) \rho_0 = [(\pi/12) (2 D_b^2 + D_c^2) h_b + (\pi/12) (D_t^2 + D_t d_t + d_t^2) h_t] \rho_f \quad (8)$$

Relative density of the preform after deformation $\rho_f = \rho_0 / \rho_f$ The equation can be written as

$$(h_b/h_0) = [3d_0^2 \rho_f / (2 D_b^2 + D_c^2)] - [((D_t^2 + D_t d_t + d_t^2) h_t) / (h_0(2 D_b^2 + D_c^2))] \quad (9)$$

From Eq. 7 the expression for the radius of curvature of bulge is $X = R - (R^2 - h_b^2/4)^{0.5}$ where, $x = (D_b - D_c)/2$
Simplifying the Eq.5, the expression for the bulge radius (R) can be obtained neglecting the x^2 term. Therefore,

$$R = h_b^2/8x. \quad (10)$$

$$R = h_b^2/4(D_b - D_c) \quad (11)$$

$$R^{0.50} = h_b/2(D_b - D_c)^{0.50} \quad (12)$$

$$R^{0.50} = [h_b/h_0][h_0/2(D_b - D_c)^{0.5}]. \quad (13)$$

Putting the value of (h_b/h_0) from Eq. 9 the bulge radius becomes as follows:

$$R^{0.50} = (h_0/2(D_b - D_c)^{0.5})x[3d_0^2 \rho_f / (2 D_b^2 + D_c^2)] - [((D_t^2 + D_t d_t + d_t^2) h_t) / (h_0(2 D_b^2 + D_c^2))] \quad (14)$$

The right hand side of Eq. 14 is the new GSF⁽²⁾ arrived at based on the radius of the bulge.
Again considering mass constancy principle for Sintered-Powder-Preform, the new GSF⁽¹⁾ can be derived as

$$(\pi/4)(h_0 d_0^2) \rho_0 = [(\pi/12) (2 D_b^2 + D_c^2) h_b + (\pi/12) (D_t^2 + D_t d_t + d_t^2) h_t] \rho_f \quad (15)$$

Relative density of the perform $\rho_f = \rho_0 / \rho_f$, so $(h_0/h_t) = [\{ (2 D_b^2 + D_c^2) (h_b/h_t) + (D_t^2 + D_t d_t + d_t^2) \} / (3 d_0^2 \rho_f)]$
The truncated cone height can be expressed as follows from above Equation

$$\ln (h_0/h_t) = \ln [\{ (2 D_b^2 + D_c^2) (h_b/h_t) + (D_t^2 + D_t d_t + d_t^2) \} / (3 d_0^2 \rho_f)] \quad (16)$$

The right hand side of Eq. 16 is the new GSF⁽¹⁾ arrived at based on the truncated cone height.

$$\text{Hoop stress can be expressed as } \sigma_\theta = [(1+2\alpha)/(2+\alpha)]\sigma_z \text{ where } \alpha \text{ is Poison's ratio} \quad (17)$$

$$\text{the representative stress can be expressed as } \sigma = 1/(2+\alpha)\{3(1+\alpha+\alpha^2)\}0.50\sigma_z. \quad (18)$$

$$\text{The hydrostatic stress is } \sigma_m = (1/3)(\sigma_\theta + \sigma_r + \sigma_z) \quad (19)$$

Usually σ_z is negative because it is compressive in nature and $\sigma_\theta = \sigma_r$.

$$\text{The true axial stress } (\sigma_z) \text{ is } \sigma_z = \text{Load} / \text{Instantaneous contact area} \quad (20)$$

$$\text{And the true axial strain } (\epsilon_z) \text{ is calculated using the expression } \epsilon_z = \ln (h_f/h_0) \quad (21)$$

where h_0 is the initial height (height before deformation) and h_f is the height after deformation. Further, hoop strain namely

$$\epsilon_\theta \text{ can be calculated as } \epsilon_\theta = \ln [D_c/d_0] \quad (22)$$

where d_0 is the initial diameter and D_c is the contact diameter. The new hoop strain considering mass constancy

$$\text{principle}(\pi/4)(h_0 d_0^2) \rho_0 = [(\pi/12) (2 D_b^2 + D_c^2) h_b + (\pi/12) (D_t^2 + D_t d_t + d_t^2) h_t] \rho_f \quad (23)$$

Since relative density $\rho_r = \rho_0/\rho_f$, the above eq. is rearranged as

$(h_0/h_f) = [\{ (2 D_b^2 + D_c^2) h_b + (D_t^2 + D_t d_t + d_t^2) h_t \} / (3 d_0^2 h_f \rho_r)]$ So thenew hoop strain can be written as

$$\text{Ln} (h_0/h_f) = \ln [\{ (2 D_b^2 + D_c^2) h_b + (D_t^2 + D_t d_t + d_t^2) h_t \} / (3 d_0^2 h_f \rho_r)] \quad (24)$$

EXPERIMENTAL VALIDATION

The atomized Al powder “Qualikem” make has been used to fabricate green performs at a selected compaction pressure of 100kN by using a die-punch of 20 mm diameter on 400 kN computerized UTM. The green preform density has been calculated by measuring its diameter, height and weight. The preforms were sintered in a endothermic atmosphere (sand-covered) inside a microprocessor controlled Muffle Furness by elevating its temperature in a controlled manner up to 450° C allowing a soaking period of 2 hours and then allowing its cooling to room temperature. The sintered preform density again hasbeen calculated. The specimens of the ratios (initial height to initial diameter ratio) namely 0.75, 1.00, 1.25 were prepared. The experiment on sintered Al was conducted with 400 kN computerized compression testing UTM. For a selected strain such as 1.5 mm/ min, 2 mm/ min, 2.5 mm/ min and 3mm/ min and for every frictional condition five specimens were stressed to different strain levels. The following parameters were measured.

1. Height of the compressed-deformed preform (h_f)
2. Contact diameters of the compressed-deformedpreform (D_{C1} and D_{C2}) where D_{C1} is the contact diameter on the top of the barreled portion and D_{C2} is the contact diameter on the bottom of the truncated cone portion, the contact diameter of the preform is $D_c = [D_{C1} + D_{C2}] / 2$.
3. Bulge diameter (D_b) and the radius of the barrel (R).
4. D_t and d_t are the maximum and minimum diameter of the truncated cone part.
5. Height of the barrel (h_b) and Height of the truncated cone part (h_t).

The load required for each deformed level was recorded from the monitor of computer400kn UTM. The barrel radii for each deformation were recorded using the radius gauges and the rest of the dimensions were measured using a digital micrometer.

RESULTS AND DISCUSSION

The graph is drawn between the diametrical strain and the linear strain (Figure 3). The plot showed a straight line relationship with a slope of 0.34, 0.35 and 0.38sssss for an aspect ratio of 1.25, 1.00 & 0.75 irrespective of lubricants considered.

The relationship between the axial strain and a new hoop strain is also a straight line with the slope of 0.73 for the aspect ratio 0.75, 0.83 for the aspect ratio 1.00 and 0.86 for the aspect ratio 1.25, irrespective of the lubricants considered (Figure 4). The new hoop strain slope is found to increase accordingly with increasing aspect ratio. The graphs (Figure 5) are drawn between the measured radius of curvature and the calculated radius with the assumption that the barrel radius fits the circular arc is correct. The calculated value conformed to the measured values irrespective of the aspect ratios and the lubricants used.

The graphs (Figure 6) are drawn between the truncated cone height of the compressed preform and $GSF^{(1)}$ arrives at by mass constancy principle. The plot showed a straight line with a slope of 0.96, 0.98, and 0.70 for the aspect ratios of 0.75, 1.0 and 1.25 respectively. The graphs (Figure 7) are drawn between the measured radius of bulge to the new geometric shape factor $GSF^{(2)}$, this also fits into a straight line with a slope of 1.90 for the aspect ratio 1.25, 1.91 for 1.00 and 2.00 for the aspect ratio of 0.75 irrespective of lubrication used. The relationship between the barrel radius and $GSF^{(2)}$ is expressed as $R = CS^{-m}$, Where R = barrel radius and S = $GSF^{(2)}$. New geometric shape factor and the constants C and m are determined imperially. The straight also implies that the rate of change of barrel radius with respect to $GSF^{(2)}$ did not exhibit a major difference for the preforms of different aspect ratios.

During compression test as the preforms are compressed the initial density ρ_0 changes to final density ρ_f , and relative density of the preform after deformation ρ_r approaches to one. Applying simple theory of plasticity, stresses namely the true axial stress (σ_z), hoop stress (σ_θ), the effective stress (δ) and the hydrostatic stress (σ_m) were calculated and

plotted against the axial strain (ϵ_z) for different aspect ratios and lubricants considered. It is noted that all stresses increase with increased strain level.

Figures 14 show that the radius of curvature of the barrel decreased exponentially with increasing values of the stress ratio parameter and for the considered aspect ratios a straight line relationship is observed with slope of -1.075 for aspect ratio of 1.25, -1.075 for aspect ratio 1.00 and -0.9868 for aspect ratio 0.75. $R = C_1 [(\sigma_m/\delta)(h_o-h_f)]^{m_1}$ Where σ_m = hydrostatic stress, δ = representative stress, C_1 and m_1 are empirically determined constants.

CONCLUSIONS

The final shape of the perform after the upsetting process can be divided into two geometries namely a barreled portion and a truncated cone portion and the new hoop strain slope is found to increase accordingly with increasing aspect ratio. It was observed the height of the truncated cone portion decreases with an increase in strain values. The

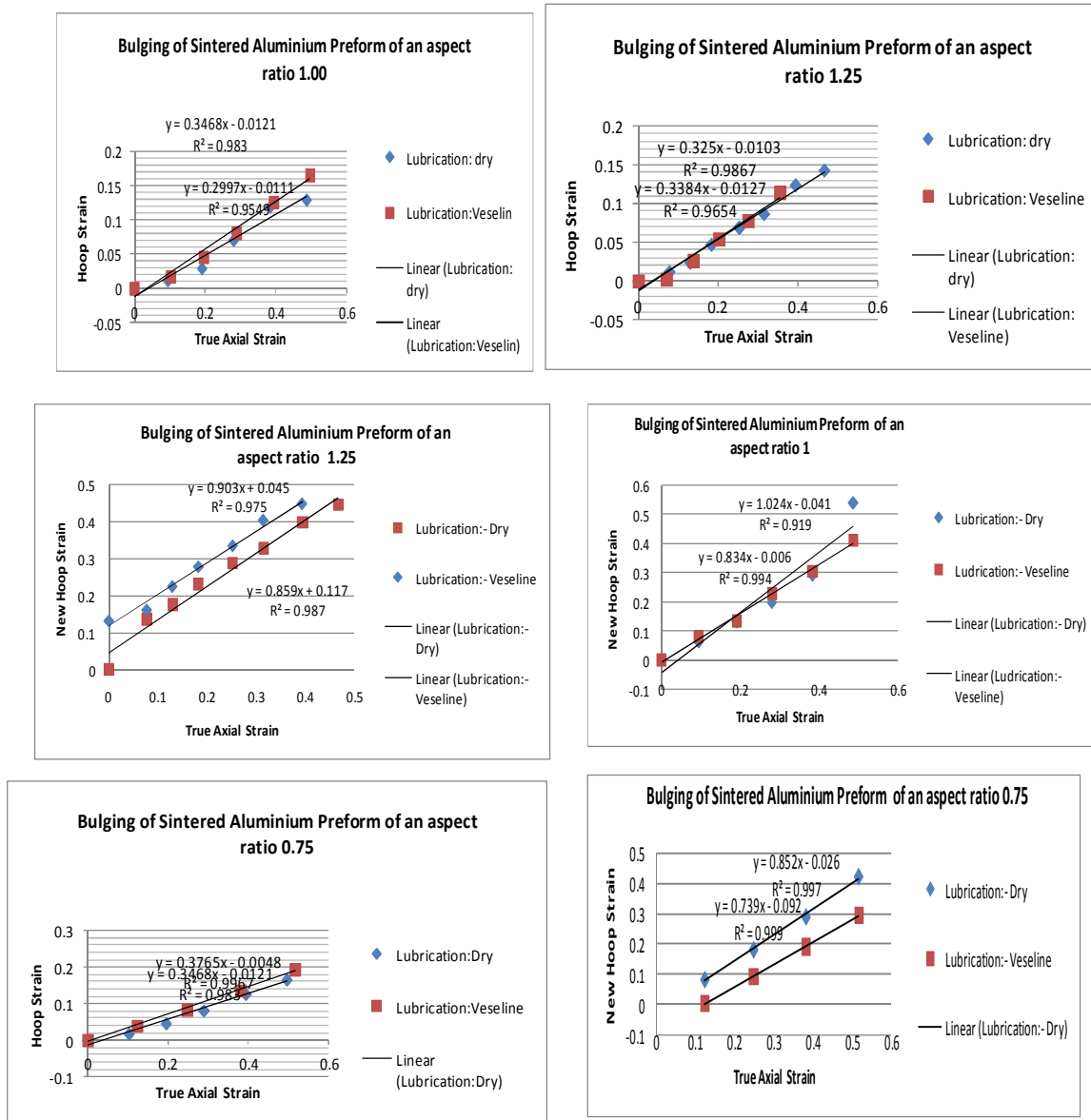


Fig.3 Relationship between hoop strain and axial strain

Fig.4 Relationship between new hoop axial strain

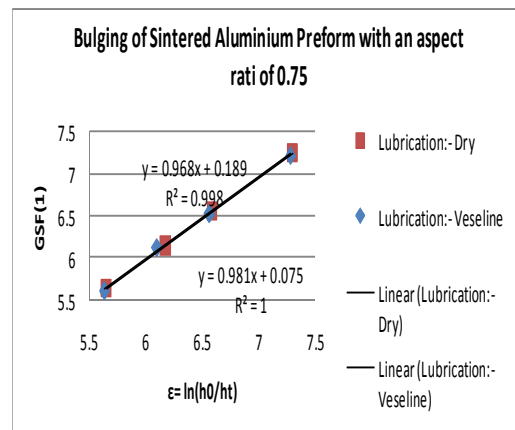
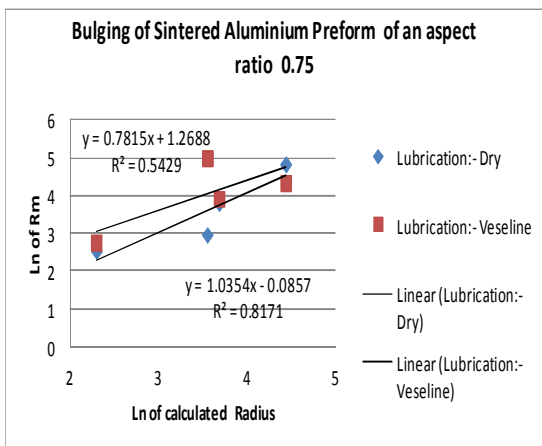
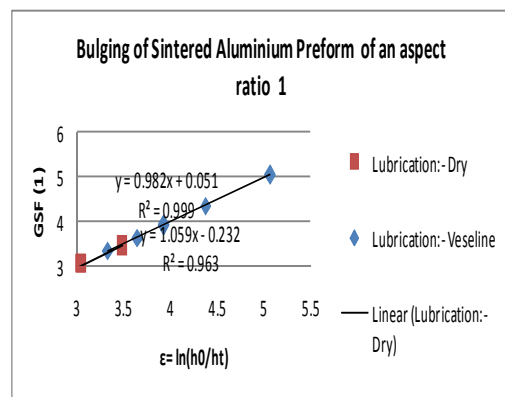
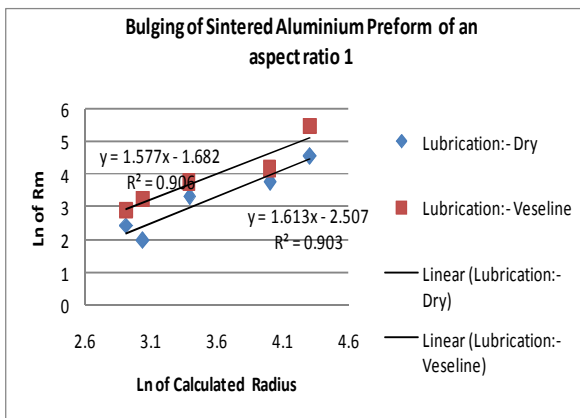
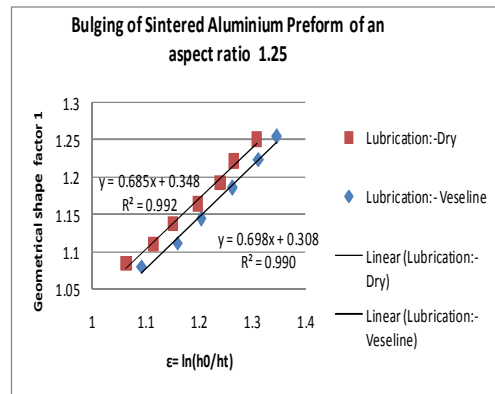
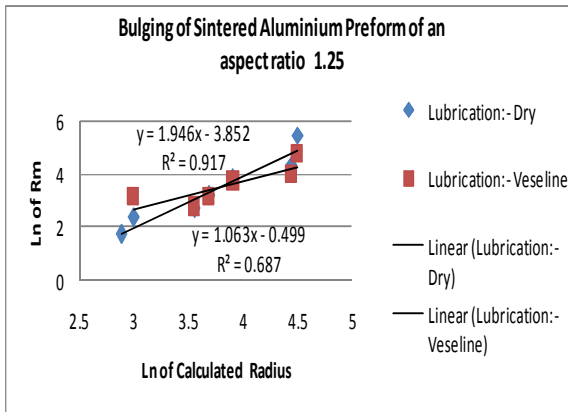


Fig.5 Relationship between measured radius and calculated radius Fig.6 Relationship between geometrical shape factor⁽¹⁾ and strain based on truncated cone height

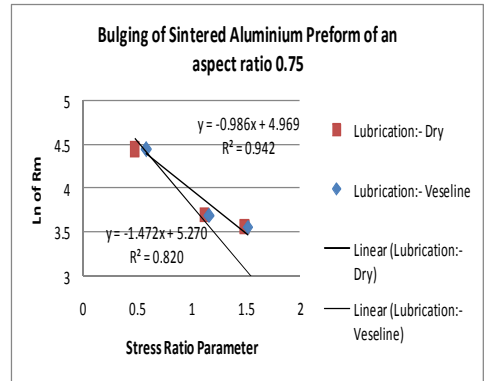
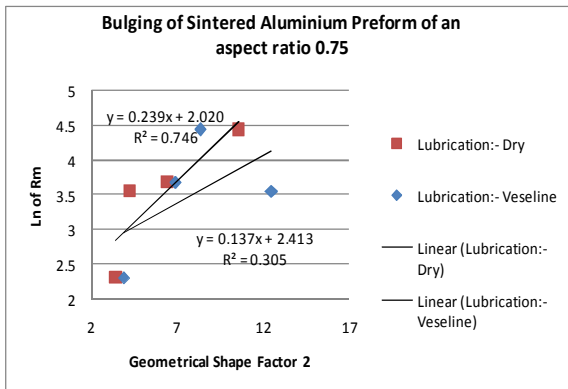
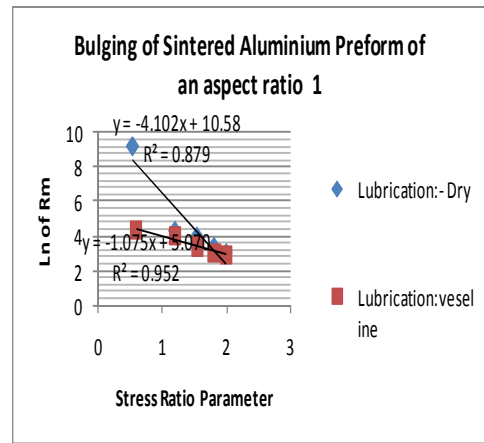
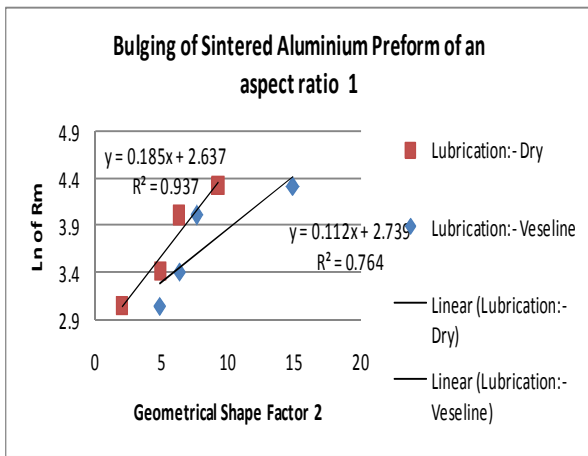
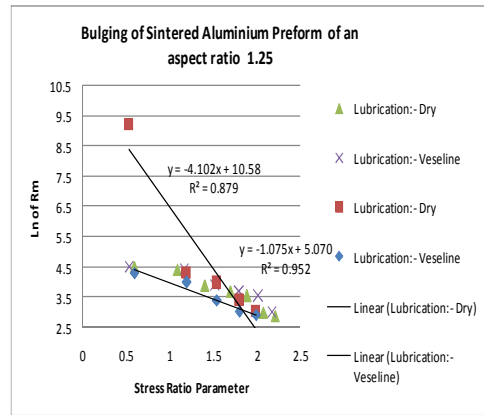
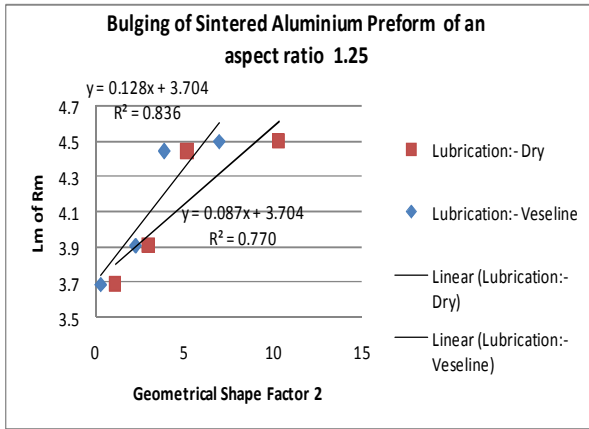


Fig.7 Relationship between measured radius and geometrical shape factor⁽²⁾

Fig.8 Relationship between measured radius and stress ratio parameter

measured radius of curvature matches one to one with the calculated radius, thus establishing the assumption that the radius of curvature of the barrel fits a circular arc. Stresses namely the hoop stress (σ_0), the effective stress (δ) and the hydrostatic stress (σ_m), are all found to increase with the increasing level of deformation and are different for different barrels. The relationship between the new hoop strain and the axial strain conformed to a straight-line behavior.

It was found that the barrel radius followed the power relationship, viz,

(a) $R=CS^{-m}$ and

(b) $R=C_1[(\sigma_m/\delta)(h_0-h_f)]^{-m_1}$

where,

R = barrel radius, S = new geometrical shape factor, σ_m = hydrostatic stress, δ = representative stress,

h_0 = initial height of the cylinder, h_f = deformed height, C, m, C_1 , and m_1 are experimentally determined constants. It was observed that the radius of curvature of the bulge decreases with increasing values of the stress ratio parameter irrespective of the aspect ratios and lubricants considered.

REFERENCES

1. Johnson W, Mellor PB, Engineering plasticity. (Van Nostrand, London, 1975) ch. 6, pp 110–114
2. Shaw C, Avery JP (1980) Forming limits – reliability, stress analysis and failure prevention methods in mechanical design. Century, Chicago, IL, ASME, pp 297–303
3. Kulkarni M, Kalpakjian S A study of barreling as an example of free deformation. *ASME J Eng Ind* 91, 743–754(1969)
4. Schey A, Venner TR, Takomana SL Shape changes in the upset-ting of slender cylinders. *ASME J Eng Ind* 104, 79–83(1982)
5. Sowerby R, O'Reilly I, Chandrasekaran N, Dung NL Materials testing for cold forging. *ASME J Eng Mater Tech* 106, 101–106(1984)
6. Banerjee Barreling of solid cylinders under axial compression. *ASMEJ Eng Mater Tech* 107:138–144
7. Shyam M, Keralavarma, A. Amine Benzerga, An approximate yield criterion for anisotropic porous media, *ELSEVIER ScienceDirect C. R. Mecanique* 336, 685-692(2008).
8. YU Shihua, HUA Lin, LI Yongzhi, YAN Shiwei, LIU sYongjun “ Deformation and Densification Laws of Powder Cold Forging” *Journal of Wuhan University of Technology-Mater. Sci. Ed.* Feb 2007
9. S. Malayappan, R. Narayanasamy, G Esakkimuthu, *ELSEVIER ScienceDirect Materials and Design* 28, 1404-1411(2007).
10. K. Manisekar, R. Narayanasamy, *EISEVIER ScienceDirect Materials and Design* 28, 592-598(2007).
11. Wikipedia, the free encyclopedia: Failure theory (Material), Hill yield criteria.
12. S. Malayappan and G. Esakkimuthu, “Barreling of aluminium solidcylinders during cold upsetting with differential frictional conditions atthe faces,” *Int. J. Adv. Manuf. Tech.* vol. 29, 41-48(2006).

Synthesis and optical properties of Zn(II) doped graphene quantum dots: Blue to purple emission

Cite as: AIP Conference Proceedings 2142, 060007 (2019); <https://doi.org/10.1063/1.5122386>
Published Online: 29 August 2019

Poonam R. Kharangarh, Vijender Singh, and Gurmeet Singh



View Online



Export Citation

AIP | Conference Proceedings

Get **30% off** all
print proceedings!

Enter Promotion Code **PDF30** at checkout



Synthesis and Optical Properties of Zn(II) doped Graphene Quantum Dots: Blue to Purple Emission

Poonam R. Kharangarh^{1,a)}, Vijender Singh² and Gurmeet Singh¹

¹*Department of Chemistry, University of Delhi-110007, New Delhi (India)*

²*Department of Physics, G.D.C. Memorial College, Bahal- 127028, Haryana (India)*

^{a)}Corresponding author: prk6@njit.edu

Abstract. The Graphene Quantum dots (GQDs), fragments of graphene have attracted considerable attention in recent years due to the size, edge effects, quantum confinement and heteroatom doping. The doping of graphene based materials can effectively tune their intrinsic properties, including electronic and optical properties, surface and local chemical reactivity. Herein, we present a comprehensive study of ZnO doped GQDs prepared by a facile hydrothermal method by using ZnO and Graphene Oxide (GO) as a source materials. All the synthesized materials were characterized by UV-Visible Spectroscopy (UV-Vis), Raman Spectroscopy, Fourier Transform Infrared (FT-IR) and Photoluminescence (PL). The morphological characterizations were confirmed by transmission electron microscopy images (TEM). The hydrothermally synthesized material had a size of 5-20 nm by uniform doping of zinc nanoparticles on graphene sheet. The results of PL of Zn(II)-GQDs showed a blue to purple emission with the variation in excitation wavelength from 280nm to 380nm. These doped GQDs were found to be an efficient approach with multicolor emission for biological applications and optoelectronic devices to make the environmental friendly, cost effective and easily scalable.

INTRODUCTION

GQDs are considered to be one of the most promising materials in recent years owing to its unique properties and novel potential applications in nanocomposite materials, fluorescence sensing, energy storage and conversion and bioimaging [1-4]. However, graphene does not show luminescence because it has no band gaps in its band structure, which is a major reason for the hindrance to show the outstanding optical properties. To overcome this limitation, we choose graphene quantum dots, fragments of graphene due to its quantum confinement effects and edge effects. Doping of GQDs with heteroatoms can tune the band gap to introduce more defect states [5] and can tailor the band gap of GQDs to the required PL properties. GQDs possess quantum confinement [6] and edge effects which induce size dependent band gap and also exhibit strong photoluminescence (PL) [7-8].

A lot of work has been done for doping with nonmetallic atoms into the graphene by introducing the additional defects during the synthesis process [9-12]. Researcher also have found the most effective way to improve the luminescent performance with co-doping of GQDs such as B-N doped GQDs [13], N-S doped GQDs [14] and N-P doped GQDs [15] by modifying the electron density. Li et al. [16] synthesized GQDs by electrochemical method with green luminescence for various optoelectronic devices. These reported methods are limited by the availability of expensive materials, multicolor emission and accessibility of special tools.

In this work, we reported Zn(II)-GQDs for the first time, by using Graphene Oxide (GO) and Zinc Oxide (ZnO) powders as source materials. Zn doped GQDs were synthesized by using a facile hydrothermal treatment which is highly dispersed in water with uniform size, and good crystalline in nature. Compared with previous methods, this method uses an inorganic water soluble organic salts making it cost effective, environmental friendly, and easy scalable. The results of Zn(II)-GQDs show distinctive optical properties when compared with graphene oxide (GO). The PL peaks of the Zn(II)-GQDs were purple shifted under a series of excitation wavelengths from 280nm to 340nm with nearly identical emission wavelengths. The position of the emission peak wavelengths in Zn(II)-GQDs shifts from purple to blue with a excitation wavelength of 380nm. In addition, Zn(II)-GQDs exhibit multicolour

emission from purple to blue . This multicolor emission might be attributed to Zn doping which introduces the additional energy levels between the valence band and conduction band.

EXPERIMENTAL DETAILS

Graphite powder was converted into graphite oxide in accordance with the procedure described by Hummers and Offemmann [17-19]. For preparation of Zn(II)-GQDs, the same procedure was used as brief in our earlier work [20-22]. In a typical synthesis, 5.95mg of ZnO were dissolved in 10 ml of GO solution & 10 ml of deionized (DI) water with stirring for 30 min and sonicate for another 30 min. The final solution was then transferred into a Teflon lined autoclave and heated at 100⁰C for 6 h by hydrothermal treatment. Furthermore, this solution was naturally brought down to room temperature and subsequently the Zn(II)-GQDs were collected by filtration through a 0.22 μ m Teflon membrane.

The morphology and size distribution of the prepared samples were examined by Transmission Electron Microscope (TEM) (FEI Technai G2 T30 electron microscope). The samples were prepared by drop casting the sample solution onto a carbon coated copper grid, followed by drying at room temperature. Photoluminescence (PL) spectra were collected by using Fluoromax-4 Spectro-fluorometer. Fourier Transform Infrared spectrum (FTIR) was used to see the presence of functional groups in samples by using PerkinElmer Spectrum RXI -Mid IR operating with a resolution of 1 cm^{-1} in the frequency range of 400-4000 cm^{-1} . Raman spectra were recorded using a Renishaw Laser Raman spectrometer via microscope system. UV-Visible absorption spectra of aqueous solutions of samples were recorded on a Perkin Elmer Lambda 35 spectrophotometer, with a slit width of 2 nm.

RESULTS AND DISCUSSION

Fig. 1 shows the HRTEM images of Zn (II)-GQDs respectively. The HRTEM images of GQDs were shown in our earlier reported work [19]. The observed Zn(II)-GQDs were spherical in shape and crystalline in nature. The majority of quantum dots in Zn(II)-GQDs were observed with a size of 5-20nm in diameter as shown in Fig. 1. This reveals the introduction of escalated density of defect states produced by Zn atoms into the hexagonal structure.

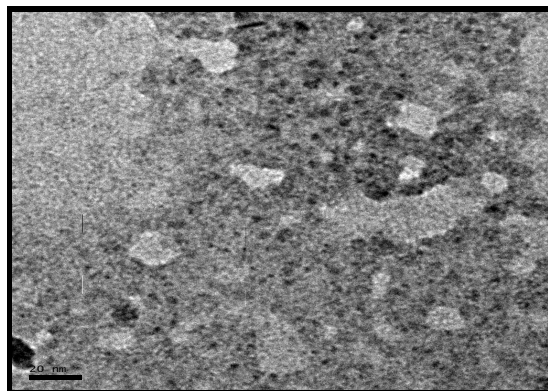


FIGURE 1. HRTEM images of Zn (II)-GQDs

Fig. 2 represents the FTIR spectra of GO, GQDs and Zn(II)-GQDs that reveals the presence of the functional groups. The FTIR spectrum (Fig. 2) of pristine GO [19] showed the vibrational peaks at C-O at 1040 cm^{-1} , C-OH at 1389 cm^{-1} , aromatic carbons at 1639 cm^{-1} , C=C-O at 1726 cm^{-1} , C-H at 2927 cm^{-1} , and stretching vibrational peaks of C-OH at 3441 cm^{-1} . In GQDs, the observed peaks were observed at 1626, 2130, and 3329 cm^{-1} . After doping with Zinc Oxide, Zn(II)-GQDs exhibit new absorption bands located at 473 cm^{-1} which might be due to the Zn related dopants into GQDs atomic lattices which is in agreement with the reported value [23]. The peak at 473 cm^{-1} can be assigned to Zn-O stretching vibration reveals that nano-sized graphene sheets has been hybridized with ZnO to form Zn-GQDs successfully [24]. Additional peaks of Zn(II)-GQDs were also detected at 684, 1188, 1543, 2354, 2842, 2916, 3156, and 3437 cm^{-1} . We observed that the intensity of band in Zn(II)-GQDs gradually decrease when band shifts to higher frequency due to the presence of the oxygen related functional groups. However, the band at

1543 cm^{-1} is assigned to the skeletal vibrations of unoxidized graphitic domain which confirms with our Raman results. The above results confirm the formation of excellent quality of Zn doped GQDs which is consistent with the reported results.

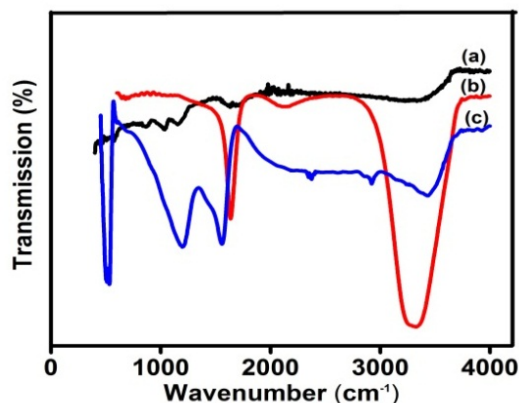
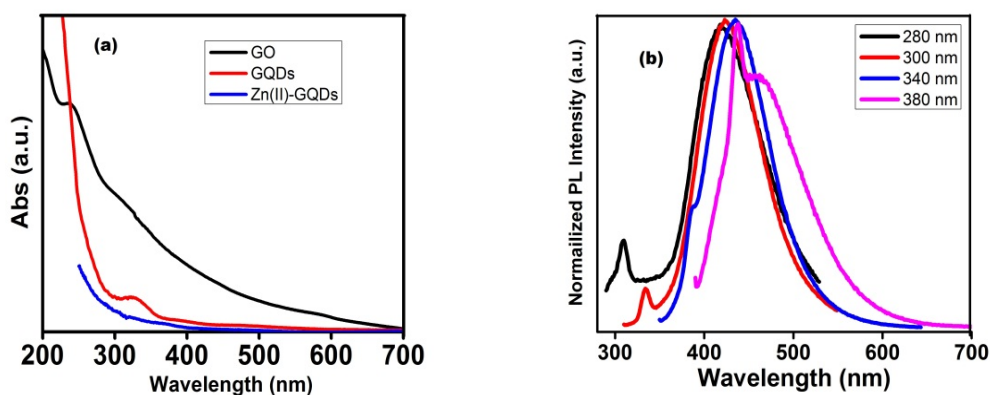


FIGURE 2. FTIR of (a) GO, (b) GQDs, and (c) Zn(II)-GQDs.

To explore the optical properties of GO, GQDs and Zn (II)-GQDs, the ultraviolet-visible (UV-Vis) absorption spectrum were recorded in aqueous solutions as shown in Fig. 4(a). In Fig. 3(a), there are two typical absorption peaks at 232nm and at 284nm in GO, which is similar to refs [21, 22]. The observed absorption peak at 232nm corresponds to π - π^* transitions of aromatic C=C bonds, leads to almost no PL signal. The second peak at 284nm is assigned from n - π^* transitions of C=O bond [25] due to the trapping of excited state energy by surface states resulting in strong emission. In GQDs, the two peaks at 273nm and 329nm were observed. In case of Zn (II)-GQDs, the π - π^* transitions peak shows a shift to 263nm and n - π^* transitions peak at wavelength 307nm [26]. The absorption bands in Zn(II)-GQDs shows a blue shift after doping with Zn in comparison to un-doped GQDs [19]. The presence of n -band is possibly due to the oxygen related functional groups which exists between π band and π^* band. This is explained by the Zn doping which introduce some additional orbitals into the GQDs, and as a result, there will be a change in electron transition pathways. In this case, UV results confirm that the band gap increases with the decrease in size of graphene fragments.



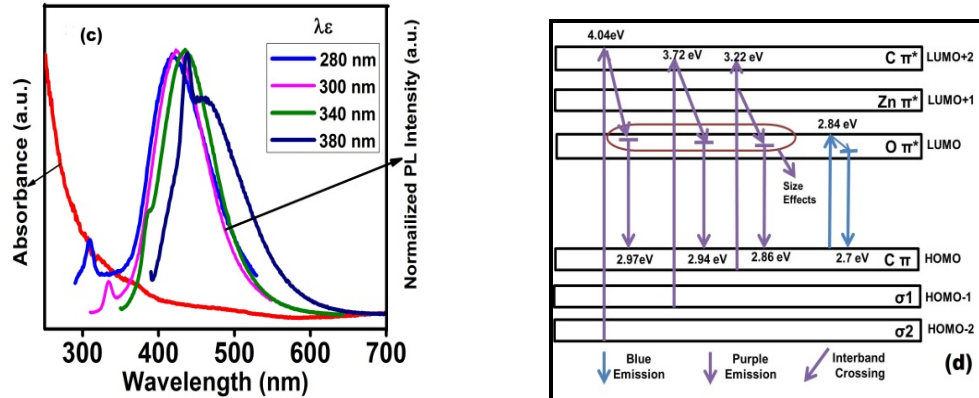


FIGURE 3. (a) UV-Vis absorption of GO, GQDs, and Zn(II)-GQDs; (b) PL spectra of Zn(II)-GQDs with different excitation wavelengths; (c) UV-Vis absorption spectra and PL of Zn(II)-GQDs; and (d) The proposed energy band diagram of Zn(II)-GQDs

The PL spectra of Zn (II)-GQDs were recorded at various excitation wavelengths from 280nm to 380nm. Fig. 3(b) shows the various normalized PL spectra recorded for Zn doped GQDs in aqueous medium by exciting at different wavelengths. This suggests a uniform particle size distribution of Zn-GQDs with the dependence of lower excitation wavelengths. Four emission peaks are observed.

The combined spectra of UV-Vis and PL of Zn (II)-GQDs is shown in Fig. 3(c). The introduced energy levels under excitations for Zn (II)-GQDs were observed at 418nm, 423nm, 435 nm and 460nm with the excitation wavelengths at 280nm, 300nm, 340nm and 380nm. These levels generate the purple PL emission when they are released to surface states with the excitation wavelengths from 280nm to 340nm. It may attribute to the number of disorder-induced states with in band gap decreases. This leads to the increase the number of small sp^2 domains resulting purple emission at shorter wavelengths in the PL spectra of Zn (II)-GQDs. As the excitation wavelength in Zn (II)-GQDs changed from 340nm to 380nm, PL peak shifts to longer wavelengths shows blue emission. The blue emission occurs due to the size effect in GQDs after doping with Zn due to the localization of electron-hole pair. It may be attributed to the relatively high surface defect concentration related to the oxygen content which can trap more excitons and lead to the blue emission. The observed peaks can be compared to reported peaks observed in undoped GQDs (emission wavelength 473 nm) [18]. Furthermore, the change in band structure leads to change in light absorption and PL properties.

Based on our excitation dependent PL results, a schematic energy band diagram of different electronic transitions of Zn (II)-GQDs is shown in Fig. 3(d). The band gap changes as it depends on the size of the graphene fragments as shown in Fig. 4(b). These results show different PL emission colors from blue to purple with different sized GQDs. Hoffmann [27] claimed that for a triplet ground state, δE should be below 1.5 eV, and since the triplet carbenes were supremely common at zigzag edges, [28]. Three different excitation bands in the PL spectra, 307 nm (4.04 eV), 384 nm (3.72eV) and 386 nm (3.22eV), were generally regarded as transitions from the σ and π orbitals to the LUMO. Thus the calculated δE was found to be 0.32 eV, and 0.82eV satisfying the required value (below 1.5 eV) for triple carbenes [28] indicates the assigned excitation bands are rational. As the three transitions were directly correlated with the observed purple PL, the purple emission should be the radiative recombination of excited electrons between the HOMO and LUMO. The introduction of new energy levels shown in energy band diagram is the key for the fine-tuning of the optoelectronic properties of GQDs, which should be suitable for different applications [29-30].

SUMMARY AND CONCLUSIONS

In summary, we have synthesized Zn doped GQDs with tunable PL by using a facile hydrothermal method with Zinc Oxide as a low-cost source material. The doped GQDs exhibit strong purple PL under the lower excitation UV light from 280nm to 340nm. It is inferred that the surface defect states that led to the band-gap variation played a

significant role in the PL of GQDs with cyclic aromatic hydrocarbon-like conjugated structure. The strong blue emission of Zn(II)-GQDs at larger wavelengths (~ 380nm) is advantageous for bio-imaging applications. These results of Zn(II)-GQDs with strong multicolor PL will bring more opportunities for future graphene based optoelectronic applications, LED emission, bio-imaging and beyond.

ACKNOWLEDGMENTS

This work was financially supported by Dr. D. S. Kothari Post-Doctoral Fellowship, UGC, India.

REFERENCES

1. F. Liu, S. Song, D. Xue, and H. Zhang, *Adv. Mater.* **24**, 1089 (2012).
2. W. Wei, C. Xu, J. Ren, B. Xu and X. Qu, *Chem. Commun.* **48**, 1284 (2012).
3. C. Liu, J. Liu, S. Ji, Y. Zhou, *Mater. Focus.* **1**, 149 (2012).
4. S. J. Zhu, J. H. Zhang, S. J. Tang, C. Y. Qian, L. Wang, and H. H. Wang, *Chem. Commun.* **47**, 6858 (2012).
5. P. R. Kharangarh, S. Umapathy, and G. Singh, *Jour. of Applied Physics* **122**, 145107 (2017).
6. C. O. Girit, J. C. Meyer, R. Erni, M. D. Rossell, C. Kisielowski, L. Yang, C. H. Park, M. F. Crommie, M. L. Kohen, S. G. Louie, *Sci.* **323**, 1705-1708 (2009).
7. S. R. M. Santiago, T. N. Lin, C. T. Yuan, J. L. Shen, H. Y. Huang and C. A. J. Lin, *Phys.Chem.Chem. Phys.* **18**, 22599 (2016).
8. F. Liu, T. Tang, Q. Feng, M. Li, Y. Liu, N. Tang, W. Zhong, and Y. Du, *J. App. Phy.* **115**, 164307 (2014).
9. X. M. Li, S. P. Lau, L. B. Tang, R. B. Ji and P. Z. Yang, *Nanoscale* **6**, 5323–8 (2014).
10. J. Gu, X. Zhang, A. Pang, J. Yang, *Nanotechnology* **27**, 165704 (2016).
11. Y. Li, Y. Zhao, H. Cheng, Y. Hu, G. Shi, L. Dai and L. Qu, *J. Am. Chem. Soc.* **134**, 15–18 (2012).
12. H. Liu, Y. Liu, D. Zhu, *J. Mater. Chem.* **21**, 3335 (2011).
13. L. B. Tang, R. B. Ji, X. M. Li, K. S. Teng and S. P. Lau, *J. Mat. Chem. C* **1**, 4908–15 (2013).
14. H. Fei, Y. Ruquan, Y. Gonglan, G. Yongji, P. Zhiwei, F. Xiujun, L. G. Errol, M. A. Pulickel, and M. T. James, *ACS Nano* **8(10)**, 10837–10843 (2014).
15. B. X. Zhang, H. Gao, and X. L. Li, *New J. Chem.* **38**, 4615 (2014).
16. Y. Li, Y. Hu, Y. Zhao, G. Shi, L. Deng, Y. Hou, and L. Qu, *Adv. Mater.* **23**, 776–780 (2011).
17. W. S. Hummers Jr and R. E. Offeman, *J. Am. Chem. Soc.* **80**, 1339 (1958).
18. P. R. Kharangarh, A. Kumar, R. K. Sharma, and G. Singh, *Adv. Mater. Proceedings* **2(3)**, 171 (2017).
19. P. R. Kharangarh, S. Umapathy, G. Singh, R. K. Sharma, and A. Kumar, *Emerging Materials Research (EMR)* **6**, 227 (2017).
20. P. R. Kharangarh, S. Umapathy, and G. Singh, *Integ. Ferroelectrics* **183**, 1, 2017.
21. P. R. Kharangarh, S. Umapathy, and G. Singh, *ECS J. Solid State Sci. Technol.* **7(3)**, M29-M34 (2018).
22. P. R. Kharangarh, S. Umapathy and G. Singh, *Appl. Surf. Sci.* **449**, 363-370 (2018).
23. J. L. Wu, X. P. Shen, L. Jiang, K. Wang, K. M. Chen, *Appl. Surf. Sci.* **256**, 2826-2830 (2010).
24. V. Etacheri, R. Roshan, V. Kumar, *ACS Appl. Mater. Interfaces* 2717–2725 (2012).
25. A. C. Ferrari, J. C. Meyer, V. Scardaci, C. Casiraghi, M. Lazzeri, F. Mauri, S. Piscanec, D. Jiang, K. S. Novoselov, S. Roth, and A. K. Geim, *Phys. Rev. Lett.* **97**, 187401 (2006).
26. D. Graf, F. Molitor, K. Ensslin, C. Stampfer, A. Jungen, C. Hierold and L. Wirtz, *Nano Lett.* **7**, 238-242 (2007).
27. R. Hoffmann, *J. Am. Chem. Soc.* **90**, 1475–1485(1968).
28. L. R. Radovic and B. Bockrath, *J. Am. Chem. Soc.* **127**, 5917–5927 (2005).
29. V. Singh and P. Aghamkar, *Appl. Phys. Lett.* **104**, 111112 (2014).
30. V. Singh and P. Aghamkar, *Applied optics* **51**, 13, 2288 (2012).

Preface: Advances in Basic Sciences (ICABS19)

Cite as: AIP Conference Proceedings **2142**, 010001 (2019); <https://doi.org/10.1063/1.5122323>
Published Online: 29 August 2019



[View Online](#)



[Export Citation](#)

AIP | Conference Proceedings

Get **30% off** all
print proceedings!

Enter Promotion Code **PDF30** at checkout



Preface: Advances in Basic Sciences (ICABS19)

We are honoured to bring this beautiful collection of research articles which were presented in the International Conference on Advances in Basic Sciences (ICABS19), which was organized by Department of Physics, GDC Memorial College, Bahal (Bhiwani), Haryana, INDIA during February 7-9, 2019.

The main target of this meeting is to bring together a multidisciplinary group of young minds, scientists from all over the country as well as from the globe to exchange their ice-breaking ideas. This meeting provided a meaningful platform for the young researchers to update and upgrade themselves. The main themes of the conference were Phase transition, Single crystals growth and characterization, Superconductivity, Magnetism & Spintronics, Nano/Bio sensors, Biomaterials, Polymers and Polymer composites, Coordination, Bio-inorganic & Organometallic Chemistry, Photonic Materials, Green Synthesis and Green Chemistry, Glass and ceramics, Soft Condensed Matter Physics etc.

ICABS19 received a great response throughout the globe and almost 387 papers were registered. In this conference 12 Invited talks were there. The foreign delegates from Croatia, Russia, Korea, and Malasia etc. also graced the meeting.

Last but not the least; the Editors would like to thank to Sh. H.K. Chaudhary (Chairman), HKC Foundation & BRHD Charitable Trust; Dr. Surender Sharma (Vice-Chairman), GDC Memorial College; Dr. S. K. Sinha (Director) BRCM Education Society; Dr. S. K. Mishra (Principal) GDC Memorial College for constant support and motivation to make the conference a grand success. In addition to these, the Editors thankfully acknowledge the Advisory Committee for their valuable suggestion. The Editors are also thankful to the Organizing Committee for managing the things properly throughout the conference and Mr. Praveen Kanth for designing and maintaining the conference website. At last, the Editors are also thankful to Team of AIP Conference Proceedings for publishing the papers.

Editors

Sanjay Gaur, Arindam Ghosh and Vijender Singh

Bahal, INDIA

February 7-9, 2019

AIP Conference Proceedings



BUY PRINT BOOKS

HOME BROWSE INFO FOR AUTHORS FOR ORGANIZERS

SIGN UP FOR ALERTS

Browse Volumes

2142

Browse Volumes

2151 (2019) ▾

2142 (2019) ▴

[Issue 1, August 29](#)

2141 (2019) ▾

Table of Contents

< PREV NEXT >

ADVANCES IN BASIC SCIENCE (ICABS 2019)



Conference date: 7-9 February 2019
Location: Bahal, India
ISBN: 978-0-7354-1885-1
Editors: Sanjay Gaur, Arindam Ghosh and Vijender Singh
Volume number: 2142
Published: Aug 29, 2019

Volume dependence of isothermal bulk modulus and its higher pressure derivatives

Cite as: AIP Conference Proceedings 2142, 050013 (2019); <https://doi.org/10.1063/1.5122379>
Published Online: 29 August 2019

Sanjay Kumar, and Vijender Singh



View Online



Export Citation

AIP | Conference Proceedings

Get **30% off** all
print proceedings!

Enter Promotion Code **PDF30** at checkout



Volume Dependence of Isothermal Bulk Modulus and its Higher Pressure Derivatives

Sanjay Kumar^{a)} and Vijender Singh^{b)}

^{a)}*BVS, Model Town, Panipat-132103, Haryana, India*

^{b)}*Department of Physics, RPS Degree College, Mahendergarh-123029, Haryana, India*

^{a)}Corresponding author: sanjay2076@gmail.com

^{b)}chahal_gju@rediffmail.com

Abstract. In the present communication, we introduced a new K -prime equation of state (EoS). It is applied here to understand the elastic properties of the lower mantle and core regions of the Earth. It is found that the present EoS yield similar results as given by Stacey EoS.

Keywords: Equations of State; Thermodynamic properties

INTRODUCTION

The equation of state (EoS) is having very important role for studying thermal and elastic properties of any solids under high temperatures and high pressures [1, 2]. Equation of state provides pressure-volume-temperature relationship for solids. It is effectively important for the estimation of elastic properties for any researcher. The first pressure derivative of bulk modulus [isothermal bulk modulus (K_T), adiabatic bulk modulus (K_S)], is an important parameter for developing various equations of state. This concept was used by different researchers [3-5]. Stacey and Davis [1] have found that the seismic data based on geophysical model such as the Preliminary Reference Earth Model (PREM) [6] are more accurate than the laboratory data [7] because laboratory data involve uncertainty due the pressure calibration. The K -prime EoS is very convenient to investigate higher pressure derivatives of bulk modulus along with other elastic properties up to extreme compression [8]. It is found that lower mantle region lies nearly between 23 GPa to 136 GPa. However, the core region from 136 to 360 GPa.

The present study introduces a new K -prime equation of state by using the concept of dimensionless thermoelastic parameter kappa (k). Results obtained by the formulated equation of state are compared with those obtained by the Stacey reciprocal K -prime equation of state [4]. The formulations of equation of state are given in Section 2 and results and discussions are given in Section 3 and the conclusions of the manuscript are explained in Section 4.

FORMULATIONS OF THE EQUATION OF STATE

Sharma [9] used to study the volume dependence of the Gruneisen parameter (γ) with the following expression

$$K'_T = K'_\infty + (K'_0 - K'_\infty) \left(\frac{V}{V_0} \right)^k \quad 1)$$

where K'_∞ is an important parameter [1, 4] in the field of equation of state at extreme compression or pressure. All equations of state for which K'_∞ is greater than zero satisfies the following relationship

$$\left(\frac{P}{K} \right)_\infty = \frac{1}{K'_\infty} \quad 2)$$

K'_0 is the first pressure derivative of isothermal bulk modulus (K_T) at zero pressure and kappa (k) is known as dimensionless thermoelastic parameter which has been used by many researchers [10-13] to solve thermoelastic properties for solids.

K'_T is defined as

$$K'_T = -\frac{V}{K_T} \left(\frac{dK_T}{dV} \right) \quad (3)$$

where V is the volume and K_T is the isothermal bulk modulus

Using Eq. (1) with Eq. (3), we get the following relationship for volume dependence of bulk modulus

$$\left(\frac{K_T}{K_0} \right) = \left(\frac{V}{V_0} \right)^{-K'_\infty} \exp \left[\left(\frac{K'_0 - K'_\infty}{k} \right) \left\{ 1 - \left(\frac{V}{V_0} \right)^k \right\} \right] \quad (4)$$

The pressure-volume relationship cannot be obtained directly through Eq. (1) but an approximate value, which is near to real, can be obtained by the following way. The term inside the square bracket of Eq. (4) can be expanded up to second order as higher order terms are not very significant. Therefore, Eq. (4) can be expressed as follows:

$$\left(\frac{K_T}{K_0} \right) = \left(\frac{V}{V_0} \right)^{-K'_\infty} \left[1 + m \left\{ 1 - \left(\frac{V}{V_0} \right)^k \right\} + \frac{m^2}{2} \left\{ 1 - \left(\frac{V}{V_0} \right)^k \right\}^2 \right] \quad (5)$$

where

$$m = \left(\frac{K'_0 - K'_\infty}{k} \right) \quad (6)$$

Using the basic definition of isothermal bulk modulus

$$K_T = -V \left(\frac{dP}{dV} \right) \quad (7)$$

Using Eq. (5) with Eq. (7), we obtain the following expression for Pressure

$$P = K_0 \left[\left(\frac{1 + m + m^2/2}{K'_\infty} \right) \left\{ \left(\frac{V}{V_0} \right)^{-K'_\infty} - 1 \right\} + \frac{m(m+1)}{(k - K'_\infty)} \left\{ \left(\frac{V}{V_0} \right)^{k - K'_\infty} - 1 \right\} - \frac{m^2}{2(2k - K'_\infty)} \left\{ \left(\frac{V}{V_0} \right)^{2k - K'_\infty} - 1 \right\} \right] \quad (8)$$

RESULTS AND DISCUSSIONS

The reciprocal K' -prime EoS due to Stacey [4] is expressed as follows

$$\frac{1}{K'_T} = \frac{1}{K'_0} + \left(\frac{1}{K'_\infty} - \frac{1}{K'_0} \right) K'_\infty \frac{P}{K} \quad (9)$$

Integration of Eq. (9) gives

$$\frac{K_T}{K_0} = \left(1 - K'_\infty \frac{P}{K} \right)^{-K'_0/K'_\infty} \quad (10)$$

and

$$\ln\left(\frac{V}{V_0}\right) = \left(\frac{K'_0}{K_\infty}\right) \ln\left(1 - K'_\infty \frac{P}{K_T}\right) + \left(\frac{K'_0}{K_\infty} - 1\right) \frac{P}{K_T} \quad (11)$$

TABLE 1. Input parameters used in the present study

Parameters	K_0	K'_0	K'_∞	k
Lower mantle	206.06[1]	4.2[1]	2.41[1]	3.153
Outer core	124.553[1]	4.9599[1]	3.0[1]	3.095

TABLE2. Computed values of volume dependence of K_T (GPa) and K'_T from (a) Stacey EoS and (b) present study

$\left(\frac{V}{V_0}\right)$	Lower mantle				$\left(\frac{V}{V_0}\right)$	Outer core			
	K_T (GPa)		K'_T			K_T (GPa)		K'_T	
	(a)	(b)	(a)	(b)		(a)	(b)	(a)	(b)
0.7144	667.17	671.68	3.0790	3.0299	0.5396	1301.35	1359.58	3.3171	3.2904
0.7221	645.43	650.14	3.0955	3.0512	0.5438	1267.81	1325.30	3.3227	3.2975
0.7240	640.04	644.94	3.0997	3.0566	0.5494	1225.90	1281.21	3.3300	3.3070
0.7353	610.11	614.97	3.1246	3.0889	0.5558	1179.46	1232.99	3.3387	3.3182
0.7490	575.69	580.67	3.1563	3.1296	0.5583	1128.70	1214.75	3.3489	3.3227
0.7634	541.96	546.84	3.1911	3.1741	0.5715	1073.81	1123.68	3.3609	3.3469
0.7786	508.80	513.43	3.2297	3.2231	0.5812	1015.11	1061.97	3.3749	3.3654
0.7946	476.06	480.58	3.2730	3.2770	0.5921	952.87	997.40	3.3914	3.3871
0.8118	443.62	447.73	3.3221	3.3376	0.6046	887.40	929.01	3.4110	3.4129
0.8303	411.40	414.97	3.3786	3.4059	0.6190	818.09	856.99	3.4344	3.4441
0.8503	379.31	382.31	3.4446	3.4835	0.6354	748.33	782.80	3.4625	3.4816
0.8721	347.27	349.65	3.5231	3.5727	0.6544	675.51	706.01	3.4970	3.5276
0.8962	315.14	316.76	3.6187	3.6770	0.6628	645.93	674.86	3.5129	3.5488
0.9093	298.88	300.17	3.6756	3.7363					

TABLE 3. Computed values of volume dependence of pressure P (GPa) from (a) Stacey EoS and (b) present study

$\left(\frac{V}{V_0}\right)$	Lower Mantle		$\left(\frac{V}{V_0}\right)$	Outer core	
	(a)	(b)		(a)	(b)
0.7144	135.75	136.29	0.5396	328.85	337.98
0.7221	128.71	129.25	0.5438	318.75	327.76
0.7240	126.97	127.55	0.5494	306.15	314.64
0.7353	117.35	117.86	0.5558	292.22	300.33
0.7490	106.39	106.88	0.5583	277.04	294.93
0.7634	95.76	96.20	0.5715	260.68	268.06
0.7786	85.43	85.80	0.5812	243.25	249.96
0.7946	75.36	75.73	0.5921	224.85	231.13
0.8118	65.52	65.82	0.6046	205.60	211.31
0.8303	55.90	56.13	0.6190	185.64	190.60
0.8503	46.46	46.66	0.6354	165.12	169.45
0.8721	37.29	37.41	0.6544	144.19	147.80
0.8962	28.29	28.34	0.6628	135.75	139.10
0.9093	23.83	23.87			

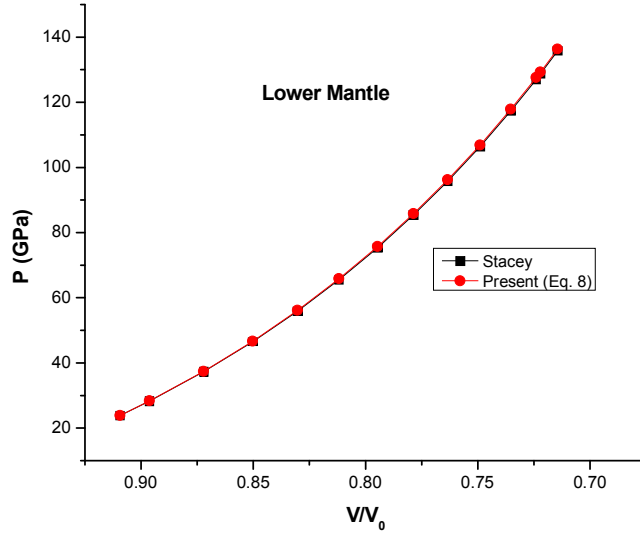


FIGURE 1. Comparison of pressure-volume data calculated through Eq. (8) and Stacey EoS [4]

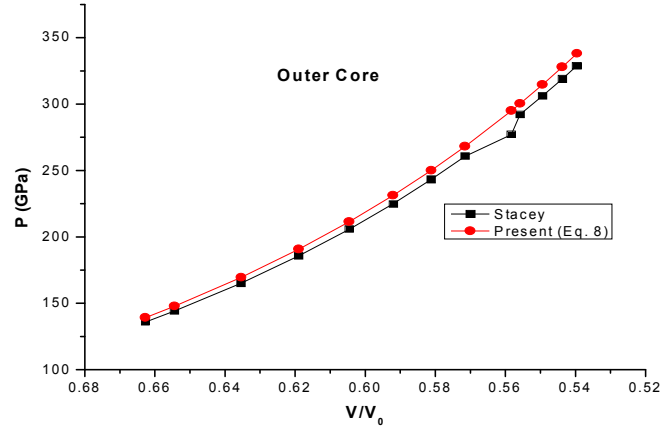


FIGURE 2. Comparison of pressure-volume data calculated through Eq. (8) and Stacey EoS [4].

We estimated the values of volume dependence of K_T and K_T' for lower mantle and outer core regions of the Earth through Eqs. (4) and (1) respectively. Computed data through Eqs. (4) and (1) are compared with those predicted values with the help of Stacey Equations of State (10) and (9) respectively in Table 2. It is apparent from Table 2 that the predicted values are found to be in good agreement with data predicted by Stacey Equation of state. Our equation of state shows the compatibility with the more stable EoS (Stacey EoS). The input data used in the present study are shown in Table 1. The calculated pressure-volume relationship for lower mantle and outer core is shown in Table 3 along with the data obtained from Stacey EoS. An excellent agreement between our data and data extracted through Stacey EoS reveals the validity of pressure-volume relationship obtained with the help of Eq. (1) in the form of Eq. (8). Computed values of pressure-volume data through Eqs. (8) and (11) are compared in Figs. 1 and 2 for lower mantle and outer core respectively. It is clear from Figs. 1 and 2 that the data in the present study are compatible with the Stacey EoS throughout the compression used.

Now, differentiating Eq. (1) with respect to pressure, we obtain

$$K_T K_T'' = -k(K_T' - K_\infty') \quad (12)$$

Again differentiating Eq. (12) with respect to pressure, we obtain

$$K_T^2 K_T''' = k(K_T' - K_\infty')(K_T' + k) \quad (13)$$

And the ratio $\left(\frac{K_T^2 K_T'''}{K_T K_T''}\right)$ for K -prime EOS is given below by using Eqs. (12) and (13)

$$\left(\frac{K_T^2 K_T'''}{K_T K_T''}\right) = -(K_T' + k) \quad (14)$$

One can easily find out the values of $K_T K_T''$ and $K_T^2 K_T'''$ through Eqs. (12) and (13).

CONCLUSIONS

In the present study, we introduced a new K -prime Equation of state. It is concluded that the newly developed EoS is compatible to the Stacey K -Prime EoS. The EoS is useful to understand the interior properties of the Earth.

REFERENCES

1. F. D. Stacey and P.M. Davis, *Phys. Earth Planet. Inter.* **142**, 137-184 (2004).
2. O. L. Anderson, *Equations of State for Geophysics and Ceramic Science* (Oxford University Press, New York, 1995).
3. A. Keane, *Aust. J. Phys.* **7**, 322-333 (1954).
4. F. D. Stacey, *Geophys. J. Int.* **143**, 621-628 (2000).
5. P. Sinha, S. K. Srivastava and N. Verma, *Physica B* **406** 2488-2491 (2011).
6. A. M. Dziewonski and D. L. Anderson, *Phys. Earth Planet. Inter.* **25** 297-356 (1981).
7. H. K. Mao, Y. Wu, L. C. Chen, J. F. Shu and A. P. Jephcoat, *J. Geophys. Res.* **95** 21737-21742 (1990).
8. J. Shanker, B. P. Singh and H. K. Baghel, *Physica B* **387** 409-414 (2007).
9. S. K. Sharma, *Mod. Phys. Lett. B* **22/31** 3113-3123 (2008).
10. O. L. Anderson and D. G. Isaak, *J. Phys. Chem. Solids* **54** 221-227 (1993); *Geophys. Res. Lett.* **19** 1987-1990 (1992).
11. S. Gaurav, B. S. Sharma, S. B. Sharma and S. C. Upadhyaya, *J. Phys. Chem. Solids* **65** 1635-1641 (2004).
12. J. Shanker, B. P. Singh and K. Jitendra, *Earth and Life* **2/2** 3 (2007), <http://www.geofinds.com>.
13. S. K. Srivastava, S. K. Sharma and P. Sinha, *J. Phys. Chem. Solids* **70** 255-260 (2009).

Study of DC conductivity of MoO₃ based bismuth borate and lead borate glasses

Cite as: AIP Conference Proceedings 2142, 070033 (2019); <https://doi.org/10.1063/1.5122425>

Published Online: 29 August 2019

Sanjay, Suman Devi, Shalini, Sudesh Kumar, Mukesh Kumar, N. Kishore, Rajni, Arindam Ghosh, and Vijender Singh



View Online



Export Citation

AIP | Conference Proceedings

Get **30% off** all
print proceedings!

Enter Promotion Code **PDF30** at checkout



Study of DC Conductivity of MoO₃ based Bismuth Borate and Lead Borate Glasses

Sanjay^{1a}, Suman Devi², Shalini², Sudesh Kumar², Mukesh Kumar³, N. Kishore⁴,
Rajni⁵, Arindam Ghosh¹, Vijender Singh¹

¹Department of Physics, GDC Memorial College, Bahal (Bhiwani) Haryana-127028 (INDIA)

²Department of Chemistry, Banasthali Vidyapith, P.O. Banasthali Vidyapith (Rajasthan)-304022 (INDIA)

³Department of Chemistry, Vaish College, Rohtak (Haryana)-124001 (INDIA)

⁴Department of Physics, Central University of Haryana, Mahendergarh (Haryana)-123031 (INDIA)

⁵Department of Physics, Maharishi Dayanand University, Rohtak (Haryana)-124001 (INDIA)

^aCorresponding author: gaur1010san@gmail.com

Abstract. Heavy metal based oxide glass series of composition $x\text{MoO}_3 \cdot (40-x)\text{M} \cdot 60\text{B}_2\text{O}_3$ ($\text{M} = \text{Bi}_2\text{O}_3$ and PbO) have been prepared by the standard melt-quenching technique. The amorphous nature of the present systems was estimated by XRD patterns. The SEM pattern has been used to study the microstructure of the sample. The effect of temperature on DC conductivity has been measured in the temperature range 523-623K for the compositions. In this temperature range, the DC conductivity increases in $\text{MoO}_3\text{-Bi}_2\text{O}_3\text{-B}_2\text{O}_3$ glasses with increase in MoO_3 content is due to small polaron hopping mechanism between Mo^{5+} and Mo^{6+} ions whereas it decreases in $\text{MoO}_3\text{-PbO-B}_2\text{O}_3$ glasses with an increasing MoO_3 content which is due to predominantly to Pb^{2+} ions.

INTRODUCTION

It is reported that in the presence of B_2O_3 , glass formation is possible with Bi_2O_3 because B_2O_3 is established as glass forming oxide whereas Bi_2O_3 is a conditional glass former. The oxide B_2O_3 is one of the most common glass formers and played a crucial role in the formation of glass network. According to Krogh-Moe [1], the structure of vitreous B_2O_3 consists of a random network of six membered boroxol rings and BO_3 triangles connected by B-O-B linkages. Further, it has been shown that the addition of Bi_2O_3 leads to improvements in the chemical durability and thermal stability of oxide glasses [2]. It is reported that the glasses containing bismuth oxide exhibit high refractive index, IR transmission and nonlinear optical susceptibilities. It was observed in earlier studies that when PbO is added to other network forming oxide glasses, it acts mainly the network modifier (with PbO_6 structural units) and by network former in both covalent and ionic bonding with $\text{PbO}_{4/2}$ pyramidal units connected in puckered layers, depending upon its concentration in the glass [3-4]. The introduction of Transition Metal (TM) oxide such as MoO_3 in the glass system may enter either as a network former or as a modifier. When the TM oxide is acting as a modifier it modifies glass structure and affects its electrical behaviour [5]. The interest for the present glass series is determined by the presence of two network forming oxides, the classical B_2O_3 and unconventional Bi_2O_3 . At the same time, both boron and bismuth are known to have stable coordination more than one, i.e. boron triangles and tetrahedra, and bismuth pyramidal and octahedral structural units. Furthermore, bismuth is able to form independent interconnected network of the borate groups [6]. The glasses containing transition metal ions such as MoO_3 have attracted interest because of their potential use in electrochemical, electronic and electro-optic devices [7-8]. The molybdenum cation could act as a network former as well as network modifier depending upon its concentration [5] for example, large molybdenum concentration leads to the formation of various molybdenum units that enter into the glass network by cross-linking borate chains [8-9]. Selecting Molybdenum oxide as a transition metal oxide, we have shown a wide glass range inside the $\text{MoO}_3\text{-M-B}_2\text{O}_3$ ($\text{M} = \text{Bi}_2\text{O}_3$ and PbO) ternary system. Ternary borate

glasses are very interesting for glass scientists and technologists due to their wide range of technological applications such as memory switching devices, light modulation, infrared windows and gas sensors [10-11]. For the present studies, we have prepared semiconducting oxide glasses with B_2O_3 as a glass former having iron, molybdenum and vanadium as transition metal ions in presence of Bi_2O_3 and PbO content. The main aim of the present glass series is to study the effect of TMO (transition metal oxide) on the XRD, SEM patterns and the DC electrical conductivity of glass systems: $MoO_3-Bi_2O_3-B_2O_3$ (MBB) and $MoO_3-PbO-B_2O_3$ (MPB).

EXPERIMENTAL DETAILS

Heavy metal based oxide glass series of composition $xMoO_3.(40-x)M.60B_2O_3$ ($M= Bi_2O_3$ and PbO) have been prepared from AR grade chemicals MoO_3 , Bi_2O_3 , PbO and H_3BO_3 by the standard melt quenching technique. The weighted quantities of the starting materials (99.99% purity) were thoroughly mixed in appropriate proportions and it was heated in porcelain crucible at a temperature of $300^\circ C$ to convert boric acid into B_2O_3 via the reaction $2H_3BO_3 \rightarrow B_2O_3 + 3H_2O \uparrow$. The homogenized melt is obtained by heating at 1473K in an electrical muffle furnace and then got the coin-shaped samples of 1-2mm thickness with the help of two stainless steel plates. After preparation, the samples were stored in the vacuum desiccators to prevent any further oxidation or degradation. X-ray diffraction (XRD) patterns of the samples were recorded using Rigaku X-ray diffractometer to determine the glass-forming region of the synthesized samples. The micrograph of each glass sample has been recorded using scanning electron microscopy (SEM) of model JEOL JSM- 6510. For the measurement of direct current conductivity, a constant voltage 50 V is applied across the sample and the current is measured by using Keithley 6485 picoammeter in the temperature range 523K-623K.

RESULTS AND DISCUSSION

X-ray Diffraction and SEM Studies

The structureless X-ray diffraction (XRD) spectra obtained from Rigaku X-ray diffractometer suggest that the samples are indeed amorphous in nature. The typical XRD patterns of each series for $x = 0$ and $x = 6$ are presented in Fig.1 (a) & Fig.2 (a) respectively, which confirms the amorphous nature of the sample with no traces of crystalloid. The study indicates that all the added amount of MoO_3 (at least up to $x = 6$) has entered the glass network. The microstructure of the prepared samples is identified by scanning electron microscopy (SEM) studies. Scanning Electron Microscope is used to study the microstructure of the samples. Fig.1 (b) & Fig. 2 (b) shows the typical SEM micrograph of studied glasses for $x = 4$ (mol %), which is found to be the amorphous nature of the studied sample.

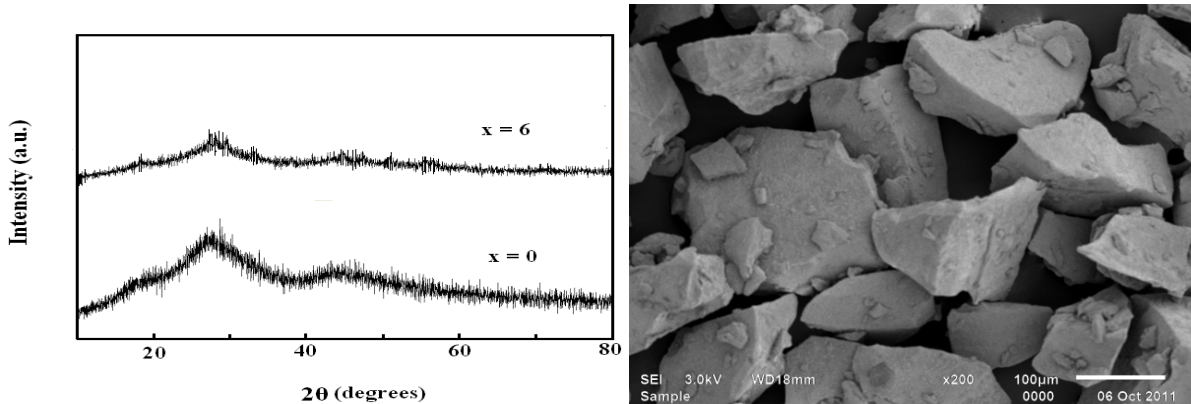


FIGURE 1. X-ray diffraction patterns of two samples of $MoO_3-Bi_2O_3-B_2O_3$ series (a). Typical SEM photograph of glass: $4MoO_3-36Bi_2O_3.60B_2O_3$ (b).

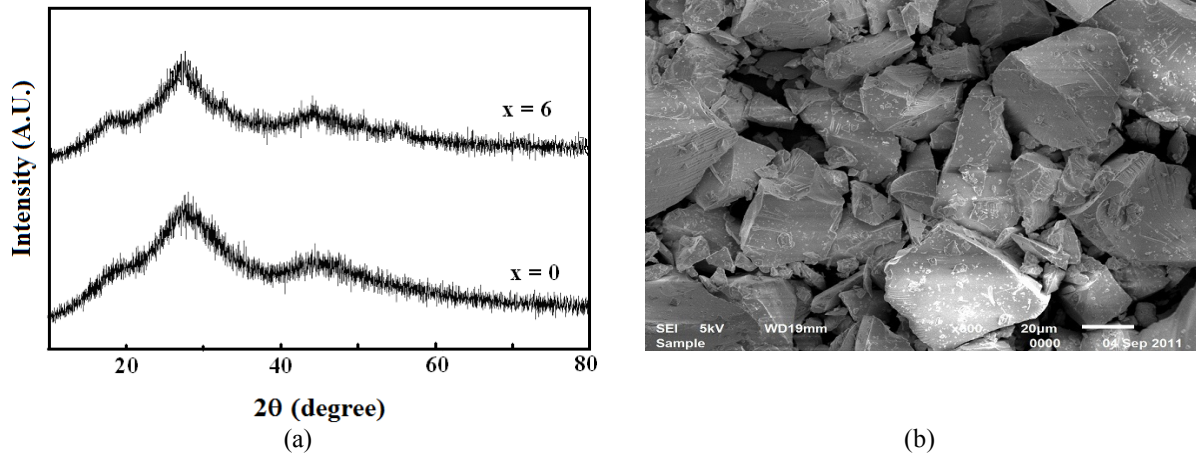


FIGURE 2. X-ray diffraction patterns of two samples of $\text{MoO}_3\text{-PbO-B}_2\text{O}_3$ series (a). Typical SEM photograph of glass: $4\text{MoO}_3\text{-}36\text{PbO.}60\text{B}_2\text{O}_3$ (b).

DC Conductivity

Conductivity is a structure sensitive property, because the structure decides both the potential barriers for the transport of mobile ions as well as the mobile ion concentration. The conductivity can be changed by changing temperature and/or by the concentration of constituents in oxide glasses [12]. The direct current (DC) electrical conductivity is measured in the temperature range from room temperature to 623K for MBB and MPB glasses. DC electrical conductivity is calculated from the relation:

$$\sigma_{\text{DC}} = 1/\rho_{\text{DC}} = (1/R)(t/A) = (I/V)(t/A) \quad (1)$$

where ρ_{DC} is the resistivity and R is the resistance of the sample, I is the current flowing through the sample, V is voltage applied for very short period in the sample, t is the thickness and A is the cross-sectional area of the sample. The conduction processes in glasses containing transition metal ions have been studied by Mott [13] in terms of phonon-assisted hopping of small polaron between localized states. The inverse of temperature dependence of DC conductivity (σ) for different glass compositions has been studied, is found to obey Arrhenius relation, in the measured temperature range as described by equation:

$$\sigma = \sigma_0 \exp (- W/k_B T) \quad (2)$$

where σ_0 is the pre-exponential factor, W is the activation energy, k is the Boltzmann constant and T is the temperature at which the conductivity to be measured. Fig. 3(a) shows that the DC conductivity increases with rise in temperature. Further, it is observed that DC conductivity increases with increase in $\text{MoO}_3\text{:Bi}_2\text{O}_3$ ratio keeping B_2O_3 constant for all compositions. In the present glasses, it is expected that the DC conductivity may have contribution in the form of electronic conductivity due to electron hopping from the lower valence state to the higher valence state which is in accordance with the mechanism of conduction proposed in other transition metal oxide glasses and interaction between the electrons and lattice, is sufficiently strong to produce a small polaron [14]. The transport of electrons in transition metal oxide (TMO) glasses is usually termed as small polaron hopping. Fig. 3(b) exhibits the temperature dependence of DC electrical conductivity of MPB glasses. Perusal of Fig. 3(b) shows that the DC conductivity increases with rise in temperature and it decreases with increase in $\text{MoO}_3\text{:PbO}$ ratio keeping B_2O_3 constant. It is well known that TMI (Mo) exists in two different valence states: Mo^{5+} and Mo^{6+} . Mo^{5+} has unpaired electron and exhibits EPR signal (hfs) whereas Mo^{6+} does not. However, EPR studies of MPB glasses indicated no EPR signal (hfs) corresponding to Mo (Mo^{5+}) [15-16] but exhibit EPR (hfs) signal corresponding to vanadyl ions only. This suggests that concentration of Mo^{5+} , if it all it exists, is too small to be detected using EPR studies. However, negligible small number of Mo^{5+} ions may exist along with Mo^{6+} ions and hence some contribution to conductivity might be due to small polaron hopping of electron between Mo^{5+} and Mo^{6+} ions. Therefore, DC conductivity in these glasses is due predominantly to Pb^{2+} ions. Thus, in MPB glasses, modifying

Pb²⁺ cations are assumed to be the charge carriers due to redox reaction assumed to occur during glass melting. As the Pb²⁺ ions are heavy, their mobility is lower which results in low conductivity. However, the formation of non-bridging oxygen ions may contribute to the increase in conductivity in borate glasses [17]. Hence, we consider that the larger conductivity at temperature higher than 500K is due to the formation of non-bridging oxygens in the B₂O₃ matrix. For the past few years, the glasses with B₂O₃ and MoO₃ as glass former oxides are well studied from the viewpoint of their structure and properties [18]. Both MoO₃ [19-21] and PbO [22] enter the structure in two forms: as a network former and/or a network modifier and affect the conductivity.

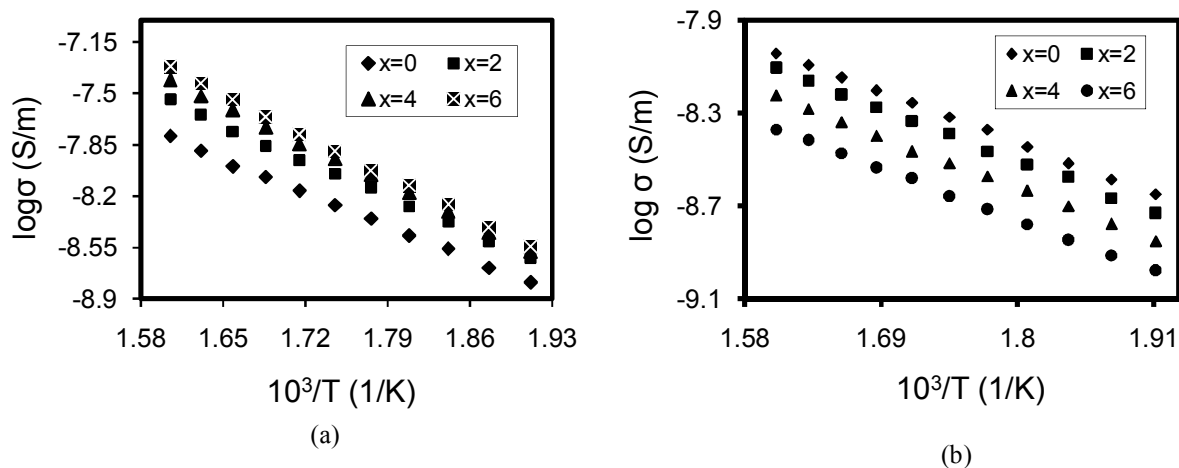


FIGURE 3. Variation of $\log \sigma$ versus $10^3 T^{-1}$ of MoO₃-Bi₂O₃-B₂O₃ glass system (a). Variation of $\log \sigma$ versus $10^3 T^{-1}$ of MoO₃-PbO-B₂O₃ glass system (b).

“**TABLE 1,**” DC conductivity at two different temperatures, activation energy and pre-exponential factor of MoO₃-Bi₂O₃-B₂O₃ and MoO₃-PbO-B₂O₃ glass systems.

Glass	x (mol %)	$\log \sigma_0$ (S/m)	$\sigma_{at 523}$ (S/m)	$\sigma_{at 623}$ (S/m)	W (eV)
MBB1	0	2.63	1.62×10^{-9}	1.62×10^{-8}	0.64
MBB2	2	1.94	2.38×10^{-9}	2.91×10^{-8}	0.69
MBB3	4	1.33	2.65×10^{-9}	3.91×10^{-8}	0.75
MBB4	6	0.95	2.85×10^{-9}	4.82×10^{-8}	0.79
MPB1	0	4.84	2.25×10^{-9}	9.06×10^{-9}	0.40
MPB2	2	4.86	1.86×10^{-9}	7.85×10^{-9}	0.40
MPB3	4	5.00	1.41×10^{-9}	5.99×10^{-9}	0.39
MPB4	6	5.15	1.05×10^{-9}	4.27×10^{-9}	0.38

CONCLUSIONS

The glass systems MoO₃-Bi₂O₃-B₂O₃ and MoO₃-PbO-B₂O₃ have been prepared by standard melt-quenching technique. From the XRD profile, amorphous nature of the prepared samples has been confirmed. The SEM pattern has been used to study the microstructure of the glasses. It is found that DC conductivity increases with rise in temperature in both glass systems but it decreases of MoO₃-PbO-B₂O₃ glass system with an increase in MoO₃ content which is due to PbO (Pb²⁺ ions) as Mo⁵⁺ is almost absent as it could not be detected in EPR studies. The DC conductivity increases with increasing MoO₃ content of MoO₃-Bi₂O₃-B₂O₃ glass system is due to “small polaron hopping” mechanism between Mo⁵⁺ and Mo⁶⁺ ions.

ACKNOWLEDGMENTS

Financial assistance provided by DRDO (IRDE Dehradun), DST (FIST), UGC (SAP) for procurement of various R & D facilities (IAVD Plant, SEM, UV-VIS-NIR Spectrophotometer, Ellipsometer, XRD, DSC-DTA-TGA, Furnace, etc.) is thankfully acknowledged.

REFERENCES

1. J. Krogh-Moe, *J. Phys. Chem. Glasses* **3**, 101 (1962).
2. H. S. Liu, P.Y. Shih, T. S. Chin, *Phys. Chem. Glasses* **38**, 123 (1997).
3. A. Veerabhadra Rao, C. Laxmikanth, B. Appa Rao, N. Veeraiyah, *J. Phys. Chem. Solids*, **67**, 2263 (2006).
4. K. J. Rao, B. G. Rao, S. R. Elliot, *J. Mater. Sci.* **20**, 1678 (1985).
5. I. Ardelean, S. Cora, V. Ionco, *J. Optoelect. Adv. Mater.* **8**, 1843 (2006).
6. H. H. Qiu., H. Sakata, T. Hirayama, *J. Ceram. Soc. Japan* **104**, 1004 (1996).
7. M. Jamnicky, P. Znasic, D. Tunega, M. D. Ingram, *J. Non-Cryst. Solids* **185**, 151 (1995).
8. U. Selvaraj, K. J. Rao, *J. Non-Cryst. Solids* **72**, 315 (1985).
9. J. F. Zynch, M. Sayer, S. L. Segel, G. Rosenblatt, *J. Appl. Phys.* **42**, 2587 (1971).
10. S. Chakraborty, H. Satou, H. Sakata, *J. Appl. Phys.* **82**, 5520 (1997).
11. Z. Hussain, *J. Electron. Mater.* **31**, 615 (2002).
12. V. N. Bogomolov, E. K. Kudinov, Yu. Firsov, *Sov. Phys. Solid State* **9**, 2502 (1968).
13. H. Doweidar, A. A. Megahed, I. A. Gohar, *J. Phys. D: Appl. Phys.* **19**, 1939 (1986).
14. Austin I G & Mott N F, *Adv Phys*, **18**, 41 (1969).
15. H.G. Hecht, T. S. Johnston, *J. Chem. Phys.* **46**, 23 (1967).
16. L. D. Bogomolova, V. A. Jachkin, N. A. Krasilnikova, *J. Non-Cryst. Solids* **241**, 509 (1998).
17. J. C. Bazan, J. A. Duffy, M. D. Ingram, M. R. Mallacc, *Solid State Ionics* **86-88**, 497 (1996).
18. K. V. Ramesh, D. L. Sastry, *J. Physica B*, **387**, 45 (2007).
19. U. Selvaraj, K. J. Rao, *J. Non-Cryst. Solids* **72**, 315 (1985).
20. J. F. Zynch, M. Sayer, S. L. Segel, G. Rosenblatt, *J. Appl. Phys.* **42**, 2587 (1971).
21. S. Mandal, A. Ghosh, *J. Phys: Condens. Matter.* **8**, 829 (1996).
22. P. J. Bray, M Leventhal, H. O. Hooper, *J. Phys. Chem. Glasses*, **4**, 37 (1963).

Measurements of third-order optical nonlinearity using Z-scan technique: A review

Cite as: AIP Conference Proceedings **2142**, 140035 (2019); <https://doi.org/10.1063/1.5122548>
Published Online: 29 August 2019

Vijender Singh, Poonam R. Kharangarh, Parveen Kumar, Davender Singh, Sanjay, Arindam Ghosh, and Sanjay Kumar



[View Online](#)



[Export Citation](#)

AIP | Conference Proceedings

Get **30% off** all
print proceedings!

Enter Promotion Code **PDF30** at checkout



Measurements of Third-Order Optical Nonlinearity using Z-Scan Technique: A Review

Vijender Singh^{a*}, Poonam R. Kharangarh^b, Parveen Kumar^c, Davender Singh^a, Sanjay^d, Arindam Ghosh^d and Sanjay Kumar^e

^a Department of Physics, RPS Degree College, Mahendergarh-123029, Haryana, India

^b Department of Chemistry, University of Delhi-110007, New Delhi, India

^c Department of Mathematics, RPS Degree College, Mahendergarh-123029, Haryana, India

^d Department of Physics, GDC Memorial College, Bahal-127028, Haryana, India

^e BVPS, Model Town, Panipat-132103, Haryana, India

*Corresponding author: vijenderchahal@gmail.com

Abstract: Optical materials exhibiting a large third-order optical nonlinearity are in great demands because of their functional applications in optical limiting, optical switching, optical data storage etc. A well-known single Z-scan technique is employed to determine third-order nonlinear optical properties of nonlinear optical materials. Z-scan is a simple experimental technique to measure intensity dependent nonlinear susceptibilities of third-order nonlinear optical materials. It was originally introduced by Sheik Bahae et.al. In this technique, the sample is translated in the z-direction along the axis of a focused Gaussian beam, and the far field intensity is measured as function of sample position. Consequently, increases and decreases in the maximum intensity incident on the sample produce wavefront distortions created by nonlinear optical effects. This is a simple and sensitive single beam technique to measure the sign and magnitude of both real and imaginary part of the third order nonlinear susceptibility $\chi^{(3)}$ of nonlinear optical materials.

INTRODUCTION

Third-order nonlinearities involve the nonlinear susceptibility tensor $\chi^{(3)}$ in equation:

$$P_i = \epsilon_0 \chi^{(1)} E + \epsilon_0 \chi^{(2)} E^2 + \epsilon_0 \chi^{(3)} E^3 + \dots \quad (1.1)$$
$$= P^{(1)} + P^{(2)} + P^{(3)} + \dots$$

The quantities $\chi^{(1)}$, $\chi^{(2)}$ and $\chi^{(3)}$ are known as the first-, second- and third-order nonlinear optical susceptibilities, respectively. We shall refer to P_i as induced polarization while $P^{(1)}$, $P^{(2)}$ and $P^{(3)}$ are the first-, second- and third-order nonlinear polarization, respectively. This term governs many nonlinear phenomena like third harmonic generation, optical Kerr effect, stimulated Raman scattering and stimulated Brillouin scattering. In general, $\chi^{(3)}$ couples together four frequency components: in other words, three fields interact to produce a fourth field.

$$P(\omega_4) = \epsilon_0 \chi^{(3)} E(\omega_3) E(\omega_2) E(\omega_1) \quad (1.2)$$

in a lossless medium the susceptibility coefficients of $\chi^{(3)}$ are real. In this case, the primary nonlinear optical effects are the generation of new frequency components and the intensity dependent refractive index change (Kerr effect).

In third-order interactions involving absorption, the imaginary part of $\chi^{(3)}$ describes Raman and Brillouin scattering and two-photon absorption [1].

The development of photonic technology during the past decade has intensified research activities on searching for new materials that display unusual and interesting nonlinear optical (NLO) properties. New NLO materials are the key elements to future photonic technologies in which their functions can be integrated with other electrical, optical and magnetic components that have become important in the era of optical communication. Organic molecular and

polymeric materials are relatively newcomers in the field of nonlinear optics compared with inorganic materials. The third-order optical nonlinearities of inorganic materials are large but their response time is relatively slow [2-3]. Large third order NLO susceptibilities have been measured in inorganic semiconductors using them as quantum wire and quantum dot materials.

Recently, research activities have been directed towards developing new organic molecular and polymeric materials. The superiority of organic materials has been realized because of their versatility and possibility of tailoring material properties by applying the techniques of molecular engineering to them for particular end-uses. In addition organic materials also exhibit large nonlinear figure of merit, high damage thresholds, and ultrafast response time.

The applications of NLO materials are widespread in the field of solid state technology that includes harmonic generators, optical computing, telecommunications, laser lithography, image processing and sensors, other optical systems. This shows that the study of NLO properties is truly an interdisciplinary area of research. The development of new materials can shed light on the theoretical understanding of the origin of NLO processes. Every year a wide variety of new NLO molecular and polymeric materials are discovered and the field continues to expand rapidly. Since the level of integration is also increasing rapidly in photonic technologies, organic polymers seem more promising compared with inorganic counterparts because of their compatibility with a variety of materials used in fabrication technology. Organic liquids, molecular solids, conjugated polymers and related model compounds, NLO chromophore functionalized polymers, organometallic compounds, organic composites, liquid crystals, semiconductors, nanoparticles etc. are different types of nonlinear materials used for various applications in the photonic industry [4-8].

NONLINEAR EXPERIMENTAL TECHNIQUES

The characterization of the nonlinear optical properties of various NLO materials for various applications like frequency mixing, optical short pulse generation and measurement, optical communication, optical switching, optical limiting etc. is a fascinating field in modern optics [9-12]. The magnitude and response of third order nonlinear susceptibility is one of the important parameters of this class of materials and several techniques are available for the measurement of such parameters. Degenerate Four Wave Mixing (DFWM), Third Harmonic Generation (THG), optical Kerr effect, Z-scan etc. [1] are some of the techniques used for this purpose. Degenerate four-wave mixing can give both the magnitude and response of the third order nonlinearity. Similarly THG is another technique used for the measurement of the magnitude of the third order susceptibility tensor. While optical Kerr effect is used for the photo physical processes determining the nonlinearity. Using z-scan technique, the sign and magnitude of the third order susceptibility tensor can be calculated.

Z-SCAN

The z-scan technique is a simple and popular experimental technique to measure intensity dependent nonlinear susceptibilities of materials and it was originally introduced by Sheik Bahae et.al [13-14]. In this method, the sample is translated in the z-direction along the axis of a focused Gaussian beam, and the far field intensity is measured as function of sample position. Consequently increases and decreases in the maximum intensity incident on the sample produce wavefront distortions created by nonlinear optical effects in the sample being observed. This is a simple and sensitive single beam technique to measure the sign and magnitude of both real and imaginary part of the third order nonlinear susceptibility $\chi^{(3)}$ of materials. The z-scan is obtained by moving the sample along a well-defined, focused laser beam, and thereby varying the light intensity in the sample. In the original single beam configuration, the Investigations of nonlinear transmittance of the sample is measured, as the sample is moved, along the propagation direction of a focused Gaussian laser beam. A laser beam propagating through a nonlinear medium will experience both amplitude and phase variations. If transmitted light is measured through an aperture, placed in the far field with respect to focal region, the technique is called closed aperture z-scan experiment [13-14]. By varying the aperture in front of the detector, one makes the z-scan transmittance more or less sensitive to either the real or imaginary parts of the nonlinear response of the material, i. e., nonlinear refractive index and nonlinear absorption, respectively.

In the closed aperture z-scan the transmitted light is sensitive to both nonlinear absorption and nonlinear refraction. In this case, phase distortion suffered by the beam while propagating through the nonlinear medium is converted into corresponding amplitude variations and the real part of the susceptibility tensor can be calculated. On the other hand, if transmitted light is measured without an aperture the z-scan obtained is known as open aperture z-

scan and in this case entire light from the sample is collected [14]. In the open aperture z-scan the output intensity is sensitive only to the nonlinear absorption of the sample and the imaginary part of the susceptibility tensor can be calculated from the data obtained.

Z-scan technique is highly sensitive to the profile of the beam and also to the thickness of the samples [13-15]. Any deviation from the Gaussian profile of the beam and also from thin sample approximation will give rise to erroneous results. To enhance its sensitivity and applicability new extensions have been added. A two color Z-scan is used to perform the studies of non-degenerate optical nonlinearities [16]. A much more sensitive technique, EZ-scan (eclipsed Z-scan), has been developed which utilizes the fact that the wings of a circular Gaussian beam are much more sensitive to the far-field beam distortion [17]. A reflection z-scan technique was introduced to study the optical nonlinearities of surfaces [18]. Z-scan with top-hat, investigations of nonlinear beams and elliptical Gaussian beams has been performed resulting in better sensitivity [19]. The dual wavelength (two-color) extension of the standard z-scan technique has been used to measure the non-degenerate nonlinearities [16]. This has been further used to time resolve the dynamics of the nonlinear process by introducing a delay between the pump and probe beams [16]. Z-scan measurements can also be done with astigmatic Gaussian beams [20]. In the case of astigmatic Gaussian beam, a slit is used instead of a (circular) aperture. Z-scan measurement for non-Gaussian beams with arbitrary sample thickness [21] and arbitrary aperture [22] has also been suggested. In the case of the former, nonlinear parameters are measured in comparison with a standard sample, mostly carbon disulphide (CS₂) [23]. The Z-scan technique has been used extensively to study different materials like semiconductors, nano-crystals, semiconductor-doped glasses, liquid crystals, organic materials, biomaterials etc. [4-8, 24-25].

CLOSED APERTURE Z-SCAN

In order to measure the nonlinear refraction or the real part of $\chi^{(3)}$ a sample is moved using a translation stage along the propagation direction of the tightly focused beam and the transmitted light is collected through an aperture placed in front of a detector as shown in Fig. 1.

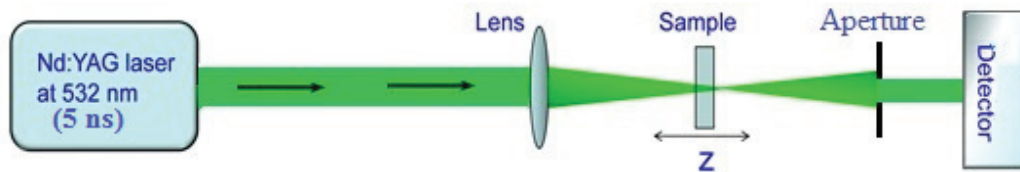


Figure 1 Closed aperture z-scan setup for nonlinear refraction measurements.

When the Gaussian beam propagates through the sample, due to the nonlinear refractive index change in the transverse direction the sample acts as converging or diverging lens as displayed in Fig. 2.

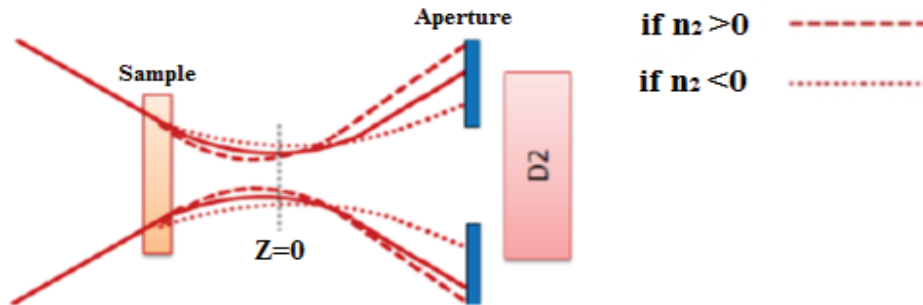


Figure 2 Depending on the sign of the change of the nonlinear refractive index, the sample may act as a converging or diverging lens.

For a positive refractive index change it would act as converging lens and for a negative refractive index change it would act as a diverging lens. The normalized transmittance through the aperture is shown in Fig. 3 for both positive and negative refractive index changes. The graph obtained by dividing the closed aperture z-scan data by

the open aperture z-scan data measured simultaneously is known as "divided z-scan graph" [14]. In the "divided z-scan" the effect of nonlinear absorption is cancelled out and the measured nonlinear effect is due to the nonlinear refraction alone.

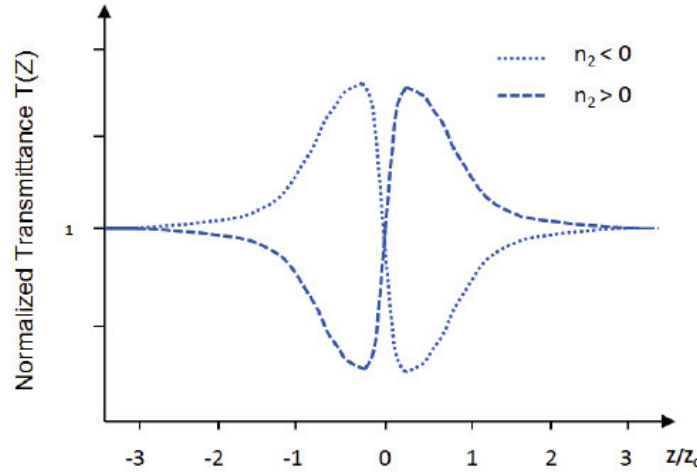


Figure 3 Z-scan traces for the transmission through the aperture for negative and positive nonlinear refractive index change.

Thus the curve for Z versus transmittance has a peak followed by a valley for a negative refractive nonlinearity. The curve for a positive refractive nonlinearity will give rise to the opposite effect, i.e. a valley followed by a peak [13-14]. The former is called self-defocusing and the latter is called self-focusing. Fig. 3 shows a typical closed aperture z-scan curve of samples having negative and positive nonlinearities respectively.

One of the mechanisms of self-focusing is optical Kerr effect [26] which has instantaneous response. In this case the electric field of a light beam exerts a torque on anisotropic molecules by coupling to oscillating dipole induced in the molecule by the field itself. Resulting light induced molecular reorientation is the main mechanism for optical nonlinearity in a transparent liquid. Nonlinear refractive index depends linearly on light intensity. Other mechanism of optical Kerr effect includes off resonant excitation of narrow band absorbers and consequent distortion of electronic distribution among energy levels in the materials. The resultant intensity dependent refractive index is responsible for self-focusing or self-defocusing. In self-focusing beam collapses upon itself spatially. Kerr like nonlinearity has very fast response time of the order of picoseconds.

OPEN APERTURE Z-SCAN

In order to determine the nonlinear absorption of a material, the aperture in front of the light collection photodiode is fully opened or removed as shown in Fig. 4. When the normalized transmittance vs. the sample position is recorded then it will be a symmetric curve around the focus as shown in Fig. 5.

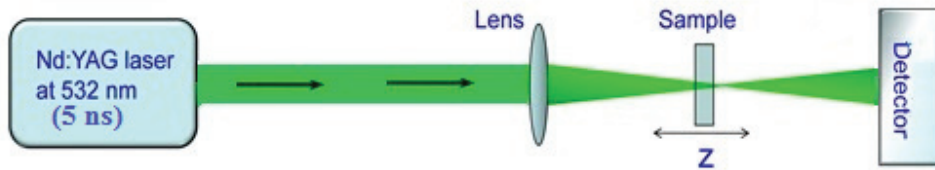


Figure 4 Open aperture z-scan setup for nonlinear absorption measurements. In order to measure the nonlinear absorption, all the transmitted light is collected by a detector.

Nonlinear absorption of the sample is manifested in the open aperture z-scan measurements. For example, if nonlinear absorption like two-photon absorption (TPA) is present, it is manifested in the measurements as a transmission minimum at the focal point [14]. On the other hand, if the sample is a saturable absorber, transmission increases with increase in incident intensity and results in a transmission maximum at the focal region. A straight-line z-scan graph is obtained in the case of samples with linear absorption. In the case of reverse saturable absorption (RSA), the sample experiences the strongest intensity and fluence at focus; therefore it absorbs the most energy and allows least transmittance.

Away from the focus in the direction of both increasing and decreasing z transmittance increases evenly because the irradiance decreases symmetrically about the focus. These features are shown in Fig. 5.

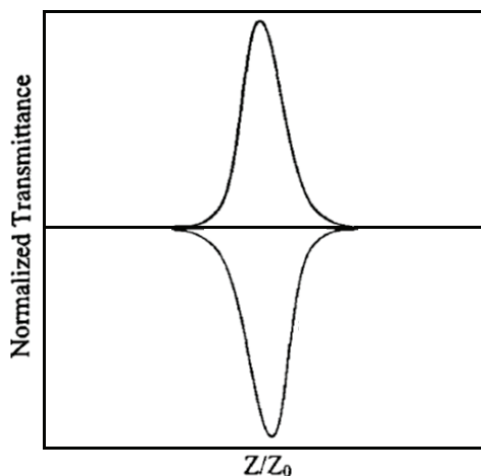


Figure 5 Open aperture z-scan curves.

ADVANTAGES AND DISADVANTAGES OF THE Z-SCAN TECHNIQUE

The Z-scan has several advantages. Among these is its simplicity. As a single beam technique, the alignment of beam is not difficult although it is to be kept centered on the aperture. It can be used to determine both the magnitude and the sign of n_2 . The sign is obvious from the shape of the transmittance curve. Generally, data analysis is quick and simple, making it a good method for screening new nonlinear materials. Under certain conditions, it is possible to isolate the nonlinear refractive and nonlinear absorptive contributions to the far-field transmittance. Thus, unlike most DFWM methods, the z-scan can determine both the real and the imaginary parts of $\chi^{(3)}$. The technique is also highly sensitive, capable of resolving a phase distortion of $\sim \lambda/300$ in samples of high optical quality. Finally, the Z-scan can also be modified to study nonlinearities on different time scales as well as higher order contributions.

Disadvantages of the technique include the fact that it requires a high quality Gaussian TEM₀₀ beam for absolute measurements. The analysis must be different if the beam is non-Gaussian. Sample distortions or wedges, or a tilting of the sample during translation, can cause the beam to walk off the-field aperture. This produces unwanted fluctuations in the detected signal. The technique cannot be used to measure off-diagonal elements of the susceptibility tensor except when a second non-degenerate frequency beam is employed. Such a technique is useful for measuring the time dependence of nonlinearities but this detracts from the simplicity and elegance of the method. The introduction of a second beam of a different frequency requires careful alignment of the two beams, taking into account difference in spot sizes and focal positions due to chromatic aberration, and physical separation and filtering of the beams prior to detection.

CONCLUSION

Nonlinear optics (NLO) is a broad field of research and technology that encompasses subject matter in the fields of Physics, Chemistry, Biology and Engineering. The z-scan technique is a simple and popular experimental

technique to measure intensity dependent nonlinear susceptibilities of materials. In this method, the sample is translated in the z-direction along the axis of a focused Gaussian beam, and the far field intensity is measured as function of sample position.

REFERENCES

1. R. L. Sutherland, D. G. McLean and S. Kirkpatrick, Handbook of Nonlinear Optics, 2nd ed. (Marcel Dekker, New York, 2003).
2. T. Kobayashi, Nonlinear Opt. 1, 91 (1991).
3. H. Nasu, T. Uchigaki, K. Kamiya, H. Kanbara and K. Kubodera, *Jpn. J Appl. Phys.* 31, 3899 (1992).
4. V. Singh and P. Aghamkar, *Appl. Phys. Lett.* 104, 111112 (2014).
5. V. Singh, P. Aghamkar and R. K. Malik, *Appl. Phys B*, 115,391 (2014).
6. V. Singh and P. Aghamkar, *Applied optics* 51, 13, 2288 (2012).
7. P. R. Kharangarh, S. Umapathy and G. Singh, *Appl. Surf. Sci.* 449,363–370 (2018).
8. P. R. Kharangarh, S. Umapathy, and G. Singh, *Journal of Applied Phys.* 122 (14), 145107 (1-7), (2017).
9. J. O. Gorman, A. F. J. Levi, T. T. Ek and R. A. Logan, *Appl. Phys. Lett.* 59, 16 (1991).
10. J. G. Fujimoto and E. P. Ippen, *Opt. Lett.* 8, 446 (1983).
11. J. S. Shirk, R. G. S. Pong, F. J. Bartoli and A. W. Snow, *Appl. Phys. Lett.* 63, 1880 (1993).
12. V. Singh, P. Aghamkar, *AIP Conf. Proc.* 1675, 030095 (2015).
13. M. S. Bahae, A. A. Said and E. W. Van Stryland, *Opt. Lett.* 14, 955 (1989).
14. M. S. Bahae, A. A. Said, T. H. Wei, D. J. Hagan and E. W. V. Stryland, *IEEE J. Quantum Electronics* 26,760 (1990).
15. F. E. Hernandez, A. Marcano and H. Maillotte, *Opt. Commun.* 134,529 (1997).
16. M. S. Bahae, J. Wang, R. De Salvo, D. J. Hagan and E. W. Van Stryland, *Opt. Lett.* 17, 258 (1992).
17. H. Ma and C. B. de Araujo, *Appl. Phys. Lett.* 66, 1581 (1995).
18. T. Xia, D. J. Hagan, M. S. Bahae and E. W. Van Stryland, *Opt. Lett.* 19,317 (1994).
19. P. B. Chapple, J. M. Staromlynska, J. A. Hermann, and T. McKay, *J. Nonlinear Opt. Phys. and Mat.* 6, 251 (1997).
20. Y. L. Huang and C. K. Sun, *J. Opt. Soc. Am. B* 17, 43 (2000).
21. P. B. Chapple, J. Staromlynska and R. G. McDuff, *J. Opt. Soc. Am. B* 11,975 (1994),
22. J. A. Herman, T. McKay and R. G. McDuff, *Opt. Commun.* 154, 255 (1998).
23. R. E. Bridges, G. L. Fischer and R. W. Boyd, *Opt. Lett.* 20, 1821 (1995).
24. P. R. Kharangarh, S. Umapathy, and G. Singh, *Integ. Ferroelectrics* 183, 1, 2017.
25. P. R. Kharangarh, S. Umapathy, and G. Singh, *ECS J. Solid State Sci. Technol.* 7(3), M29-M34 (2018).
26. T. Hattori and T. Kobayashi, *J. Chem. Phys.* 94, 3322 (1991).